Scuola di Dottorato in Fisica, Astrofisica e Fisica Applicata
Dipartimento di Fisica

Corso di Dottorato in Fisica, Astrofisica e Fisica Applicata
Ciclo XXVIII

Symmetric Block Copolymers Templates for Nano-Lithographic Applications

Supervisore: Professor Paolo MILANI

Co-Supervisore: Dottor Michele PEREGO

Coordinatore: Professor Francesco RAGUSA

Tesi di Dottorato di:
Monica CERESOLI

Anno Accademico 2015/2016

To Andrea and Chiara.

Contents

List of Figures

Introduction

This thesis develops in the framework of nanofabrication, which implies the production of objects with at least one characteristic dimension smaller than 100 nm. This field comprises many different applications such as biological and energetics technologies as well as state of the art microelectronics. Nanostructured templates indeed could be exploited in organic photovoltaics [1], nanoporous membranes [2], and next-generation lithography [3].
For this reason microelectronics represents one of the stronger boost in the study of the new physics and chemistry involved on such a small dimensional scale. Together with the other nanomanufacturing applications it has been long characterized by a top-down approach: it consists in a subtractive process which starts from large pieces of materials and reduces them to the nanoscale designing features with precise shape and size.
The process of reduction or miniaturization dramatically affects the semiconductor industry in the so called scaling of devices for the integrated circuits design. Following Moore's law, which forecasts a double device density on integrated circuits every 18 months, devices should nowadays present few-nanometers defined features.
The Semiconductor Industry Association's International Technology Roadmap for Semiconductors (ITRS) periodically plans the fabrication goals for the coming decades indicating the most promising techniques to fulfill Moore's prevision.
ITRS requirements regarding the scaling process of devices, could be represented by the definition of new dimensional nodes. In microelectronics a node corresponds to the linewidth of an equal line-space pattern in the Integrated Circuits (ICs) manufacturing process. The demand for smaller and smaller nodes continuously proposes new technological issues (coming to quantum effects), but the core of the fabrication process is probably represented by lithography. It is a a top-down method which sculpts devices features in deposited or grown materials.

Limits of Current Photolithography

Nowadays the fabrication approach employed in the industrial process flow for the definition of microelectronic devices in integrated circuits is photolithography. A typical scheme of photolithography is reported in figure 1, but it has been long refined in order to address features as small as tens of nanometers. Conventional 193 nm photolithography based on light source, masks and optics to impress the photoresist coverage of

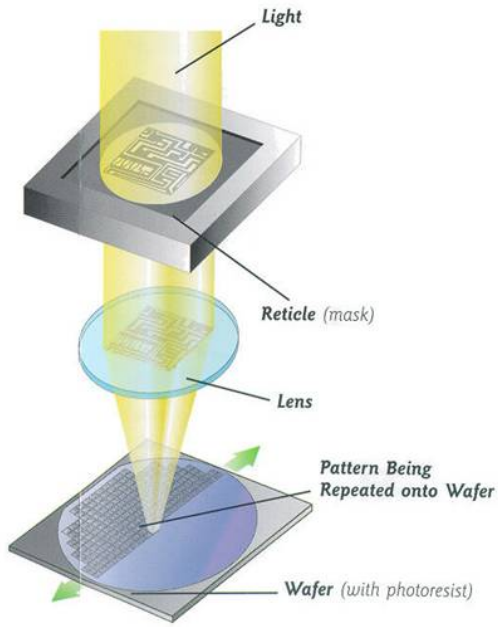

Figure 1: Typical scheme of photolithographic set up, taken from:
$http://willson.cm.utexas.edu/Research/Sub_Files/Immersion/index.php$

silicon wafers, has already faced its diffraction limit of $\lambda/4$, in the so called 45 nm node of production. New strategies such as multiple exposure [4] improved the resolution up to the 22 nm node but different approaches are required to identify non expensive solutions, for the industrial exploitation[1] of following nodes.
Top-down techniques alternative to current photolithography could be identified in Electron Beam Lithography (EBL) as well as in Extreme Ultra-Violet Lithography (EUVL). The main advantage of EBL is the possibility to directly "write" onto the photoresist surface without the need of a physical mask. Although EBL supplies for high quality performances (with features below 22 nm) on small samples for research activities, it does not represent a high throughput technique with respect to the requirements of industrial production. For this reason it is currently commercially limited to the fabrication of masks for subsequent photolithographic processes.
The EUVL line at 13.5 nm is under development, but it still represents a huge investment in terms of machine replacements costs, revealing at the same time several physical problems such as the implementation of new optics and resists materials.
In the same contest the last few decades have seen the development of many other different unconventional lithography techniques such as the nanoimprint lithography in which the template features are precisely replicated onto the sample substrate by means of a mold. The critical issue for this kind of processes then consists in the fabrication of the mold, that means a 1x mask for the definition of feature sizes down to $\approx$ 20 nm.
Nevertheless the depicted top-down approach could hardly addressed the low-cost/high-

[1] It is worth to note that such impressive results depend on the concomitant progress in masks production, deposition technologies and photoresist chemistry. All these contributions have to be taken into account in order to determine the manufactorability (in the cost/benefits balance) of the technique.

volume manufacturability in going towards 10 nm scale or even to smaller features, where the quantum properties of matter becomes fundamental potentialities of devices. A paradigm shift is required for a viable nanofabrication technique on such a small dimensional scale. The solution provided by nature is the bottom-up approach. If top-down identifies a subtractive process, bottom-up ruther stands for an additive one, in which complex functional systems, from inorganic to biological structures are built up from atomic or molecular scale components.

Self-Assembling Materials: Top-Down meets Bottom-Up

In the bottom-up framework a solution to the fabrication of ordered nanostructured templates is provided by the Self-Assembly (SA) process. SA indicates the mechanism through which atoms or molecules spontaneously organize into complex structures and patterns, corresponding to a local minimum into the energy of the material system starting from a higher energy state.
Direct Self-Assembly (DSA) refers to the possibility to drive the assembly process of these materials by means of additional regular features (most likely fabricated within a top-down technique) in the environment to guide the organization of the components and to determine the final structure they form. In this way the implementation of bottom-up into top-down techniques could lead to new possibilities of nanofabricaiton. In this contest, the possibility of integrating SA materials into the standard lithographic processes to generate sub-lithographic structures was critically reviewed in recent editions of the ITRS in the perspective of process simplification.
Examples of SA materials are functionalized Monolayers of molecules, the so called SAMS, as well as phase separating Block Copolymers (BCPs).
BCPs are a class of macromolecules formed by chemically distinct homopolymer chains covalently bonded at one end. Due to the immiscibility between the distinct blocks, a phase separation occurs. However, the chemical bond limits the scale of phase separation giving rise to self-ordered microdomains with different size and morphology.[5] This peculiar behavior makes BCPs extremely appealing for both fundamental studies and technological applications in several different fields.[3] [6] [7] In particular, when deposited in the form of thin films, they provide ideal templates for the nanofabrication of dense patterns with typical sizes ranging from 5 to 50 nm.[8] [9] [10] DSA of BCPs could be lead by adding a chemical (chemical modification of substrate surface) or a topographical (graphoepitaxy) pattern as well as applying external fields (electric, thermal, pressure etc.).
The implementation of BCPs into current photolithography allows its extension to sub-litographic features providing a simple tool for the sub-patterning of previously defined photolithographic structures. BCPs thus, revealed as the most promising candidates for the fabrication of the next generation of microelectronic devices.[11] [12] [13]

In order to prove their potential exploitation into next years industrial lithographic processes, BCPs based technology has to successfully afford some fundamental issues regarding both the synthesis and the organization of the polymeric layer and its following implementation as a lithographyc mask. In particular the main technological constrains are:

- Fast procedures for nanotemplate fabrication;

- Low cost processing steps, fully compatible with nowadays photolithographic process flow;
- High resolution (nanometer scale) and high density templates with different morphologies;
- High pattern transfer fidelity and self registration with photolithographic prestructured substrates.

The peculiar properties of BCPs naturally fulfill the needs for high density and small scale dimensions. Moreover the polymeric material, as in the case of PS-*b*-PMMA, could be properly chosen in order to be similar to the conventional resist material employed in photolithography, simplifying its integration into common process flow. Nevertheless the possibility to process these materials within techniques fully compatible with microelectronics requirements remains an open issue. Lot of research develops around the identification of the correct methods for the implementation and the organization of BCPs into the fabrication of devices towards and beyond the 22 nm node. In this contest IBM scientists very recently demonstrated the use of a BCPs based technology in the fabrication of new devices configurations such as the FinFET transistor. In particular, the definition of sublithographic Si-fins was carried out starting from BCPs striped patterns within the manufacturing process of a 29 nm pitch FinFET transistor (see figure 2). [14].

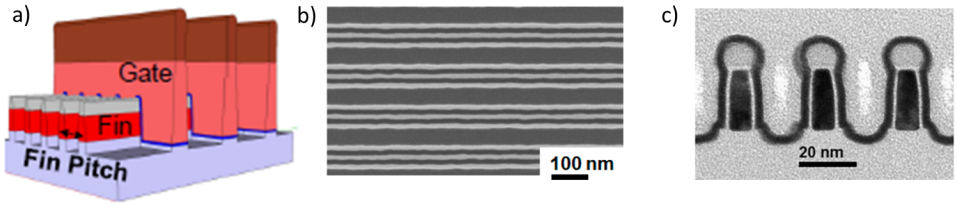

Figure 2: a) 3D scheme of a FinFET device: a group of fins is spaced following a certain fin pitch; the fin channels are controlled by a common gate line. b) and c) Top down Scanning Electron Microscope image and cross section Transmission Electron Microscope image of groups of fins fabricated with BCPs based technology. All the images are adapted from Tsai *et al.*[14]

Thesis Overview

This thesis focuses on the study of the kinetics and ordering mechanism of BCPs self-assembly in view of their possible application in the fabrication of sub-lithographic features for next microelectronics devices. The nanofabrication of a particular template configuration, the striped pattern, is discussed in detailed. The experimental samples were obtained with the block copolymer which has long represented the work horse in the field, that is polystirene-b-poly(methylmethacrylate) (PS-*b*-PMMA) and which is expected to be effectively integrated into the fabrication process of the near future.

Chapter 1, **Block Copolymers**, reports the basic theoretical concepts necessary to understand the properties of these SA materials that makes them suitable for nanofabrications. Starting from few general considerations about BCPs, the chapter highlights the various possible treatments that have been developed to address and induce the SA process.

Particular interest is focused on symmetric lamellar forming BCPs and on the choice of PS-*b*-PMMA as the material of study.

Chapter 2, **Experimental Methods**, describes in details all the techniques used for the synthesis and characterization of the BCPs based nanotemplates that are the subject of the present thesis. A complete process flow from the bare silicon substrate to the fabrication of a striped pattern is explained. An important section reports the features of the simple but peculiar thermal process employed in the organization of ordered BCPs nanodomains.

Chapter 3 (**Perpendicular Orientation of Nanostructures: Functionalization of the Substrate**) and chapter 4 (**Lateral Order of Symmetric BCPs on Featureless Substrate**) report about the main experimental results obtained in this work, following two distinct but interconnected targets: the control of the orientation of the ordered BCPs thin film morphologies with respect to the substrates, and the detailed study of the kinetics of their ordering process.

The **Conclusions** sum up the results displayed in the previous chapters, evaluating their possible exploitation as a tool for the fabrication of sub-20 nm structures in the next generation of microelectronic devices. In particular the chapter highlights future perspectives and open issues of this new fabrication approach in the route towards the integration of this technology into the industrial lithographic protocols.

At the end of this work, the Appendix (**Homopolymer blends: alternative route to obtain a neutral brush layer**) deals with an alternative strategy, with regards to that reported in chapter 3, to control the orientation of the ordered BCPs structures, with respect to the substrate.

Bibliography

[1]C. Guo, Y.-H. Lin, M. D. Witman, K. A. Smith, C. Wang, A. Hexemer, J. Strzalka, E. D. Gomez, and R. Verduzco, "Conjugated block copolymer photovoltaics with near 3% efficiency through microphase separation.", Nano letters **13**, 2957–63 (2013).

[2]W. A. Phillip, B. O'Neill, M. Rodwogin, M. A. Hillmyer, and E. L. Cussler, "Self-assembled block copolymer thin films as water filtration membranes.", ACS applied materials & interfaces **2**, 847–53 (2010).

[3]J. Bang, U. Jeong, D. Y. Ryu, T. P. Russell, and C. J. Hawker, "Block copolymer nanolithography: translation of molecular level control to nanoscale patterns.", Advanced materials **21**, 4769–92 (2009).

[4]R. F. Pease, and S. Y. Chou, "Lithography and Other Patterning Techniques for Future Electronics", in Proceeding of the ieee 96 (2008), pp. 248–70.

[5]F. S. Bates, and G. H. Fredrickson, "Block Copolymers—Designer Soft Materials", Physics Today **52**, 32 (1999).

[6]C. K. Jeong, H. M. Jin, J.-H. Ahn, T. J. Park, H. G. Yoo, M. Koo, Y.-K. Choi, S. O. Kim, and K. J. Lee, "Electrical biomolecule detection using nanopatterned silicon via block copolymer lithography.", Small **10**, 337–43 (2014).

[7]J. Lee, J. Lim, and P. Yang, "Ballistic phonon transport in holey silicon.", Nano letters **15**, 3273–9 (2015).

[8]K. Koo, H. Ahn, S.-W. Kim, D. Y. Ryu, and T. P. Russell, "Directed self-assembly of block copolymers in the extreme: guiding microdomains from the small to the large", Soft Matter **9**, 9059 (2013).

[9]S. Darling, "Directing the self-assembly of block copolymers", Progress in Polymer Science **32**, 1152–1204 (2007).

[10]H. Hu, M. Gopinadhan, and C. O. Osuji, "Directed self-assembly of block copolymers: a tutorial review of strategies for enabling nanotechnology with soft matter.", Soft matter **10**, 3867–89 (2014).

[11]H.-C. Kim, S.-M. Park, and W. D. Hinsberg, "Block copolymer based nanostructures: materials, processes, and applications to electronics.", Chemical reviews **110**, 146–77 (2010).

[12]M. P. Stoykovich, and P. F. Nealey, "Block copolymers and conventional lithography", Materials Today **9**, 20–29 (2006).

[13]L. Persano, A. Camposeo, and D. Pisignano, "Integrated bottom-up and top-down soft lithographies and microfabrication approaches to multifunctional polymers", Journal of Materials Chemistry C **1**, 7663 (2013).

[14]H. Tsai, J. W. Pitera, H. Miyazoe, S. Bangsaruntip, S. U. Engelmann, C.-C. Liu, J. Y. Cheng, J. J. Bucchignano, D. P. Klaus, E. A. Joseph, D. P. Sanders, M. E. Colburn, and M. A. Guillorn, "Two-Dimensional Pattern Formation Using Graphoepitaxy of PS- b -PMMA Block Copolymers for Advanced FinFET Device and Circuit Fabrication", ACS Nano **8**, 5227–5232 (2014).

CHAPTER 1

Block Copolymers

1.1 From Polymers to Block Copolymers

Polymers are macromolecules constituted by a large number of molecular units (monomers) that are covalently bonded together. In most cases they display a flexible backbone set-up of carbon atoms[1] and they usually represent organic compounds, containing carbon atoms together with hydrogen, oxygen, nitrogen, and halogens, etc. Figure 1.1 reports the typical example of Polystyrene (PS) in which phenyl groups appear as sidegroups of the C-C backbone chain.

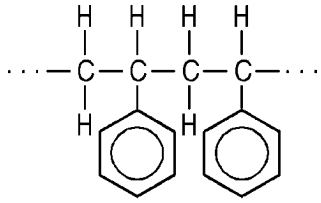

Figure 1.1: Chemical composition of PS.

These macromolecules are synthesized through a polymerization process which starts from reactive low molar mass compounds. Along the polymeric chain the monomers could be easily identified and their number determines the degree of polymerization N. Polymerization does not bring to a unique N value, but a mixture of macromolecules with various molar masses rises.
Following the procedure highlighted by G. Strobl in his ``The Physics of Polymers´´[1], we call M the molar mass and $p(M)$ the distribution function normalized with:

$$\int_0^\infty p(M)dM = 1. \tag{1.1}$$

The average molar mass thus results from:

$$\overline{M}_n = \int_0^\infty p(M)MdM. \tag{1.2}$$

[1]It is worth to note that the backbone chain could be formed even by silicon atoms, together with other elements (as in the case of poly(dimethylsiloxan)).

Because of the common high degree of polymerization, we address M as a continuos variable rather than as a discrete monomeric value. Alternatively to the number average of eq.1.2, the weight average of the molar mass may be defined as:

$$\overline{M}_w = \frac{\int_0^\infty p(M)M \cdot MdM}{\int_0^\infty p(M)MdM}. \tag{1.3}$$

When the molar mass distribution has a finite width, $\overline{M}_w$ is larger then $\overline{M}_n$ and the width of the distribution is evaluated by means of the polydispesity (PDI) defined as:

$$PDI = \frac{\overline{M}_w}{\overline{M}_n} - 1, \tag{1.4}$$

or as

$$PDI = \frac{\langle \Delta M^2 \rangle}{\overline{M}^2{}_n}, \tag{1.5}$$

with $\langle \Delta M^2 \rangle = \overline{M}_w \cdot \overline{M}_n - \overline{M}^2{}_w$, when it is directly related to the variance of $p(M)$ [1]. This parameter goes to zero only for a sample with a uniform molar mass (monodisperse). The molar mass distributions can be very different for different polymeric compounds and they are affected by the method of synthesis used in the polymerization process[2].

When the polymerization process involves a combination of different monomers a copolymer gets formed. A particular class of copolymers is represented by Block Copolymers (BCPs). These macromolecules are produced by covalently bonding two (diblock) or more chemically distinct polymer blocks. Each block is homogeneously constituted by a series of identical monomers.
Many different architectures can be classified basing on the number of chemically distinct blocks and on the kind of sequencing (linear or branched [2]). Nevertheless the most simple and studied configuration is the linear AB diblock structure sketched in figure 1.2.

Figure 1.2: Example of a diblock copolymer chain displaying two different blocks of the monomeric components A, B.

Adding further A, B blocks to the chain reported in figure 1.2, $(AB)_n$ multiblocks get formed, while introducing another type of monomer, an ABC triblock is produced with linear or branched structures, depending on the specific arrangement of the different blocks.
Beacuse of the different chemical properties of the distinct blocks it could be energetycally convenient to reduce the contacts between dissimilar monomers through a phase

[2]For example a condensation process, which proceeds by coupling groups of already linked monomers, brings to a broad molar mass distribution. Conversely a chain polymerization in which a reactive center (ion or reactive substance with one unpaired electron) reacts only with monomers and progressively shifts to the end of the chain, forms a narrower molar mass distribution.

separation. This develop of separated phases from a copolymer melt is a self-assembly process that presents interesting properties of order which could be fruitfully applied for lithographyc scope.[3].

In this thesis only diblock copolymers (diBCPs) were used, for this reason in the following sections we limit our considerations to their simple configurations.

1.2 Phase Separation and Different Morphologies

The self-assembly (SA) process corresponds to the spontaneous organization of a system in which the components form regular structures that correspond to a minimum in the free energy. For a BCP system, this process is represented by a counterbalance between the repulsive interaction given by the chemical immiscibility between the different blocks, and the attractive interaction constituted by the covalent bond between them.[4] Figure 1.3 [5] helps in delineating the influence of these contributions in the SA of a symmetric diBCP i.e. with equal numbers of monomers of the two species, which orders into a lamellar configuration. In passing from the disordered (fig. 1.3 a) to the ordered state (fig. 1.3 b), the monomeric contacts between the two species are reduced due to the stretching of the chains which lowers the number of accessible configurations and generates an entropic force that limits in turn the scale of phase separation due to the covalent bond between the blocks in a chain. The result of these contributions is the formation of an ordered lamellar phase with domains built up by a single species, alternating on a characteristic period L_0.

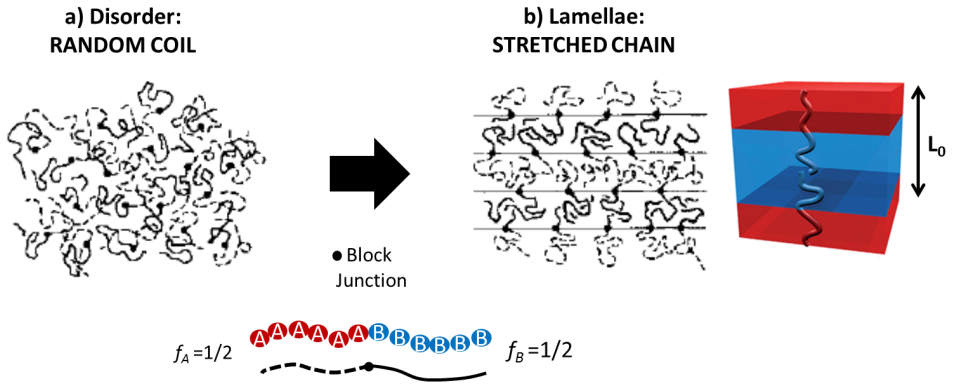

Figure 1.3: a) Disordered state of symmetric BCPs in their random coil configuration. b) Ordered state after BCPs self-assembly into a lamellar architechture.

In order to understand the main parameters that govern the phase separation process of BCPs in bulk configuration, we go through the details of the free energy terms for the simple case of symmetric AB diBCP, in the disordered and ordered states.
The free energy contribution per chain, related to the disordered state in which A and B

blocks are homogeneously mixed, can be approximated by the A-B contact energy alone [2]:

$$\frac{F_{dis}}{k_BT} \approx \chi_{AB} f_A f_B N = \frac{\chi_{AB} N}{4} \tag{1.6}$$

where f_A is the relative fraction of A monomers, N is the degree of polymerization and χ_{AB} is the so called Flory-Huggyns parameter.
The Flory-Huggyns interaction parameter represents the free energy cost per monomer of contacts between A e B monomers, as illustrated in the formula:

$$\chi_{AB} = \frac{Z}{k_BT}\Big[\varepsilon_{AB} - \frac{1}{2}(\varepsilon_{AA} + \varepsilon_{BB})\Big] \tag{1.7}$$

in which Z is the number of nearest neighbor monomers to a copolymer configuration cell and ε_{AB} is the interaction energy per monomer between A and B monomers.
If $\chi_{AB} < 0$, the free energy drives to the mixing. Conversely for $\chi_{AB} > 0$ a net repulsion between A and B takes place. It is worth to note that χ_{AB} is inversely proportional to the temperature T. That means that rising the temperature the mixing is favoured.
For a symmetric diBCP $f_A = N_A/N = f_B = 1/2$ (see figure 1.3).
The length of the chains is a very important parameter, a small chemical incompatibility on the monomeric scale could indeed generate a strong repulsion when considering large N. Besides, the mobility of the chain is also determined by its length.

In the ordered lamellar state, the free energy contribution is given by:

$$\frac{F_{lam}}{k_BT} = 3\left(\frac{L_0}{2}\right)^2 \frac{1}{2Na^2} + \frac{\gamma_{AB}}{k_BT}\Sigma. \tag{1.8}$$

The first term in eq.1.8 is approximately Hookian and it represents the stretching energy for a chain of N monomers to extend a half-period ($L_0/2$) in the lamellar phase [2]. a indicates the monomer size scale.
The second term describes the interaction energy confined at the narrow interface between A and B microdomains through the product of the A-B interfacial tension (γ_{AB}) and the interfacial area per chain (Σ).
By substituting $\gamma_{AB} = (k_BT/a^2)\sqrt{(\chi_{AB}/6)}$ and $\Sigma = (2Na^3)/L_0$ into eq.1.8, it is possible to proceed with the minimization of the equation in terms of L_0.
This procedure leads to [2]

$$F_{lam} \approx 1.19\big(\chi_{AB} N\big)^{1/3} \tag{1.9}$$

and to the dependence of L_0

$$L_0 \approx 1.03(\chi_{AB})^{1/6} N^{2/3}. \tag{1.10}$$

The free energy of the disordered state and of the ordered lamellar one match for $\chi_{AB}N \approx 10.4$ or more precisely due to a more accurate mean-field procedure proposed by Leibler [6], for $\chi_{AB}N \approx 10.5$. This value identifies the transition between the disordered and the ordered state for symmetric diBCP systems.
On the basis of this model a phase diagram for this fixed value of $f_A = f_B = 1/2$ is postulated, with different regimes depending on the value of the $\chi_{AB}N$ product [5]. This product indeed delineates the local composition profile (ϕ_A) of the diBCP system as depicted in the left panel of figure 1.4. When $\chi_{AB}N \ll 1$ a disordered copolymer

melt is formed and the A-B interactions are sufficiently weak that the individual chain maintains its Gaussian statistics [7]. For $\chi_{AB}N$ increasing to O(10) a Disorder-to-Order Transition (ODT) originates from the counterbalance between the contributions to the free energy. In this regime, called Weak Segregation Limit (WSL), the individual copolymers are still largely unperturbed, but an approximately sinusoidal composition profile for the ordered phase takes place. Finally, when $\chi_{AB}N \gg 10$ the phase behavior regime approaches the Strong Segregation Limit (SSL). In this case the interaction energy of A-B contacts is localized into the narrow [5] interfaces regions and the local composition profile appears as alternating nearly pure A and B microdomains.

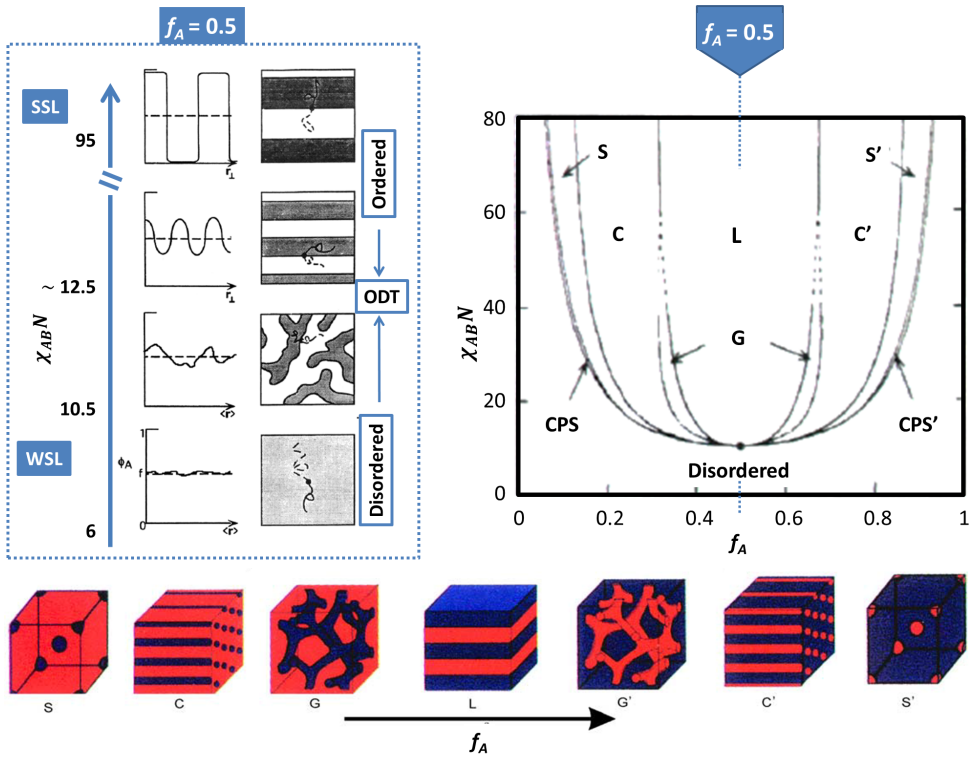

Figure 1.4: The phase diagram of AB-diBCP in a $\chi_{AB}N$ *vs.* f_A plane [2] is reported in the right picture. In the left panel the local composition profile ϕ_A for the fixed relative fraction f_A = 0.5 is investigated for increasing $\chi_{AB}N$ values [7]. The ODT transition with emerging lamellar morphology is highlighted. On the bottom the main morphologies of ordered diBCP as a function of f_A are illustrated. [2]

A more detailed description of the theory of BCPs phase separation has been addressed in the last decades by means of accurate self-consistent mean-field theories and many different computational approaches [6][8][9] [10][11][12].These theoretical models result in good agreement with experimental outcomes depending on the particular chosen regime of segregation for $\chi_{AB}N$. A deep illustration of these theories is far beyond the scoope of this thesis. In figure 1.4 we report the complete phase diagram picture for

diBCPs by considering the variation of the second fundamental parameter f_A.

For $\chi_{AB}N$ values higher than 10.5, varying the relative fraction f_A an ODT curve gets formed. Above this curve different microphase structures corresponding to different morphologies are present. With respect to f_A = 1/2, which gives rise to the lamellar phase (L), symmetric features get formed with the minority component structures embedded into a matrix made by the majority component. Considering the right half of the graph, B cylinders (C) appear as hexagonally packed into the A component for $f_A \sim$ 0.7. By increasing f_A up to 0.8 the B body-centered cubic spherical phase appears (S). Besides the above listed main morphologies (bottom of figure 1.4), regions of close-packed spheres (CPS) as well as perforated lamellae [13] and bicontinuos gyroid (G) phase were also detected.
For a given f_A value, in order to obtain smaller and smaller features, the choice of a BCP with the proper $\chi_{AB}N$ product is fundamental. In the straightforward example of symmetric AB diBPC eq.1.10 shows that the lamellar period changes with $(\chi_{AB})^{1/6}$ and $N^{2/3}$. Thus, considering the transition condition $(\chi_{AB}N)_{ODT} \approx 10.5$, it is possible to obtain $L_0 \gtrsim 5(\chi_{AB})^{-1/2}$. This evaluation allows for example for the fabrication of lamellar size ($L_0/2$) of 8, 5 and 2.5 nm for χ_{AB} of 0.1, 0.25 and 1 respectively (for the corresponding minimum values of N of 105, 42 and 11). [14] Considering the stronger dependence of L_0 on N than on χ_{AB}, the most efficient way to reduce the characteristic period seems to be the reduction of the degree of polymerization, while maintaing the product $\chi_{AB}N$ above the ODT limit.[15] Several polymers which fulfill the high-χ_{AB} low-N requirement are under study. This is the case of organic-inorganic BCPs such as the silicon based ones. [14] [16] In this contest polystyrene-*b*-polydimethylsiloxane (PS-*b*-PDMS), represents a promising candidate with a large χ_{AB} parameter of 0.11 (at 150°C [14]).

1.3 Block Copolymer Thin Films

For lithographic application the thin film configuration is preferred. In this case the above picture of BCPs bulk morphologies is strongly influenced by the energetic interactions at the interfaces and by the film thickness.[17] In particular the effects of the surfaces and interfaces on the final morphology of the thin film could lead to preferential wetting layers, film dewetting or unexpected film patterns.[4] In order to be suitable for lithographic applications, some prerequisites of an homogeneous BCP thin film have to be controlled: the film thickness (t), the orientation of the microdomains with respect to the substrate, their in plane order and alignment (lateral order) and their placement with respect to pre-existing features on the substrate (registration).
In the next paragraphs an overview of the main approaches that address each of these points is presented.

1.3.1 Effect of Film Thickness

The most common way to obtain a thin film of BCPs is the spin-coating of a solution of the diBCP in a good solvent, onto a substrate. The sample is then spun at a proper speed to allow the evaporation of most of the solvent. Besides the spin speed, at the end of this deposition process the thickness would be determined by the concentration of the

solution and the molecular weight of the polymeric component. At this point a thermal or solvent annealing is commonly applied in order to accelerate the microdomain organization of the BCP in the thin film.
Considering the common case of "soft" confinement , in which a free surface is left in direct contact with the atmosphere, the polymer domain spacing L_0 plays a fundamental role in the BCP pattern formation, especially when one of the two blocks preferentially wets the substrates giving rise to a parallel microdomains architecture with respect to the substrate. If an incommensurability between the film thickness t and the lattice spacing L_0 occurs, the film may be affected by the formation of islands or holes, whereas if the commensurability is preserved a homogeneous film gets formed.
For the lamellar forming AB diBCP, in the case of a symmetric wetting (with the same block wetting both the substrate and the free surface), the commensurability is given by t/L_0 = n (with n = 1, 2, 3...). Conversely for an anti-symmetric wetting a homogeneous coverage is obtain for t/L_0 = n + 0.5.[18] For more complex symmetries (different f_A in the starting BCP) proper commensurability conditions could be evaluated with the same principle of island/hole formation.[19] Moreover thin films, with $t < L_0$, exhibit more complicated ordering.[17]

1.3.2 Controlling the Orientation of BCPs Ordered Domains

The lithographic throughput requires the fabrication of high aspect ratio templates with low defectivity and sharp side walls for pattern transferring. These properties result mandatory in targeting the insertion of these self-assembled films in the fabrication processes of magnetic-storage media, quantum dots, and flash memory devices.[20][21] In this contest, the ability to tailor surface energies represents a fundamental step to manipulate the orientation of nanoscopic structures in thin BCPs films.[15][22][23][24]
When the BCP thin film is confined between substrate/polymer and air/polymer interfaces, the selective affinity of one block to either the substrate or the air-interface results in a parallel or perpendicular orientation of the microdomains within the polymeric film.[25][26][27][28] Figure 1.5 reports the different appearance of lamellar and cylinder forming BCPs thin films presenting parallel or perpendicular orientation with respect to the substrate.

Two of the basic elements of a lithographyc patterns, dots and stripes, can be produced in the underlying substrate by processing block copolymer thin films featuring spheres or parallel cylinder morphologies respectively. Unfortunately, these systems form intrinsically low-aspect-ratio structures and exhibit an exceedingly high defectivity due to through-film non-uniformity effects. In contrast, precisely controlled dot and stripe patterns are obtained from block copolymer thin films featuring cylinders and lamellae perpendicularly oriented [15] with respect to the underlying substrate. Therefore, the control of the domain orientation is essential for the technological application of these materials.
To achieve perpendicular orientation of the block copolymer features in thin films, a variety of distinct technological approaches [29] were introduced, including electric field alignment [30][31], solvent annealing [32], directed assembly on chemically patterned substrates [33][34], graphoepitaxy [35][36][37], and self- assembly on chemically neutral surfaces. [38][39][40][41][42][43]

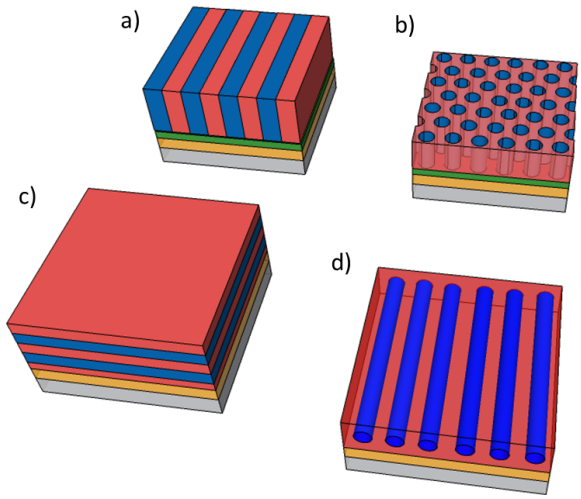

Figure 1.5: Examples of possible orientations of diblock copolymers patterns due to different interaction between BCPs and the substrate. The neutralization of the interaction at the surface brings to perpendicular orientation of either symmetric (a) or asymmetric (b) BCP patterns. On the contrary, preferential wetting of one of the two component of the BCP with the substrates gives rise to parallel lamellae (c) and cylinders (d).

In the self-assembly on chemically neutral surfaces, the perpendicular orientation can be achieved once non-preferential interactions are established at both the bottom and top interfaces [44] (see figure 1.5 a, b), whereas preferential wetting of the substrate by the block with the lower interfacial energy usually leads to parallel orientation of the block copolymer features in the domains (figure 1.5 c,d).
In this contest lot of studies about the neutralization of the substrates deal with the use of random copolymers (RCPs).[45][46] In a RCP system, the monomeric components appear in a completely random way and no patterned distributions are detectable along the polymeric chains (see figure 1.6). An amorphous and uniform coverage of the substrate with a RCP layer with the proper composition could prevent any preferential effect on the self-assembly process of a BCP overlayer.

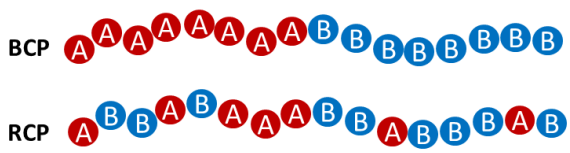

Figure 1.6: In a BCP, the block defining units repeat along the chain. In a RCP with the same polymeric components, the different monomers (A, B) do not follow any predetermined order and appear along the chain in a random way.

It was Mansky, with a seminal work in 1997 [38], to introduce the most versatile and robust strategy to control the BCP morphology orientation by means of RCPs. He firstly applied the "grafting to" approach, consisting of the chemical linking of a functional preformed (co)polymer to the substrate. He originally used a functional hydroxyl terminated poly(styrene-r-methylmethacrylate) (P(S-*r*-MMA)) random copolymer, reported in figure 1.7 for the neutralization of the interaction between an oxide substrate and a PS-*b*-PMMA BCP thin films.[3]

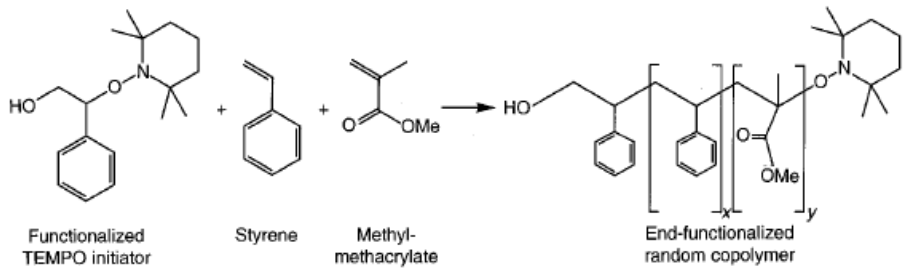

Figure 1.7: Original scheme of P(S-*r*-MMA) synthesized for the "grafting to" approach by Mansky *et al.* [38]. The OH functional group reacts with HO-Si sites of the substrate, while the polymerization initiator consists in tetramethylpiperidinyloxy (TEMPO) group.

In this case indeed the simple deposition of a PS-*b*-PMMA BCP thin film on an untreated surface would result in a parallel configuration of the ordered domains (figure 1.5).[17]. The affinity of the polar PMMA block for the hydrophilic oxide surface would lead to a preferential wetting of the substrate, while PS block would assemble at the air interface due to a lower surface energy.
The surface chemistry involved in the "grafting to" process, consists of the thermally activated reaction of HO–Si substrates with the hydroxyl groups of the functional RCP. For this reason the process is carried out at temperature well above the glass transition temperature (T_g) of the polymer. Once the unattached polymer chains have been removed by rinsing in toluene, a brush layer of a few nanometers remains grafted onto the substrate.
The final thickness of the brush layer is determined by the self-limiting nature of the ``grafting to'' reaction.[50][51] [52] When a grafted polymer layer covers the surface, the incoming chains have to diffuse against the concentration gradient formed by the already grafted chains. This diffusion process becomes progressively slower, because an increase in the grafted chains leads to a steeper gradient, this way highlighting a saturation limiting thickness for the brush layer.
The decoupling of the block copolymer from the polar silicon surface given by the brush layer is both physical and chemical. It was recently demonstrated [53] that the thickness of the RCP layer necessary to neutralize the surface interactions depends on the molar mass and the grafting density of the employed RCP. In particular, the minimum thickness required for an effective neutralization of the substrate progressively shifts towards higher values when increasing the M_n of the RCP, with a leveling off around 5–6 nm, corresponding to M_n values of approximately 10000–12000 g/mol. When the RCP-grafted

[3]This concept has been further developed as a kind of leitmotif, leading to a great variety of random copolymers bearing not only end-chain but also side-chain thermal- or photo-crosslinkable functional groups [47][48], and neutral layers for PS-*b*-PMMA can be deposited regardless of the chemistry of the underlying substrates.[49]

layer thickness is higher than 5–6 nm, then a spatial decoupling of the BCP film from the SiO_2 substrate occurs [38][49][53], resulting in an effective screening of the substrate, irrespective of the M_n value of the random copolymer used to generate the brush layer. When the minimum thickness requirement is fulfilled the orientation of the BCP nanodomains could be determined by the composition of the brush layer.
For a given BCP it is possible to determine and synthesized the RCP with the proper composition to balance the interfacial interactions at the substrates. In particular the best composition could be identified as the one that provided for the perpendicular orientation of the ordered domains on the largest window of thickness of the BCP overlayer. In the case of PS-*b*-PMMA, Ham *et al.* [26] identified the optimal styrene mole fraction of P(S-*r*-MMA) which allowed for the perpendicular orientation of given cylindrical and lamellar PS-*b*-PMMA (Styrene fraction of about 64% and 55% respectively). The proper styrene fraction appeared to be the one which brings to the more stable perpendicular configuration in a thickness (of BCP films) vs. styrene fraction (of RCP brush) diagram, as reported in figure 1.8 for a lamellar forming diBCP.

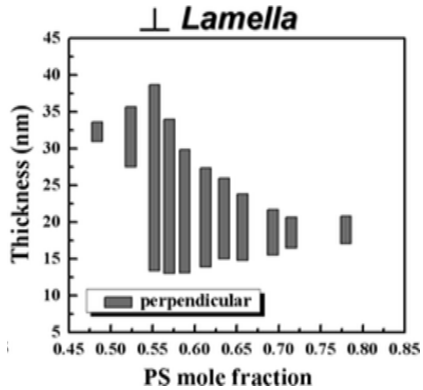

Figure 1.8: Results reported by Ham *et al.* [26] about the thickness window for the perpendicular microdomain orientation of a symmetric PS-b-PMMA (50000 g/mol) on different RCP substrates.

It is worth to note that the described procedure is relatively straightforward for thin films of thickness around the characteristic periodicity L_0, while a more general result should account for the thickness effects and needs for an accurate study of all the contributions to the free energy of the system including the one at the free surface, at the substrate, and at the interface between the different blocks.[54][48]

1.3.3 Lateral Order and Registration with the Substrate

The phase diagram depicted in the previous sections for the ordered BCPs morphologies, collects the possible configurations at the thermodynamic equilibrium. Actually when thin films of diBCPs are experimentally fabricated, they display a polycristalline morphologies with the occurrence of many defects, in contrast with the long-range order required by most of lithographic applications. Although the very early stages of

SA process are far from being controlled and understood[4], the formation of ordered morphologies, in the absence of external forces or constrains, seems to start at multiple nucleation sites giving rise to a polycristalline-patterns. Defects which disrupt the orientational and translational order, occur due to thermal fluctuations or to the formation of metastable states, depending on the segregation level of the system.[55] In this picture each ``crystal'' represents a grain, that means a region in which a uniform translational and orientational domain order is preserved.
The spontaneous SA process generates extremely defective patterns where grains are not clearly distinguishable. It is the case of the fingerprint morphology of striped pattern, obtained from perpendicular lamellae or parallel cylinders without guiding fields. An example of this kind of organization with the identification of several different defects is reported in figure 1.9. For more developed grain sizes, defects would concentrate at the

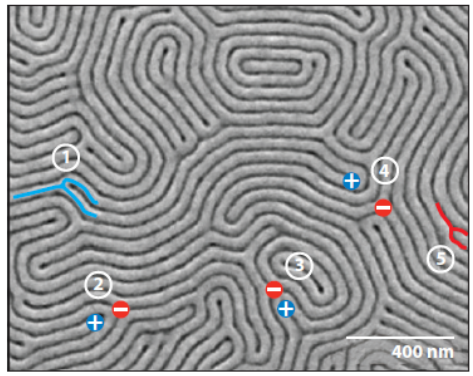

Figure 1.9: Image of a fingerprint morphology taken by Scanning Electron Microscope (SEM) for a PS-*b*-PMMA lamellar thin film.[55] The bright and dark structures correspond to PS and PMMA domains respectively. Different types of defects are indicated: 1) PMMA core dislocation; 2) disclination pair: +1/2 PS and -1/2 PMMA; 3) disclination pair: +1/2 PMMA and -1/2 PMMA; 4) disclination pair: +1/2 PMMA and -1/2 PS; and 5) PS-core dislocation. Blue and red lines illustrate the increase in the connectivity of PMMA and PS respectively. [56]

so called grain boundaries which separate grains with different orientations. Figure 1.10 reports the case of hexagonally packed perpendicular cylinders. The grain boundaries are delineated by the collection of dislocations composed by fivefold (-60° disclination) and sevenfold (+60° disclination) coordinate sites. The grain boundaries are easily detected in the software processed image in the right panel of figure 1.10.

The evolution of the lateral order of thin films morphology could be monitored through the grain coarsening process from small polycristalline structure up to single-grain-like pattern. The quantitative evaluation of the grain coarsening can be carried out within experiments of small angle X-rays scattering or neutron scattering. Such experiments provide the intensity scattered spectrum $I(\overrightarrow{q})$, where $\overrightarrow{q}$ is the scattering vector, and the correlation function of the sample $C(r)$, where $r = |\overrightarrow{r} - \overrightarrow{r'}|$ and $C(r)$ goes to 1 for r = 0

[4]The experimental study of the beginning of the phase separation process is everything but trivial. It requires a careful control of processing conditions which induce the ordering mechanism and then the ability to rapidly "freeze" it. One of the outcomes of this thesis is to provide an experimental procedure able to lead this kind of investigation.

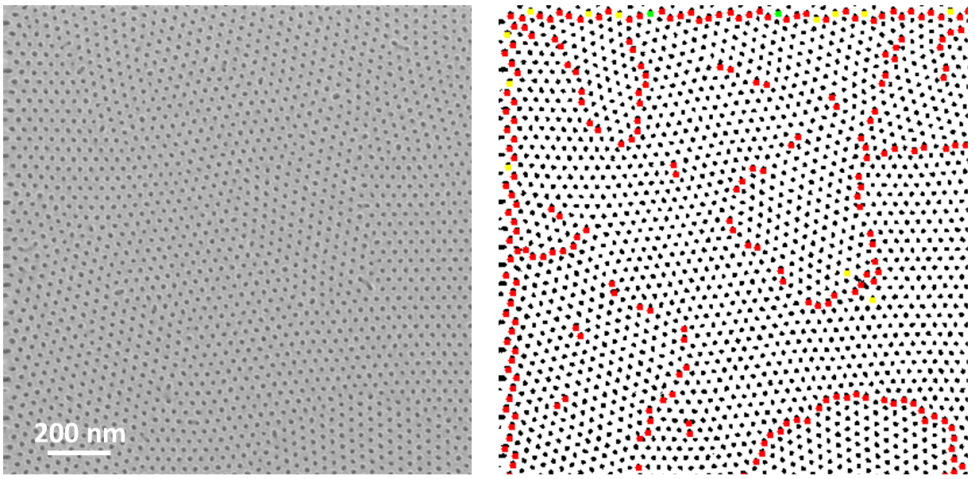

Figure 1.10: The left picture reports a SEM image of a cylindrical samples in which PMMA cylinders are ordered in an hexagonal pattern in a PS matrix. On the right the processed image reveals the presence of defects at the grain boundaries (color dots).

while it goes to 0 for $r \longrightarrow \infty$.
Nevertheless the same quantities could be estimated from TEM [57] or SEM images by means of specific analysis models.
A scalar measure of the local degree of order is given by the so called Correlation Length (ξ) [58], which is determined by the exponential fitting of the correlation function ($C(r) = exp(-r/\xi)$) and results proportional to the average separation distance between defects disrupting grain order[5]. [59]
A computational procedure for the extraction of ξ values, in the case of lamellar pattern, is described in details in the next chapter.
The study of the grain coarsening in thin films deposited on featureless substrate is fundamental in order to investigate the kinetics of ordering up to long-range ordered patterns. Starting from the spontaneous formation of domains the SA process of BCPs could be promote and fastened in order to yield the long-range order required. The most simple approach to promote the organization of the BCP layer into an ordered thin film, is thermal treatment above the T_g of the polymeric film. By raising up the temperature,[6] the polymer chains mobility is increased and the SA of ordered phases is boosted through the increase and melt of grains. The ordered configuration would be finally stable once the system is cooled down again below T_g.
With this procedure interesting results have been obtained in the definition of patterns with sub-20 nm features, with densities approaching 1 Tb/in^2, [61] [62], but the technological implementation is often precluded by the excessively long duration of the thermal treatments. Considering both the neutralization of the substrate with a RCP and the organization of BCPs layer, all the standard thermal procedures reported so far require annealing on a timescale in the range from 10^2 to 10^3 minutes. [63] [54]

[5]The grain size turns to be ξ^d where d is the dimension of the system.[58]

[6]It is worth to note that experimental results on one of the most studied diBCPs systems reveal only a weak dependence of χ_{AB} on the temperature: $\chi_{PS-PMMA} = (0.028 \pm 0.002) + (3.9 \pm 0.06)/T$.[60]

This crucial issue is specifically addressed in the ITRS along with the density of defects in the self-assembled polymeric templates. To be competitive with actual large-scale production lithographic techniques, the net time to form and fix the diBCP pattern must lie at around 240 s (see ITRS 2007 *Emerging Research Materials*). Unfortunately, scaling down the annealing time represents a drawback to the overall reduction of the defects, which is normally obtained by bringing the system slowly to an equilibrium stage in which the defects are energetically disadvantaged.
Another technique which boosts SA, while at the same time reporting promising results in terms of scaling down of the annealing time required by the diBCP thin film to self-organize, is solvent annealing.[64] [65] This treatment indeed allows the BCP organization to be obtained in less than 600 s at very low temperatures.[66] During a solvent annealing SA process, samples are exposed to solvent vapor. The solvent could be properly chosen in order to affect lot of diBCP films characteristics, depending on its selectivity for one block or the other.[18] For examples, the solvent changes the free surface preferentiality of the film biasing diBCPs orientation. By swelling the film, it also lowers the T_g and increases chains mobility while it modifies phase morphology by changing the relative volume fraction of the blocks.
These results can be further improved by introducing the microwave annealing process, as an extension of the solvent-driven process.[67] The main drawback of the aforementioned techniques is the complexity of the solvothermal setup. Moreover, the necessity to finely control all the process parameters like for instance pressure of the chamber, solvent temperature, sample temperature, etc., prevents a feasible application in VLS production.
Furthermore thermal and solvent annealing themselves are not sufficient for the fabrication of the long-range order required by lithographic applications. Though promoting grain coarsening on very large scale, a lot of defects still remain at grain boundaries. For this reason it is necessary to apply a Direct Self-Assembly (DSA) in which ¨external¨directional forces are employed to speed and stabilize the self assembly process of BCPs and to further guide their registration with pre-existing structures.
One of the possible forces involved in DSA, into the alignment of BCP domains, is represented by shear.
This method takes advantage on the differences in the mechanical properties and viscoelasticity of the different blocks. The final configuration depends on polymer (architecture, M_n, level of segregation) and processing (temperature proximity to T_g and T_{ODT}, timescale and amplitude of shear deformation) characteristics.[68] Figure 1.11 reports a scheme of different possible alignment due to different shear symmetries. The system would align by minimizing the chain mixing and the work done during shear flow. In this way the gradient of concentration between the microdomains results perpendicular to the shear velocity direction. Though better established for thick film configurations, shear alignment has been succesfully applied to thin BCP film in the last decade by applying shear through soft pads.[69] [70]
Another kind of procedure that takes advantage from an external field is the Electric Field Alignment. In this case the orientation mechanism rises from the difference in the electric permittivity (ε) of the block copolymer domains that result differently polarized when submitted to an electric field (e.g. $\varepsilon_{PS} \approx 2.4$ while $\varepsilon_{PMMA} \approx 3.6$). Lamellae and cylinders would align parallel to the electric field lines.[68]
A Magnetic Field Alignment could instead be used when dealing with an anisotropy in the magnetic susceptibility of the BCP system.

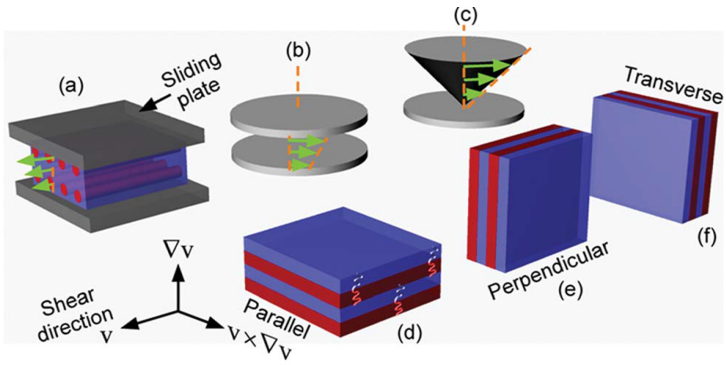

Figure 1.11: Examples of alignments of BCPs due to different shear geometries. a) Parallel cylinders aligned in the shear direction. Parallel b) and cones c) plates geometries. d) e) f) Possible lamellae configurations depending on the shear geometry applied. Adapted from [68].

Alignment of BCP domains were also obtained by driving order with a sharp temperature gradient in the so called Zone Annealing. This thermal gradient is strongly directional, depending on the particular setup employed, in contrast with the isotropic conventional thermal treatments. Recently very interesting results have been shown with Cold Zone Annealing (CZA, at temperature well below T_{ODT}) [71] and with its evolution in a Phototermal Gradient annealing.[72] These works suggest that this kind of gradients enhances the grains growth by acting on the activation energy of the ordering process.
Besides all these technological approaches, one of the most diffuse method for performing DSA, is represented by the pre-patterning of the substrates with chemical or topographical features combined with conventional or hot plate annealing. Notwithstanding a significant increment into the number of processing steps, these approaches give the main advantage of promoting at one time the orientation of the ordered domains, their long-range lateral order and their placement on the substrate.[73]
When chemical pre-patterned features are involved we talk about Chemoepitaxy.
This technique merges high-resolution lithographic patterning of a chemical surface layer, with the subsequent deposition and SA of a BCP material.
A simplified picture of this procedure is sketched in the left panel of figure 1.12. The ordering of self-assembled microdomains follows the underlying chemical template when the length scale of the latter is commensurable with the characteristic periodicity of the polymeric system.

The main benefit of this approach is the possibility to apply BCPs microdomains even to complex structures such as bends, junctions or isolated structures.[74]
Conversely an important drawback consists in the need of conventional photolithography for the definition of the chemical pattern on very small scale (near the BCP dimensions).
Topographically pre-patterned substrates are instead employed in a Graphoepitaxy process.[75] [76] This technique is based on the assumption that the topographic features would tend to nucleate the phase separation of BCPs, giving rise to microdomains with the orientation fixed along the topographic pattern direction. The self-assembled structures, in this way, would subdivide the large scale lithographic prepatterned features

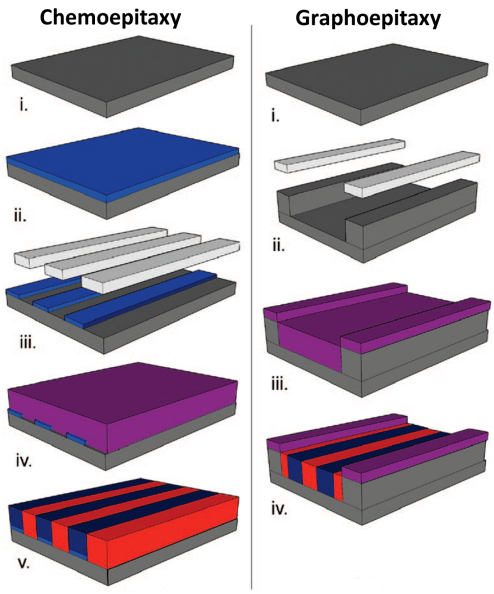

Figure 1.12: Schematic process flow of Chemoepitaxy (left panel) and Graphoepitaxy (right panel). In the Chemoepitaxy the substrate is coated with a chemical surface layer (ii), successively exposed to UV-light through a mask, and then chemical developed (iii). Finally the SA of a BCP layer takes place onto the chemical pattern (iv, v). Graphoepitaxy instead involves the lithographic patterning of topographic structures (ii) and the SA of the BCP film onto this pattern (iii, iv). Figure adapted from [73].

into sublithographic units, as briefly depicted in the right panel of figure 1.12.
Once the topographic structure has been delineated through lithography, the surface energy of both the bottom and the sidewall has to be carefully controlled. On one side if a non selective wetting is obtained for the bottom alone, a symmetric BCP forms a lamellar pattern parallel to the sidewalls. On the other, when non selectivity is assured for all the confinements, a symmetric BCP would form a lamellar pattern perpendicular to the sidewalls.[77]
The subdivision of larger topographic scale into smaller units is the main convenience of this technique which in turn lacks of easiness in addressing unconventional layout geometry.

1.4 Ordering Process in Symmetric BCPs

One of the most fundamental features in devices design, is the definition of striped patterns which could delineate for example the channel array elements of multinanowire transistor design.[78] [79] The characteristic dimension is defined by the period of the pattern that is the alternation of a line and a channel, named as pitch. The fabrication of striped patterns can be successfully accomplished using symmetric BCPs forming lamellar structures perpendicularly oriented to the surface or using asymmetric BCPs forming cylinder structures parallel to the substrate (see figure 1.5 a, d). Although the use of the latter system implies severe limitations in terms of inherently achievable aspect ratios and pattern transfer fidelity, during subsequent additive/subtractive nanofabrication steps, cylinder forming BCPs are preferred because of the fast grain coarsening revealing a rapid increment in the correlation length with time under conventional thermal treatments. [80] [81] Conversely, the main advantage of lamellar systems is related to the high achievable aspect ratio [82] that would make them very attractive for pattern transfer or sequential infiltration [83] [84] [85], once an efficient control is exerted on the evolution of the in plane lateral order over large areas.
Several studies in the literature reported about the achievement of high lateral ordered structure in asymmetric PS-*b*-PMMA resulting in large grains of parallel or perpendicular PMMA cylinders depending on the functionalization of the substrate. [86] [71] [72] The correlation length for cylinder-forming striped pattern has been reported to growth with a power low of the time of annealing: $\xi \sim t^{1/4}$ [80].
Conversely, topological constrains significantly reduce the molecular diffusion and inhibit the grain coarsening in lamellae forming BCPs, resulting in limited level of lateral order with significantly smaller growth exponents with respect to parallel cylinders.[59] Figure 1.13 reports a comparison between the growth of ξ as function of the time of annealing (t_{ann}) for thin films of parallel cylinders and perpendicular lamellae (with L_0 thickness) submitted to a thermal treatment. These data highlight the slower grain coarsening process of lamellar thin film.[81]
As previously suggested, coarsening in BCPs occurs via defects motion and annihilation that finally implies the diffusion of macromolecules. In microphase separated systems, molecular diffusion occurring along the microdomains (parallel diffusion) is favored over diffusion across the microdomains (hopping) because of the enthalpy barrier to block copolymer mixing, as illustrated in the figure 1.14.

The fast coarsening kinetics in cylindrical morphologies is strictly related to their par-

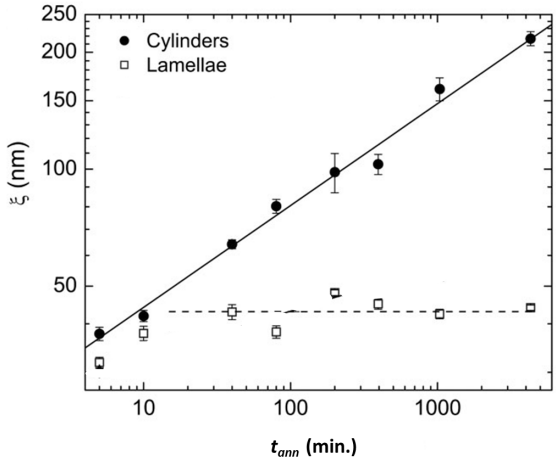

Figure 1.13: Correlation length values versus the annealing time for PS-*b*-PMMA thin films of parallel cylinders (full circles), and perpendicular lamellae (open squares), adapted from [81].

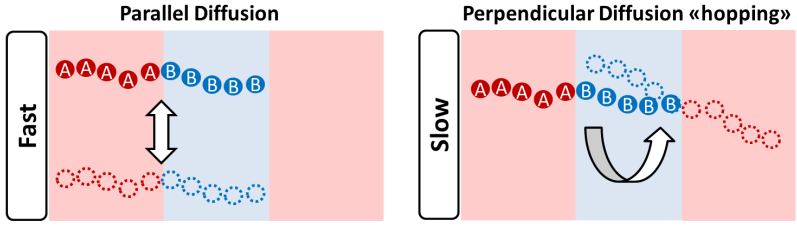

Figure 1.14: The left panel sketches the fast parallel diffusion of a symmetric diBCP along the lamellar domains. The right panel highlights the slow hopping diffusion process across different domains due to the enthalpy barrier to mixing.

ticular topology, since the matrix of the cylindrical phase provides a simple channel for layer breaking by molecular motion around the cylinder cores. In contrast, in lamellar morphologies, defect annihilation requires layer breaking with molecular diffusion across the microdomains, resulting in a high activation energy for the annihilation process and in a slow rate of pattern coarsening and ordering development. [87] The influence of this topological constrain was properly depicted by Ruiz *et al.* [59] as reported in figure 1.15.

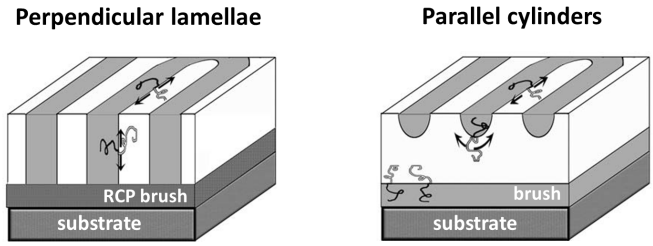

Figure 1.15: BCPs striped patterns fabricated by perpendicular lamellae or parallel cylinders. The arrows indicate the parallel diffusion of macromolecules for both the morphologies highlighting a higher freedom for molecular diffusion for the parallel cylinders embedded in a continuous matrix. Schemes were adapted from ref.[59].

Many approaches were proposed to increase the lateral order of perpendicularly oriented PS-*b*-PMMA lamellae in order to enable their industrial exploitation A reduced defect density was addressed through solvent annealing [56] while interesting results for the alignment of lamellar pattern on large areas were achieved by applying a shear stress through a moving pad [70] as well as by a thermal treatment on pre-patterned substrates. [88]
In this contest, the study and the investigation of the organization of symmetric diBCPs on featureless regions still represents a fundamental step into the comprehension of the ordering mechanism of these systems [80] [87] [89] and consequently into their implementation into existing lithographic process flow.[90] [67] Moreover, for some applications, the organization on featureless regions of the surface is required and a general route toward rapid ordering is fundamental. [91] [92] [93]
This thesis fits with this intense research activity [59] [81] [56], focusing on the ordering mechanism of symmetric diBCPs microdomains on unpatterned substrates, highlighting the particular interest for simple technological set up, such as thermal annealing, which would surely have feasible applications in semiconductor industry. Although conventional thermal treatments resulted generally inadequate to promote a high level of lateral order [59] in symmetric diBCPs, the technological route is still open. Very recently, for example, an efficient procedure to organize micro-sized grains of aligned lamellae by thermal annealing was identified by blending the PS-*b*-PMMA with short RCP chains.[94]

1.5 The choice of PS-*b*-PMMA

The framework just outlined highlights the main characteristics that a BCP thin film must fulfill in order to be suitable implemented into a lithography process flow, which is basically determined by the miniaturization process of devices size and by the increase of their density. Besides encoding the morphological characteristics of the pattern the BCPs also dictates the further processing steps for pattern transfer from polymers to the substrate. For this reason the choice of the proper BCP is fundamental.
Most of the known literature deals with the standard exemplar system of PS-*b*-PMMA ($\chi_{AB} \approx 0.03$ at 150°C [14]). It has been the work-horse in the field for many years and it is the best candidate for the implementation of BCPs systems into next generation lithography.
With respect to higher χ_{AB} BCPs, the self-assembly of PS-*b*-PMMA could be promoted within a simple thermal treatment and the perpendicular orientation of the ordered microdomains with respect to the substrate could be easily obtained. The surface interactions of the two blocks at the free surface indeed is balanced above a certain temperature threshold while any preferential interaction with the substrate could be neutralized by grafting a PS-*r*-PMMA brush layer.
Interesting results in terms of feature size reduction were obtained with PS-*b*-PMMA thin films by electric-field assisted thermal treatment (hexagonally packed cylinders of PMMA with characteristic diameters of about 14 nm [95]) and very recently with the experimental setup described later on in this thesis (hexagonally packed cylinders of PMMA with diameters of about 12 nm for Mn= 39000 g/mol [16]).
PS-*b*-PMMA provides for several advantages even in terms of pattern fabrication. Although PS-*b*-PMMA does not present a particularly enhanced etching resistance [84], PMMA domains can be easily removed using ultraviolet exposure and oxygen plasma (for a lamellar pattern), or ultraviolet exposure and oxygen plasma in combination with acetic acid treatment (for cylinders), leaving nanoporous PS film that can be used as soft mask for successive processes. [26] [96] [97] Furthermore PS-*b*-PMMA could be easily implemented into the standard lithographic process flow because of its similarities with the commonly employed photoresist materials. Finally in the last years PS-*b*-PMMA demonstrates its versatility into Sequential Infiltration Synthesis (SIS) which applies the principles of Atomic Layer Deposition technique to the issue of optimizing pattern transfer. This last consideration will be further considered in the conclusions and perspectives of this thesis.
For all these reasons the present study focuses on PS-*b*-PMMA $\sim L_0$ thick films deposited on PS-*r*-PMMA brush layers, working in a range of temperature (above 225°C) in which the interfacial interactions at the free surface of PS-*b*-PMMA are balanced.[98]

Bibliography

[1] G. R. Strobl, *The Physics of Polymers - Concepts for Understanding Their Structures and Behavior* (Springer, 1997).

[2] F. S. Bates, and G. H. Fredrickson, "Block Copolymers—Designer Soft Materials", Physics Today **52**, 32 (1999).

[3] D. J. Herr, "Directed block copolymer self-assembly for nanoelectronics fabrication", Journal of Materials Research **26**, 122–139 (2011).

[4] R. A. Farrell, T. G. Fitzgerald, D. Borah, J. D. Holmes, and M. A. Morris, "Chemical interactions and their role in the microphase separation of block copolymer thin films.", International journal of molecular sciences **10**, 3671–712 (2009).

[5] F. S. Bates, and G. H. Fredrickson, "Block copolymer thermodynamics: theory and experiment.", Annual review of physical chemistry **41**, 525–57 (1990).

[6] L. Leibler, "Theory of Microphase Separation in Block Copolymers", Macromolecules **13**, 1602–1617 (1980).

[7] J. H. Rosedale, F. S. Bates, K. Almdal, K. Mortensen, and G. D. Wignall, "Order and Disorder in Symmetric Diblock Copolymer Melts", Macromolecules **28**, 1429–1443 (1995).

[8] E. Helfand, and Z. R. Wasserman, "Block Copolymer Theory. 5. Spherical Domains", Macromolecules **11**, 960–966 (1978).

[9] A. N. Semenov, "Contribution to the theory of microphase layering in block-copolymer melts", Sov. Phys. JETP **61**, 733 (1985).

[10] M. W. Matsen, and F. S. Bates, "Unifying Weak- and Strong-Segregation Block Copolymer Theories", Macromolecules **29**, 1091–1098 (1996).

[11] M. W. Matsen, and M. Schick, "Stable and unstable phases of a diblock copolymer melt", Physical Review Letters **72**, 2660–2663 (1994).

[12] M. W. Matsen, and M. Schick, "Microphase Separation in Starblock Copolymer Melts", Macromolecules **27**, 6761–6767 (1994).

[13] S. Qi, and Z.-G. Wang, "On the Nature of the Perforated Layer Phase in Undiluted Diblock Copolymers", Macromolecules **30**, 4491–4497 (1997).

[14] C. Sinturel, F. S. Bates, and M. A. Hillmyer, "High χ-Low N Block Polymers: How Far Can We Go?", ACS Macro Letters, 1044–1050 (2015).

[15]K. Koo, H. Ahn, S.-W. Kim, D. Y. Ryu, and T. P. Russell, "Directed self-assembly of block copolymers in the extreme: guiding microdomains from the small to the large", Soft Matter **9**, 9059 (2013).

[16]G. Seguini, T. J. Giammaria, F. F. Lupi, K. Sparnacci, D. Antonioli, V. Gianotti, F. Vita, I. F. Placentino, J. Hilhorst, C. Ferrero, O. Francescangeli, M. Laus, and M. Perego, "Thermally induced self-assembly of cylindrical nanodomains in low molecular weight PS-b-PMMA thin films.", Nanotechnology **25**, 045301 (2014).

[17]H.-C. Kim, S.-M. Park, and W. D. Hinsberg, "Block copolymer based nanostructures: materials, processes, and applications to electronics.", Chemical reviews **110**, 146–77 (2010).

[18]J. N. Albert, and T. H. Epps, "Self-assembly of block copolymer thin films", Materials Today **13**, 24–33 (2010).

[19]R. A. Segalman, "Patterning with block copolymer thin films", Materials Science and Engineering: R: Reports **48**, 191–226 (2005).

[20]J. Bang, U. Jeong, D. Y. Ryu, T. P. Russell, and C. J. Hawker, "Block copolymer nanolithography: translation of molecular level control to nanoscale patterns.", Advanced materials **21**, 4769–92 (2009).

[21]M. Li, and C. K. Ober, "Block copolymer patterns and templates", Materials Today **9**, 30–39 (2006).

[22]I. Hamley, "Ordering in thin films of block copolymers: Fundamentals to potential applications", Progress in Polymer Science **34**, 1161–1210 (2009).

[23]S. E. Mastroianni, and T. H. Epps, "Interfacial manipulations: controlling nanoscale assembly in bulk, thin film, and solution block copolymer systems.", Langmuir **29**, 3864–78 (2013).

[24]S. Sakurai, "Progress in control of microdomain orientation in block copolymers – Efficiencies of various external fields", Polymer **49**, 2781–2796 (2008).

[25]E. Huang, S. Pruzinsky, T. P. Russell, J. Mays, and C. J. Hawker, "Neutrality Conditions for Block Copolymer Systems on Random Copolymer Brush Surfaces", Macromolecules **32**, 5299–5303 (1999).

[26]S. Ham, C. Shin, E. Kim, D. Y. Ryu, U. Jeong, T. P. Russell, and C. J. Hawker, "Microdomain Orientation of PS- b -PMMA by Controlled Interfacial Interactions", Macromolecules **41**, 6431–6437 (2008).

[27]E. Kim, S. Choi, R. Guo, D. Y. Ryu, C. J. Hawker, and T. P. Russell, "Transition behavior of PS-b-PMMA films on the balanced interfacial interactions", Polymer **51**, 6313–6318 (2010).

[28]C. M. Bates, T. Seshimo, M. J. Maher, W. J. Durand, J. D. Cushen, L. M. Dean, G. Blachut, C. J. Ellison, and C. G. Willson, "Polarity-switching top coats enable orientation of sub-10-nm block copolymer domains.", Science **338**, 775–9 (2012).

[29]M. Luo, and I. Thomas H. Epps, "Directed Block Copolymer Thin Film Self-Assembly: Emerging Trends in Nanopattern Fabrication", Macromolecules, 7567 (2013).

[30]T. L. Morkved, M. Lu, A. M. Urbas, E. E. Ehrichs, H. M. Jaeger, P. Mansky, and T. P. Russell, "Local Control of Microdomain Orientation in Diblock Copolymer Thin Films with Electric Fields", Science **273**, 931–933 (1996).

[31]H. Xiang, Y. Lin, and T. P. Russell, "Electrically Induced Patterning in Block Copolymer Films", Macromolecules **37**, 5358–5363 (2004).

[32]C. Sinturel, M. Vayer, M. Morris, and M. A. Hillmyer, "Solvent Vapor Annealing of Block Polymer Thin Films", Macromolecules **46**, 5399–5415 (2013).

[33]S. O. Kim, H. H. Solak, M. P. Stoykovich, N. J. Ferrier, J. J. De Pablo, and P. F. Nealey, "Epitaxial self-assembly of block copolymers on lithographically defined nanopatterned substrates.", Nature **424**, 411–4 (2003).

[34]E. Han, I. In, S.-M. Park, Y.-H. La, Y. Wang, P. F. Nealey, and P. Gopalan, "Photopatternable Imaging Layers for Controlling Block Copolymer Microdomain Orientation", Advanced Materials **19**, 4448–4452 (2007).

[35]J. Y. Cheng, A. M. Mayes, and C. A. Ross, "Nanostructure engineering by templated self-assembly of block copolymers.", Nature materials **3**, 823–8 (2004).

[36]I. Bita, J. K. W. Yang, Y. S. Jung, C. A. Ross, E. L. Thomas, and K. K. Berggren, "Graphoepitaxy of self-assembled block copolymers on two-dimensional periodic patterned templates.", Science **321**, 939–43 (2008).

[37]S. Park, D. H. Lee, J. Xu, B. Kim, S. W. Hong, U. Jeong, T. Xu, and T. P. Russell, "Macroscopic 10-terabit-per-square-inch arrays from block copolymers with lateral order.", Science **323**, 1030–3 (2009).

[38]P. Mansky, Y. Liu, E. Huang, T. P. Russell, and C. Hawker, "Controlling Polymer-Surface Interactions with Random Copolymer Brushes", Science **275**, 1458–1460 (1997).

[39]R. D. Peters, X. M. Yang, T. K. Kim, B. H. Sohn, and P. F. Nealey, "Using Self-Assembled Monolayers Exposed to X-rays To Control the Wetting Behavior of Thin Films of Diblock Copolymers", Langmuir **16**, 4625–4631 (2000).

[40]D. Y. Ryu, K. Shin, E. Drockenmuller, C. J. Hawker, and T. P. Russell, "A generalized approach to the modification of solid surfaces.", Science **308**, 236–9 (2005).

[41]S. Ji, G. Liu, F. Zheng, G. S. W. Craig, F. J. Himpsel, and P. F. Nealey, "Preparation of Neutral Wetting Brushes for Block Copolymer Films from Homopolymer Blends", Advanced Materials **20**, 3054–3060 (2008).

[42]M.-S. She, T.-Y. Lo, and R.-M. Ho, "Long-range ordering of block copolymer cylinders driven by combining thermal annealing and substrate functionalization.", ACS nano **7**, 2000–11 (2013).

[43]C. M. Bates, J. R. Strahan, L. J. Santos, B. K. Mueller, B. O. Bamgbade, J. A. Lee, J. M. Katzenstein, C. J. Ellison, and C. G. Willson, "Polymeric Cross-Linked Surface Treatments for Controlling Block Copolymer Orientation in Thin Films", Langmuir **27**, 2000–2006 (2011).

[44]G. T. Pickett, T. A. Witten, and S. R. Nagel, "Equilibrium surface orientation of lamellae", Macromolecules **26**, 3194–3199 (1993).

[45]D. G. Walton, G. J. Kellogg, A. M. Mayes, P. Lambooy, and T. P. Russell, "A Free Energy Model for Confined Diblock Copolymers", Macromolecules **27**, 6225–6228 (1994).

[46]G. J. Kellogg, D. G. Walton, A. M. Mayes, P. Lambooy, T. P. Russell, P. D. Gallagher, and S. K. Satija, "Observed Surface Energy Effects in Confined Diblock Copolymers", Physical Review Letters **76**, 2503–2506 (1996).

[47]S. Ji, C.-C. Liu, J. G. Son, K. Gotrik, G. S. W. Craig, P. Gopalan, F. J. Himpsel, K. Char, and P. F. Nealey, "Generalization of the Use of Random Copolymers To Control the Wetting Behavior of Block Copolymer Films", Macromolecules **41**, 9098–9103 (2008).

[48]E. Han, K. O. Stuen, M. Leolukman, C.-C. Liu, P. F. Nealey, and P. Gopalan, "Perpendicular Orientation of Domains in Cylinder-Forming Block Copolymer Thick Films by Controlled Interfacial Interactions", Macromolecules **42**, 4896–4901 (2009).

[49]E. Han, and P. Gopalan, "Cross-Linked Random Copolymer Mats As Ultrathin Nonpreferential Layers for Block Copolymer Self-Assembly", Langmuir **26**, 1311–1315 (2010).

[50]S. T. Milner, T. A. Witten, and M. E. Cates, "Theory of the grafted polymer brush", Macromolecules **21**, 2610–2619 (1988).

[51]A. Kopf, J. Baschnagel, J. Wittmer, and K. Binder, "On the Adsorption Process in Polymer Brushes: A Monte Carlo Study", Macromolecules **29**, 1433–1441 (1996).

[52]B. Zhao, and W. Brittain, "Polymer brushes: surface-immobilized macromolecules", Progress in Polymer Science **25**, 677–710 (2000).

[53]K. Sparnacci, D. Antonioli, V. Gianotti, M. Laus, F. F. Lupi, T. J. Giammaria, G. Seguini, and M. Perego, "Ultrathin random copolymer-grafted layers for block copolymer self-assembly.", ACS applied materials & interfaces **7**, 10944–51 (2015).

[54]E. Han, K. O. Stuen, Y.-H. La, P. F. Nealey, and P. Gopalan, "Effect of Composition of Substrate-Modifying Random Copolymers on the Orientation of Symmetric and Asymmetric Diblock Copolymer Domains", Macromolecules **41**, 9090–9097 (2008).

[55]W. Li, and M. Müller, "Defects in the Self-Assembly of Block Copolymers and Their Relevance for Directed Self-Assembly.", Annual review of chemical and biomolecular engineering **6**, 187–216 (2015).

[56]I. P. Campbell, C. He, and M. P. Stoykovich, "Topologically Distinct Lamellar Block Copolymer Morphologies Formed by Solvent and Thermal Annealing", ACS Macro Letters **2**, 918–923 (2013).

[57]B. A. Garetz, N. P. Balsara, H. J. Dai, Z. Wang, M. C. Newstein, and B. Majumdar, "Orientation Correlations in Lamellar Block Copolymers", Macromolecules **29**, 4675–4679 (1996).

[58]C. Harrison, P. M. Chaikin, D. A. Huse, R. A. Register, D. H. Adamson, A. Daniel, E. Huang, P. Mansky, T. P. Russell, C. J. Hawker, D. A. Egolf, I. V. Melnikov, and E. Bodenschatz, "Reducing Substrate Pinning of Block Copolymer Microdomains with a Buffer Layer of Polymer Brushes", Macromolecules **33**, 857–865 (2000).

[59]R. Ruiz, J. K. Bosworth, and C. T. Black, "Effect of structural anisotropy on the coarsening kinetics of diblock copolymer striped patterns", Physical Review B **77**, 054204 (2008).

[60]T. P. Russell, R. P. Hjelm, and P. A. Seeger, "Temperature dependence of the interaction parameter of polystyrene and poly(methyl methacrylate)", Macromolecules **23**, 890–893 (1990).

[61]X. Yang, L. Wan, S. Xiao, Y. Xu, and D. K. Weller, "Directed Block Copolymer Assembly versus Electron Beam Lithography for Bit-Patterned Media with Areal Density of 1 Terabit/inch(2) and Beyond.", ACS nano **3**, 1844–58 (2009).

[62]R. Ruiz, H. Kang, F. A. Detcheverry, E. Dobisz, D. S. Kercher, T. R. Albrecht, J. J. de Pablo, and P. F. Nealey, "Density multiplication and improved lithography by directed block copolymer assembly.", Science **321**, 936–9 (2008).

[63]D. Y. Ryu, S. Ham, E. Kim, U. Jeong, C. J. Hawker, and T. P. Russell, "Cylindrical Microdomain Orientation of PS- b -PMMA on the Balanced Interfacial Interactions: Composition Effect of Block Copolymers", Macromolecules **42**, 4902–4906 (2009).

[64]K. W. Gotrik, A. F. Hannon, J. G. Son, B. Keller, A. Alexander-Katz, and C. A. Ross, "Morphology Control in Block Copolymer Films Using Mixed Solvent Vapors", ACS Nano **6**, 8052–8059 (2012).

[65]J. G. Son, J.-B. Chang, K. K. Berggren, and C. A. Ross, "Assembly of sub-10-nm block copolymer patterns with mixed morphology and period using electron irradiation and solvent annealing.", Nano letters **11**, 5079–84 (2011).

[66]J. Gong, H. Ahn, E. Kim, H. Lee, S. Park, M. Lee, S. Lee, T. Kim, E.-A. Kwak, and D. Y. Ryu, "Rapid structural reorganization in thin films of block copolymer self-assembly", Soft Matter **8**, 3570 (2012).

[67]X. Zhang, K. D. Harris, N. L. Y. Wu, J. N. Murphy, and J. M. Buriak, "Fast assembly of ordered block copolymer nanostructures through microwave annealing.", ACS nano **4**, 7021–9 (2010).

[68]H. Hu, M. Gopinadhan, and C. O. Osuji, "Directed self-assembly of block copolymers: a tutorial review of strategies for enabling nanotechnology with soft matter.", Soft matter **10**, 3867–89 (2014).

[69]D. E. Angelescu, J. H. Waller, R. A. Register, and P. M. Chaikin, "Shear-Induced Alignment in Thin Films of Spherical Nanodomains", Advanced Materials **17**, 1878–1881 (2005).

[70]S. Pujari, M. A. Keaton, P. M. Chaikin, and R. A. Register, "Alignment of perpendicular lamellae in block copolymer thin films by shearing", Soft Matter **8**, 5358 (2012).

[71]K. G. Yager, N. J. Fredin, X. Zhang, B. C. Berry, A. Karim, and R. L. Jones, "Evolution of block-copolymer order through a moving thermal zone", Soft Matter **6**, 92–99 (2010).

[72]P. W. Majewski, and K. G. Yager, "Millisecond Ordering of Block Copolymer Films via Photothermal Gradients.", ACS nano **9**, 3896–3906 (2015).

[73]C. T. Black, "Polymer self-assembly as a novel extension to optical lithography.", ACS nano **1**, 147–50 (2007).

[74]M. P. Stoykovich, H. Kang, K. C. Daoulas, G. Liu, C.-C. Liu, J. J. de Pablo, M. Müller, and P. F. Nealey, "Directed self-assembly of block copolymers for nanolithography: fabrication of isolated features and essential integrated circuit geometries.", ACS nano **1**, 168–75 (2007).

[75]R. Tiron, X. Chevalier, C. Couderc, J. Pradelles, J. Bustos, L. Pain, C. Navarro, S. Magnet, G. Fleury, and G. Hadziioannou, "Optimization of block copolymer self-assembly through graphoepitaxy: A defectivity study", Journal of Vacuum Science & Technology B: Microelectronics and Nanometer Structures **29**, 06F206 (2011).

[76]M. Maret, R. Tiron, X. Chevalier, P. Gergaud, A. Gharbi, C. Lapeyre, J. Pradelles, V. Jousseaume, G. Fleury, G. Hadziioannou, N. Boudet, and C. Navarro, "Probing Self-Assembly of Cylindrical Morphology Block Copolymer Using in Situ and ex Situ Grazing Incidence Small-Angle X-ray Scattering: The Attractive Case of Graphoepitaxy", Macromolecules **47**, 7221–7229 (2014).

[77]S.-M. Park, C. T. Rettner, J. W. Pitera, and H.-C. Kim, "Directed Self-Assembly of Lamellar Microdomains of Block Copolymers Using Topographic Guiding Patterns", Macromolecules **42**, 5895–5899 (2009).

[78]W. A. Lopes, and H. M. Jaeger, "Hierarchical self-assembly of metal nanostructures on diblock copolymer scaffolds.", Nature **414**, 735–8 (2001).

[79]T. Thurn-Albrecht, J. Schotter, G. A. Kastle, N. Emley, T. Shibauchi, L. Krusin-Elbaum, K. Guarini, C. T. Black, M. T. Tuominen, and T. P. Russell, "Ultrahigh-Density Nanowire Arrays Grown in Self-Assembled Diblock Copolymer Templates", Science **290**, 2126–2129 (2000).

[80]C. Harrison, D. H. Adamson, Z. Cheng, J. M. Sebastian, S. Sethuraman, D. A. Huse, R. A. Register, and P. M. Chaikin, "Mechanisms of Ordering in Striped Patterns", Science **290**, 1558–1560 (2000).

[81]R. Ruiz, R. L. Sandstrom, and C. T. Black, "Induced Orientational Order in Symmetric Diblock Copolymer Thin Films", Advanced Materials **19**, 587–591 (2007).

[82]S.-M. Park, M. P. Stoykovich, R. Ruiz, Y. Zhang, C. T. Black, and P. F. Nealey, "Directed Assembly of Lamellae- Forming Block Copolymers by Using Chemically and Topographically Patterned Substrates", Advanced Materials **19**, 607–611 (2007).

[83]J. Kamcev, D. S. Germack, D. Nykypanchuk, R. B. Grubbs, C.-Y. Nam, and C. T. Black, "Chemically enhancing block copolymers for block-selective synthesis of self-assembled metal oxide nanostructures.", ACS nano **7**, 339–46 (2013).

[84]Y.-C. Tseng, Q. Peng, L. E. Ocola, J. W. Elam, and S. B. Darling, "Enhanced Block Copolymer Lithography Using Sequential Infiltration Synthesis", The Journal of Physical Chemistry C **115**, 17725–17729 (2011).

[85]M. Ramanathan, Y.-C. Tseng, K. Ariga, and S. B. Darling, "Emerging trends in metal-containing block copolymers: synthesis, self-assembly, and nanomanufacturing applications", Journal of Materials Chemistry C **1**, 2080 (2013).

[86]S. Ji, C.-C. Liu, W. Liao, A. L. Fenske, G. S. W. Craig, and P. F. Nealey, "Domain Orientation and Grain Coarsening in Cylinder-Forming Poly(styrene- b -methyl methacrylate) Films", Macromolecules **44**, 4291–4300 (2011).

[87]C. Harrison, Z. Cheng, S. Sethuraman, D. A. Huse, P. M. Chaikin, D. A. Vega, J. M. Sebastian, R. A. Register, and D. H. Adamson, "Dynamics of pattern coarsening in a two-dimensional smectic system", Physical Review E **66**, 011706 (2002).

[88]A. M. Welander, H. Kang, K. O. Stuen, H. H. Solak, M. Müller, J. J. de Pablo, and P. F. Nealey, "Rapid Directed Assembly of Block Copolymer Films at Elevated Temperatures", Macromolecules **41**, 2759–2761 (2008).

[89]C. T. Black, and K. W. Guarini, "Structural evolution of cylindrical-phase diblock copolymer thin films", Journal of Polymer Science Part A: Polymer Chemistry **42**, 1970–1975 (2004).

[90]S. O. Kim, B. H. Kim, K. Kim, C. M. Koo, M. P. Stoykovich, P. F. Nealey, and H. H. Solak, "Defect Structure in Thin Films of a Lamellar Block Copolymer Self-Assembled on Neutral Homogeneous and Chemically Nanopatterned Surfaces", Macromolecules **39**, 5466–5470 (2006).

[91]C. K. Jeong, H. M. Jin, J.-H. Ahn, T. J. Park, H. G. Yoo, M. Koo, Y.-K. Choi, S. O. Kim, and K. J. Lee, "Electrical biomolecule detection using nanopatterned silicon via block copolymer lithography.", Small **10**, 337–43 (2014).

[92]J. Tang, H.-T. Wang, D. H. Lee, M. Fardy, Z. Huo, T. P. Russell, and P. Yang, "Holey silicon as an efficient thermoelectric material.", Nano letters **10**, 4279–83 (2010).

[93]C. Garozzo, C. Bongiorno, S. D. Franco, M. Italia, A. L. Magna, S. Scalese, P. M. Sberna, and R. A. Puglisi, "Nanofabrication processes for innovative nanohole-based solar cells", Physica status solidi (a) **210**, 1564–1570 (2013).

[94]B. H. Kim, S. J. Park, H. M. Jin, J. Y. Kim, S.-W. Son, M.-H. Kim, C. M. Koo, J. Shin, J. U. Kim, and S. O. Kim, "Anomalous Rapid Defect Annihilation in Self-Assembled Nanopatterns by Defect Melting", Nano Letters **15**, 1190–1196 (2015).

[95]T. Xu, H.-C. Kim, J. DeRouchey, C. Seney, C. Levesque, P. Martin, C. Stafford, and T. Russell, "The influence of molecular weight on nanoporous polymer films", Polymer **42**, 9091–9095 (2001).

[96]I. A. Zucchi, E. Poliani, and M. Perego, "Microdomain orientation dependence on thickness in thin films of cylinder-forming PS-b-PMMA.", Nanotechnology **21**, 185304 (2010).

[97]E. Han, H. Kang, C.-C. Liu, P. F. Nealey, and P. Gopalan, "Graphoepitaxial assembly of symmetric block copolymers on weakly preferential substrates.", Advanced materials (Deerfield Beach, Fla.) **22**, 4325–9 (2010).

[98]P. Mansky, T. P. Russell, C. J. Hawker, J. Mays, D. C. Cook, and S. K. Satija, "Interfacial Segregation in Disordered Block Copolymers: Effect of Tunable Surface Potentials", Physical Review Letters **79**, 237–240 (1997).

CHAPTER 2

Experimental Methods

2.1 Synthesis and Processing

The standard fabrication procedure to prepare nanostructured polymeric layer involves essentially two steps: substrate surface neutralization and diblock copolymer self-assembly. In the first step, the surface neutralization, i.e. the non preferential wettability of the substrate with respect to the blocks, can be obtained through a thermally induced grafting reaction of the substrate with OH-terminated RCP. The second step consists of the deposition of the BCP layer and subsequent annealing treatment to promote self-assembly of the investigated microphase separated morphology (the lamellar one in this thesis).
In this section the polymeric materials as well as the details of the process flow for BCP nanostructures self-assembly and the characteristic of the specific set ups used to treat these polymeric films are described.

2.1.1 Polymers

A α-hydroxyl ω-TEMPO functional RCP PS-*r*-PMMA with styrene fraction of XS = 0.58 (Mn = 11 400 g/mol, polydispersity index (PDI) = 1.64) and a symmetric BCP PS-*b*-PMMA with styrene fraction of XS = 0.50 (Mn = 51 000 g/mol and PDI = 1.06, PMMA syndiotactic-rich contents 78%) were purchased from Polymer Source Inc. and used as received without further purification.
The RCP and the BCP were marked as TR58 and B50, where R and B stand for random and block, respectively, T for TEMPO, and the number represents the percent styrene unit. The chemical structure of TR58 is reported in figure 2.1.

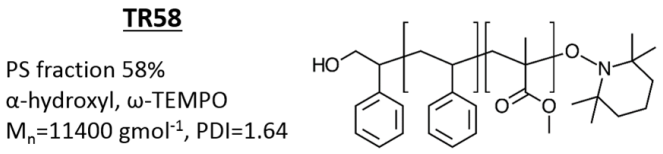

Figure 2.1: Chemical structure of TR58.

A second RCP was properly synthesized as follows. 2-Hydroxyethyl(2-bromoisobutyrate) (HEBIB), tris(2-(dimethylamino)ethyl)amine (Me6TREN), copper(II) bromide (CuBr2), tin(II)2-ethylhexanoate ($Sn(EH)_2$), and solvents were purchased from Aldrich and used

as received.
Styrene and methylmethacrylate were purchased from Aldrich and purified by passing through an inhibitor removal column (Aldrich) before use.
The α-hydroxyl ω-Br functional RCP BrR58 (Mn = 13 200 g/mol, PDI =1.36, XS = 0.58) was obtained by ARGET ATRP of styrene and methyl methacrylate initiated by HEBIB and catalyzed by $CuBr_2/Me_6TREN$ complex in the presence of $Sn(EH)_2$ as the reducing agent. In detail, 2.40 mg of $CuBr_2$ (10.3 μmol) and 2.8 μL of Me_6TREN (10.3 μmol) were dissolved in 6.0 mL of degassed anisole and transferred via degassed syringes to a dry Schlenk flask, purged by flushing with nitrogen. Then 8.0 mL of degassed styrene (69.7 mmol), 4.0 mL of degassed methyl methacrylate (37.4 mmol), and 80.0 μL of HEBIB (0.55 mmol) were added, and the mixture was degassed by three freeze-thaw cycles. Next, a purged solution of $Sn(EH)_2$ (84.0 μmol) and Me_6TREN (84.0 μmol) in degassed anisole (1.0 mL) was added, and the mixture was sealed under nitrogen. The polymerization was carried out at 90°C for 22 h, and then the reaction mixture was cooled to room temperature and diluted with tetrahydrofuran (THF, 5 mL). The copolymer was precipitated into methanol, washed with methanol, and purified by precipitation from THF solution into methanol. The copolymer composition was evaluated by ^1H NMR spectroscopy, and the styrene unit fraction resulted in XS = 0.58. The molar mass and first polydispersity index were determined by SEC and resulted in Mn = 13 200 g/mol and PDI = 1.36, respectively. The chemical structure of BrR58 is reported in figure 2.2.

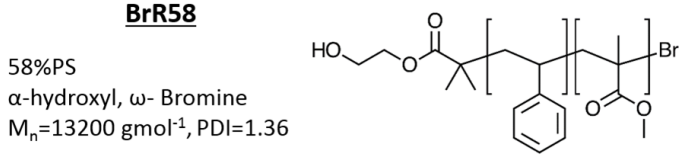

Figure 2.2: Chemical structure of BrR58.

2.1.2 Sample Preparation

The standard procedure followed in the preparation of the BCPs samples is briefly sketched in figure 2.3
a) All the samples were fabricated starting from (100) silicon substrates ($\approx$ 1 cm^2) covered with a thermal silicon dioxide layer[1] or with native oxide. In order to remove any organic residual and to increase the density of hydroxyl groups at the surface, the samples were treated in Piranha solution (H_2SO_4/H_2O_2 with 3/1 vol. ratio) at 80°C for 40 minutes. This step of the process is effective in reducing the water contact angle of the substrates from about 63.5° to 8°. Samples were then rinsed in H_2O, dried in N_2 flow, and then processed in an ultrasonic bath in 2-propanol.
b) A thin layer of RCP was deposited on the hydroxyl group rich-surface in order to neutralize the surface prior to BCP deposition. A solution of TR58 or BrR58 in toluene (18.0 mg in solution with 2.00 mL of toluene) was spin coated on the Si substrates for 30

[1]Layers of 100 nm or 50 nm of silicon dioxide were employed or, as an alternative, a 2 nm native oxide layer. The choice of the oxide between these, didn't cause any specific effect on the following deposition and organization of RCP or BCP layers.

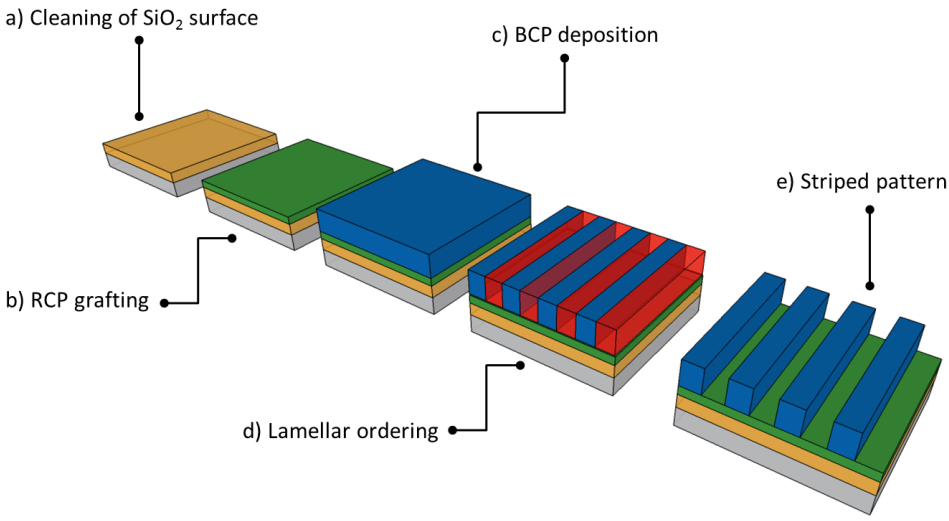

Figure 2.3: Process steps for the fabrication of BCPs striped patterns, starting from SiO_2 substrates.

s at 3000 rpm. The samples were then RTP treated for different time and temperature (as reported in detailed in the following chapters) in N_2 atmosphere to promote the grafting reaction. The non-grafted fraction was removed with an ultrasonic bath in toluene and the samples were dried again under N_2 flow.
c) About 25 nm thin films of B50 (in a solution of 16.0 mg of polymer in 2.00 mL of toluene) were then spin coated onto the grafted substrates (30 s at 3000 rpm).
d) Finally, to promote the organization of the BCP, the resulting samples were processed in RTP for different times and temperatures. To improve the contrast during the characterization of the sample by SEM, the PMMA phase was selectively degraded and removed, by exposure to UV radiation (5 mW·cm^{-2}, λ = 253.7 nm) for 15 minutes followed by processing in oxygen plasma for 60 s at 40 W.
e) The complete removal of the PMMA phase brings to the formation of a PS matrix for striped pattern transfer.

2.1.3 Rapid Thermal Process (RTP)

A Rapid Thermal Processing (RTP) machine is a standard semiconductor manufacturing equipment usually employed to rapidly heat samples to extremely high temperature for short processes. RTP was originally developed for dopant activation in ion implanted samples. The instrument is now used on a wide range of treatments such as oxidation, silicide formation, chemical vapor deposition, depending on the specific set up (e.g. a typical oxidation process is carried out in O_2 atmosphere, at 1200 °C, for about 10 minutes).[1].
The rapidity of the process is assured by the radiative power of halogen lamps which govern the heating transfer mechanism in RTP annealing. Figure 2.4 illustrates the open RTP lid, showing the set of halogen lamps used to heat the target sample. Figure 2.5

highlights the inner structure with halogen lamps, sample position and thermocouple control.

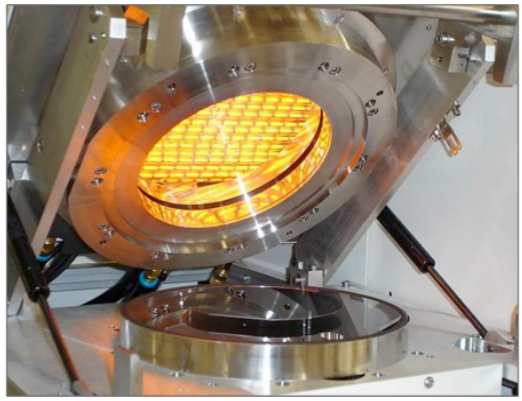

Figure 2.4: Open lid of a common RTP machine.

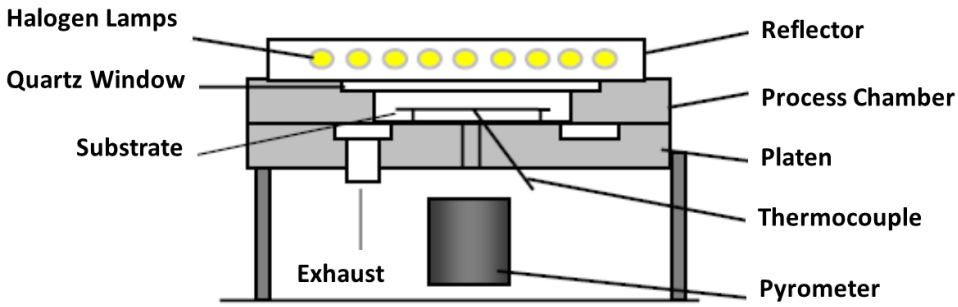

Figure 2.5: Inner structure of the heating chamber in a common RTP machine.

Two different kind of temperature control can be used to govern the feedback of lamp power: a non contact optical pyrometer (above 400°C) or a thermocouple (from room temperature and preferably at low temperature). By setting the RTP in its relatively low range of temperature (below the thermal degradation limit) under a N_2 flux, it is possible to adapt this technology to the process of polymeric samples.
There are two main advantages of this approach. The first one is the *in situ* monitoring of the temperature induced in the sample, during the entire treatment. This possibility is assured in the studied range of temperature, by the feedback control governed by a thermocouple connected to the sample[2].
The second one is the use of radiation sources to rapidly drive the polymeric film above the glass transition temperature (T_g), this way allowing for BCP ordering process.

[2]The constant monitoring of the temperature will play a fundamental role in the use of RTP to study the ordering mechanism on very short time of annealing, avoiding the loading and unloading temperature fluctuations commonly reported for other thermal treatments.[2]

Similarly to the standard thermal annealing performed with a furnace or hotplate, the annealing process in RTP is divided into three phases (see figure 2.6): (a) the heating ramp, (b) the isothermal step and (c) the cooling ramp.

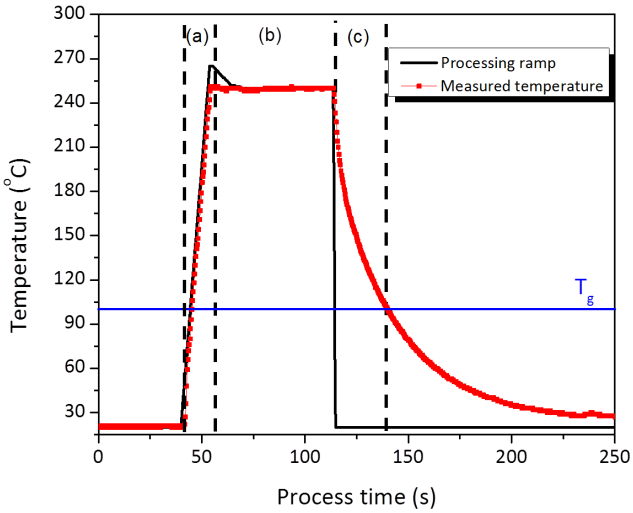

Figure 2.6: Scheme of a characteristic RTP annealing: (a) Heating ramp brings BCP above T_g. (b) A nominal overheating of halogen lamps allows the measured temperature to be kept constant for the duration of the chosen isothermal step. (c) The cooling ramp is influenced by the proper time of cooling of RTP.

The heating ramp (2.6 (a)) constitutes the very peculiar step of RTP in processing BCP. The heating rate (HR) at which the sample reaches the target temperature (T_{target}), that it will maintain for the successive isothermal step, is definitely faster than what reported for common furnace (up to 50°C/s according to the machine specifications, with respect to 3-5°C/min) and definitely more monitored than on a hot plate.
Most of the treatments performed in this thesis operates with HR = 18°C/s. This value enables a very fast heating ramp (it takes 6 s to get above the T_g) while avoiding any extreme stress to the thermocouple performance which would shorten its working life.
The isothermal step (2.6 (b)) is characterized by a plateau at the chosen T_{target}, hold for a determined time of annealing (t_{ann}). In order to adapt the use of RTP to thermal treatment characterized by a short plateau and a relatively low temperature compared to the common ones of semiconductor processes, it is necessary to set a slight overheating in the nominal temperature (black line in figure 2.6). This procedure forces the radiative power of halogen lamps making the measured temperature stable (red line in figure 2.6).
Finally a cooling ramp (2.6 (c)) brings the temperature experienced by the sample back to the room one (20°C for the clean-room environment in which the measures were carried out). The cooling rate is fixed by the refreshing process of the machine. Playing with the N_2 flux it is possible to gain a certain discretion on the refreshing time of RTP. By the way this choice is upper limited (a strong flux could involve a displacement in the samples position) and the main contribution to the recovery time of the machine remains a prerogative of the cooling flux of cold water around the halogen lamps chamber.

For this reason the same N_2 flux was used for all the treatments (1000 sccm which e.g. corresponds to about 20 s to bring the temperature back below T_g from 250°C), this way making the cooling ramp a constant contribution, once T_{target} has been defined.
Depending on the three steps of the process, it is possible to precisely control the time interval in which the samples remains above the polymeric T_g.
Nevertheless it is worth to note that, since the heating and the cooling ramp are the same for almost every process here reported, in the following, the grafting treatment of RCP as well as the ordering processes of BCP are labeled through the effective T_{target} and t_{ann} rather then through the less indicative complete process time (e.g. the RTP treatment sketched in figure 2.6 is considered as a 60 s long annealing, at 250°C). In chapter 4 the ordering process of BCP within RTP is systematically addressed on stressed annealing condition ranges. For this reason it will require a more physical insight into the motivation and justification of this point, with a detailed investigation of the effect that each single step of the RTP process would induce on the ordering mechanism.

All the samples were processed in a JIPELEC JetFirst 100 RTP system (more technical characteristics can be found at the link *thesemcogroup.com/rtp-rta*). For this kind of system the range of temperature for RTP treatments is between 200°C and 1300°C with possible heating rates of 20-200°C/s and a maximum power of lamps of about 30kW (our BCPs ordering process works at about the 20% of this power and the maximum investigated temperature was 350°C).

2.2 Characterization Techniques

2.2.1 Spectroscopic Ellipsometry

Spectroscopic Ellipsometry (SE) is a non-destructive and contactless technique for the optical investigation of the thickness and the optical properties of thin films, such as the optical constants, the composition, the roughness or the doping concentration.[3] It basically consists in the measure of a change in the amplitude ratio (Ψ) and phase difference (Δ) in the polarization, when light reflects or transmits from a material sample.
This technique owes its name to the most common polarization state, the elliptical one, that comes from the combination of orthogonal waves of arbitrary amplitude and phase. A common experimental setting, as the one employed in this thesis, is reported in figure 2.7. All the measures were carried out by a M-2000U spectroscopic ellipsometer (J. A. Wollam Co. Inc.) using a Xe lamp at 70° incident angle.

A lamp (right arm of figure 2.7) produces an unpolarized beam light which is sent through a polarizer. The originally linearly polarized light, becomes elliptically polarized in reflecting from the sample surface, and it travels through an analyzer constituted by another polarizer. Finally it comes to a detector (left arm of figure 2.7). The analyzer allows for passing only a certain amount of light which depends on the polarizer orientation with respect to the electric field ``ellipse´´arriving from the sample.
The plane of incidence is determined by the incident and the reflected beam. We talk about *s*-polarized and *p*-polarized light when it is polarized parallel or perpendicular to the plane of incidence respectively. The polarization state of the incident light can be described through its *s* and *p* components. After reflection, the polarization change of these components would be determined by the properties of the sample. The reflected

Figure 2.7: Example of experimental setting for a SE instrument (taken from *www.jawoollam.com*).

components (normalized to their initial values) are denoted as *Rs* and *Rp*, respectively. Their ratio describes the polarization change in the following equation [4]:

$$\rho = \frac{Rp}{Rs} = tan(\Psi)e^{i\Delta} \tag{2.1}$$

Due to the stringent relationship between the change in the polarization of the sample and the optical properties and thickness of the material under investigation, SE can be used to characterize single layers as well as complex multilayer stacks ranging from sub-nanometers to a few microns with an excellent accuracy.
However, the measured Ψ and Δ values in general cannot be converted directly into the optical constants of the sample. For this reason a model layer for data analysis must be established, which considers the optical constants and thickness parameters of all individual layers of the sample including the correct layer sequence. The sample is considered as a discrete number of defined layers that are homogeneous and isotropic. At this point a software proceeds by an iterative regressive method in varying the values of the unknown optical constants and/or thickness of the sample, in order to improve the agreement between calculation and experiment. In this way the values of Ψ and Δ which best match the experimental data are determined, providing the optical constants and thickness parameters of the sample. An estimation of the difference between the curves could be highlighted through the Mean Squared Error (MSE). The lower the MSE value appears, the better the agreement between the experimental and the model data is.
Many different models of data analysis could be employed in the determination of the thickness, depending on the particular material under investigation. Among them, the Cauchy layer which is commonly used for transparent or partially transparent films such as dielectrics, could be suitably implemented into block copolymer films analysis[3].
The thicknesses of both the RCP and BCP films were measured at each step of the fabrication process flow in which a polymeric layer was involved. A single Cauchy layer was adopted in evaluating the thickness of the BCP layer considered as an homogeneous layer with effective optical properties given from PS and PMMA contribution

[3]Considering the refractive index as the sum of a real contribution (n), and of an extinction coefficient (k), the Cauchy model provides $n(\lambda) = A + \frac{B}{\lambda^2} + \frac{C}{\lambda^4}$, where A, B, C are variable fit parameters that determine the index dispersion.

indistinctly[4].

2.2.2 Oxygen Plasma

Plasma treatments are commonly used in microelectronics to alter the surface of a sample by exposing it to a controlled vacuum plasma. In order to generate a plasma, a gas or mixture of gases are introduced inside a sealed, low-pressure vacuum plasma chamber. Then a ionization source (e.g. microwave) is applied on the gas atmosphere in the chamber. Due to the different gas employed, several different interactions between plasma components and the sample surface occur such as sputtering, adsorbtion, etc. The use of an oxygen plasma is widely diffused for photoresist ashing into the fabrication of integrated circuits. In this process the organic components of the sample are oxidised and reduced to ashes and then pumped-out by the vacuum system of the chamber.
A similar treatment can be properly adapted for PS-*b*-PMMA thin films treatment, at the end of a UV-exposition. UV light source degrades the PMMA molecular structure this way making it easily removable during an oxygen plasma treatment, while the PS chains result to be cross-linked.
All the samples in which a B50 layer was deposited and ordered, were processed in oxygen plasma for 60 s at 40 W at the end of a UV exposition. The indicated power and time of treatment are optimised to improve the contrast between the two phases, this way getting easier to take well-resolved SEM images of the lamellar pattern. Conversely, in order to completely remove the PMMA phase, more aggressive treatments are required. It is worth to note that the opening of the lamellar pattern is a very complex issue concerning the ability of pattern transfer, as will be addressed in the conclusions of this thesis. Nevertheless Oxygen Plasma revealed very useful for an in-depth investigation of our samples. By alternating successive plasma treatments, at the low 40 W power for constant time-steps, with a SEM top-view imaging of the samples, it is possible to collect a ``layer-by-layer'' analysis of the morphological organization of the BCP thin film across its whole thickness.

2.2.3 Scanning Electron Microsopy (SEM)

A Scanning Electron Microscopy (SEM) was used for the morphological characterization of the self-assembled BCP thin films.
The peculiar characteristics of SEM imaging process makes it suitable for the analysis of BCPs thin films. The concept at the base of SEM is the detection of the signal resulting from the interaction of a primary electron beam, which scans the surface of a sample with atoms at or near its surface. The interaction between the primary beam and the sample induces secondary products referred to an interaction volume called excitation bulb, as reported in figure 2.8.

The most common secondary electron imaging mode, can produce very high-resolution images with details smaller than 1 nm. The range of possible magnifications indeed is extremely wide from about 10 times (more or less equivalent to that of a powerful hand-lens) to more than 500000 times (which closes 250 times the magnification limit of the

[4]When the PMMA component is completely removed more detailed model could be employed, further considering the full/empty percentage in the polymeric film.

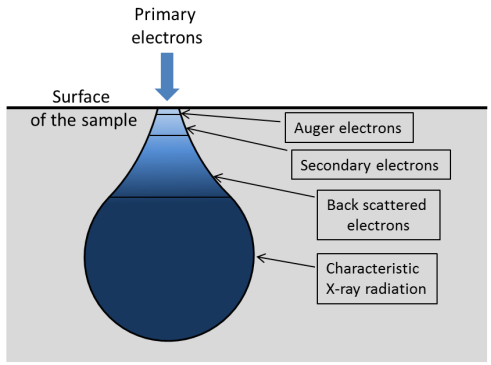

Figure 2.8: Excitation bulb scheme for an imaging process of SEM.

best light microscopes).
The secondary electrons have typically low energy value (< 50 eV). They are generated through inelastic scattering of the primary electrons on the atomic core or on the electrons of the atomic shell of the sample material. It is possible to subdivide the secondary electrons into three classes: SE1 generated in the spot centre, SE2 generated after multiple scattering (they leave the surface at greater distance from the spot centre) and SE3 generated by the back scattered electrons far away from the spot centre
The back scattered electrons are instead characterized by energy values higher than 50 eV and they are generated through elastic scattering in a deeper range of the interaction volume. Their information is strongly related to the atomic number of the material under investigation. For this reason they can provide information about the distribution of different elements in the sample.
When the electron beam removes an inner shell electron from the sample, causing a release of energy when a higher energy electron fills the shell, the characteristic X-rays radiation is emitted. These X-rays help in identifying the composition and the abundance of different elements in the sample.
A lot of information is thus available depending on the particular detection system used.

The SEM machine employed in this thesis was a Zeiss Supra 40 system as the one reported in figure 2.9.
It is a field emission (FE) SEM based on the highly performing Gemini® column, which guarantees high resolution imaging at the nanoscale, over the entire voltage range (from 20 eV up to 30 keV). The core of the electron optical setup is the accelerating column. It mainly consists of an emitter gun, condenser lenses, shutter, field lenses, aperture, projector lens, deflecting coils and secondary electron detector.
Once the primary electron beam scans the sample, in order to collect information relatively to the sample surface only SE1 and SE2 need to be detected. Indeed they are produced directly in or near the spot centre and they come from the surface part of the excitation bulb.
The detector which most suits this kind of analysis, and that we adopted in this thesis, is the In-lens one. The detection efficiency of this tool depends on its geometric position in the beam path and from the combination with the electrostatic/electromagnetic lens.

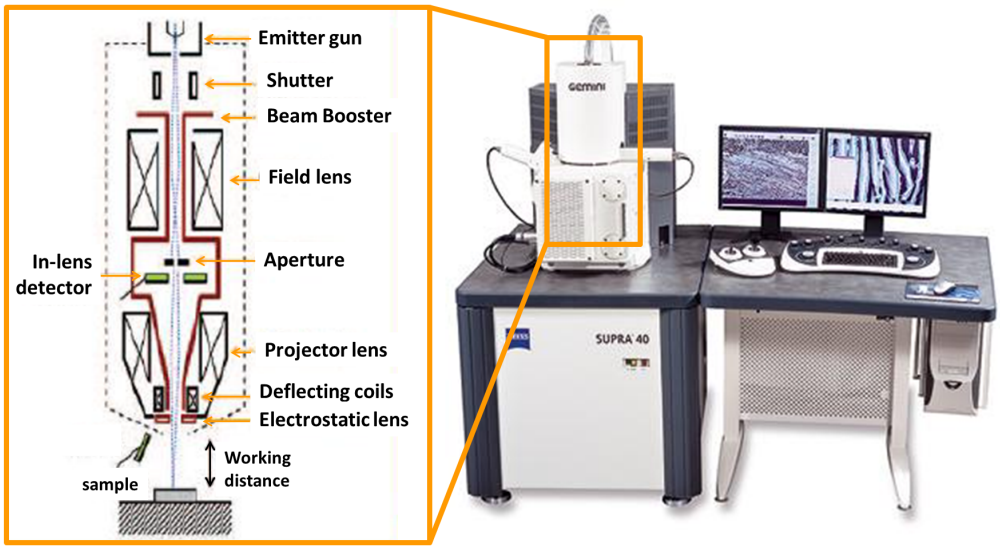

Figure 2.9: Supra 40 Gemini® FE-SEM. The left insert displays the inner structure of the accelerating column.

The configuration of the In-lens detector in the beam path is shown in figure 2.10.

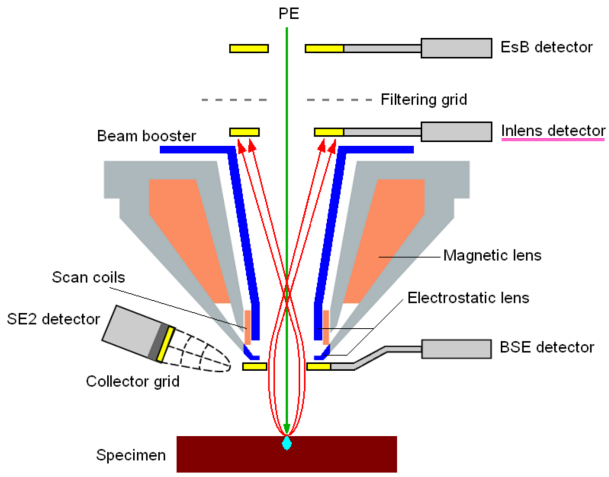

Figure 2.10: Configuration of different detectors in the SEM setup. The In-lens detector position is highlighted, in the beam path. The vacuum level in the sample chamber for this analysis is about 10^{-6} mbar.

2.2.4 Measurements of Thermal Stability and Determination of Solvent Content.

Thermogravimetric Analysis.
Thermogravimetric Analysis (TGA) were at the basis of the determination of the thermal stability of the polymeric samples involved in this thesis.
TGA is a method of thermal analysis in which the physical and chemical changes of the material properties are monitored as a function of increasing temperature at constant heating rate or, conversely, as a function of time at constant temperature. The thermal stability can be evaluated in terms of mass lost by the sample in varying the temperature of the analysis. Given a particular range of temperature indeed, the sample is thermally stable if no mass change is detected. The temperature that corresponds to a significant variation into the mass of the analyzed species highlights instead the beginning of the degradation.
In order to evaluate the thermal stability of the polymeric thin films under study a hyphenated **Thermo Gravimetric Analysis-Mass Spectrometry (TGA-GC-MS)** method was used.[5]
The use of hyphenated thermal and mass spectrometric techniques is well established and many studies were addressed to the investigation of the polymer structures under distinct thermal conditions.[6] [7] However, in most cases, the thermal conditions were set to induce a complete polymer degradation. Comparatively few studies were devoted to the assessment of the effects of relatively mild thermal treatments on the final polymer structure and stability.[8] [9] In this contest, the addition of a Gas Chromatographic (GC) stage between TGA and MS could be highly effective in improving the analytical performance for material amounts to be analyzed at the nanoscale level. In the resulting TGA-GC-MS configuration, the TGA can operate to impart a precise and reproducible thermal history to the samples. Hyphenation of TGA with GC-MS allows the separation of the evolved gas mixture into single components. For this reason an optimised TGA-GC-MS method, such as the one adopted in this work has the capability to precisely and accurately discriminate the different thermal degradation behaviors of the polymeric systems employed.[5]
The interface setup utilized in order to connect the GC-MS instrument to the TGA is represented in figure 2.11. The apparatus consists of three components: a heated transfer line (HTL1) from TGA to an automatic gas sampling system (autoinjector), an autoinjector (AI) equipped by a switch valve and a prefixed volume loop, and a second heated transfer line (HTL2) from the AI to the GC-MS injector port. The AI controls the repetitive pulsed transfer of known amounts of the evolved gas, with the desired frequency, in the injector of the GC-MS instrument by a system consisting of a multi-position valve, switched by a nitrogen gas flux. The second heated transfer line (HTL2) from the AI enters directly in the GC-MS injector since it intercepts the carrier gas that flow in the GC column.

The above set up allows analysis in different modalities to be performed since the gas stream from TGA can be sampled either at regularly prefixed intervals or at different intervals during the thermogravimetric experiment.
The MS signal was acquired both in full-scan mode and in Single Ion Monitoring (SIM) mode. The first analysis evaluates the entire number of species involved in the degradation product, in the range of mass versus charge values of 20–350 m/z. The second one is used to follow the evolution of the degradation for a single species by acquiring, one at a time, the signals corresponding to styrene (S) at $m/z = 104$, methylmethacrylate (MMA)

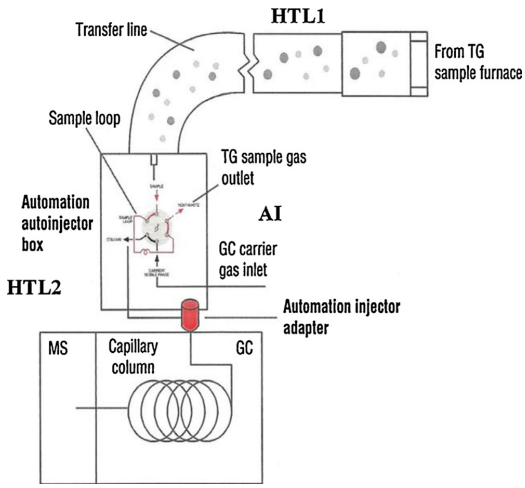

Figure 2.11: Scheme of TGA-GC-MS interface configuration.

at m/z = 100, of their dimers and trimers and of TEMPO (m/z = 156) and toluene (m/z = 92).
Among those products, the main contribution to the degradation for both the RCP PS-*r*-PMMA and the BCP PS-*b*-PMMA is given by the S and MMA monomers. Nevertheless the sensibility of the MS detector provides for better resolved results for styrene than for methylmethacrylate depending on the easiness of fragmentation and ionization of the molecule under investigation. For this reason most of the results reported in following chapters display the Styrene data alone.
Fig. 2.12 shows a typical output result of a SIM mode analysis, corresponding to chromatogram in which the mass loss is reported as a function of the temperature scan at a fixed sampling rate. Subsequently a profile is built up by joining the points relative to the maxima of successive styrene or methylmethacrilate peaks in the chromatogram, to obtain a continuous curve describing the overall monomers evolution as a function of sample temperature.

Direct Exposure Probe Analysis.
Another technique which can be used for the analysis of the thermal stability of a polymeric material is the Direct Exposure Probe (DEP). In this instrument a single drop (about 3 μL) of the polymeric material in solution, is directly deposited onto a thin filament hyphenated with a quadrupolar mass spectrometer. The filament is a wire of rhenium with a loop at the end inserted in a ceramic base. The current flow in the filament provides for the desorption of the material as a function of the temperature. The DEP tool can be coupled with a GC-MS detector, for the mass loss characterization of the desorbed material.
Because of the possibility to rapidly heat the polymeric material, the DEP analysis makes possible to reproduce on the bare polymeric material, the thermal treatments performed on samples within a RTP process. Moreover it gives the possibility to track the mass loss for a specific polymeric component as a function of time for a given temperature profile. An example of this kind of analysis performed in this thesis is reported in figure 2.13a. The treatment reported in the figure consists in an initial conditioning step (90 s

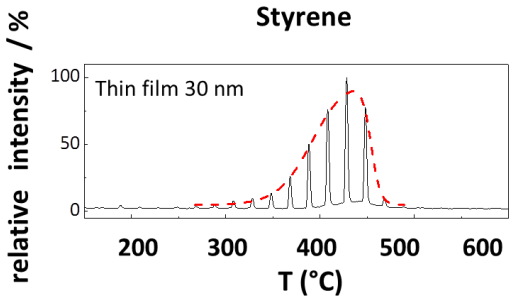

Figure 2.12: Example of a TGA-GC-MS chromatogram, acquired in the SIM scan mode for the evolution of styrene monomer degradation for a TR58 thin film of 30 nm. The peaks structure reproduces the fixed scan rate of the measure, while the red dot-line fits the various peaks giving an idea of the continuous evolution of styrene degradation profile. Data were adapted from [10].

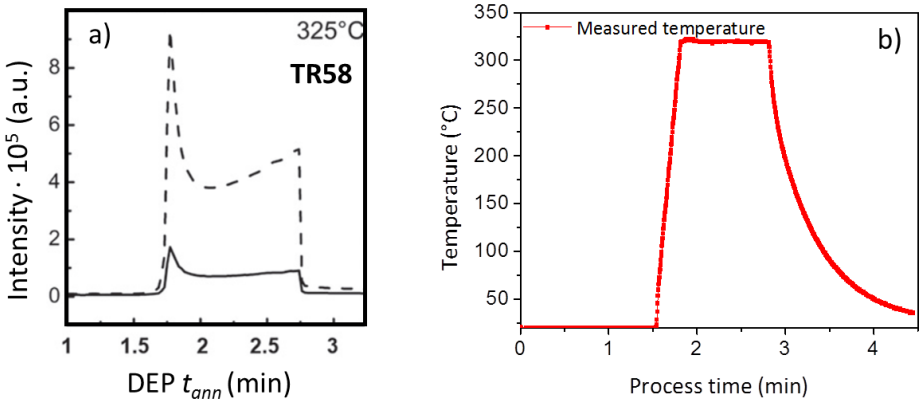

Figure 2.13: On the left: example of a DEP scan for the evolution of styrene (dashed line) and methylmethacrylate (continuous line) monomer degradation for TR58. On the right: RTP temperature profile for the treatment corresponding to the DEP simulation.

at 25°C), followed by a heating step (from 25°C to 325°C at a constant rate of 20°C/s), an isothermal step (60 s at 325°C) and finally a cooling step performed by simply switching off the electric current in the filament.
In figure 2.13b the RTP treatment corresponding to the one simulated by DEP is reported for comparison.

Determination of Toluene Content
A GC-MS analysis gives also the possibility to determine the solvent content (toluene in this thesis) both in as received bulk materials and in thin films at different steps of the lamellar fabrication process flow. A more detailed description of this procedure is reported elsewhere [11].

2.3 Image Processing

2.3.1 Correlation Length Measure

A quantitative measure of the level of lateral order of a lamellar pattern organized on featureless substrates, is given by the evaluation of the correlation length ξ.
This parameter can be extracted from the analysis of SEM images of the samples, provided that a good resolution (pixel/nm) of imaging is obtained. Unfortunately a complete and univoque method for determining ξ is still lacking, but most of the literature dealing with grain coarsening, bases its calculation on the seminal works of Harrison [12] and of Yokojima [13], which were well summed up by Ruiz *et al.* [2]
The fundamental idea of the procedures they proposed, is to treat the striped patterns obtained from perpendicular lamellae as well as from single layer of parallel cylinders, as smectic A_2 systems, since the layer repeat unit occurs over a distance equals to the radii of gyration of two molecules.[14]
Since the overall order of the striped pattern is determined by the variation into the orientation of the cylinders (or lamellae) a local orientational parameter of order could be suitable defined as:

$$\psi(\vec{r}) = exp[2i\theta(\vec{r})], \tag{2.2}$$

where $\vec{r}$ is the position vector, the factor 2 stems for the twofold degenerate symmetry of the lamellar system and θ is defined as the orientation of the director normal to the striped pattern $\hat{n}(\vec{r})$.
Several top-view SEM images are taken for each sample and converted into a 8-bit grey scale image (TIFF format)[5]. Each one is then processed to obtain the local orientational parameter of eq.2.2.
θ comes from $arctan(n_y/n_x)$ and $\hat{n}(\vec{r})$ is calculated from:

$$\hat{n}(\vec{r}) = \frac{\vec{\nabla} I}{|\vec{\nabla} I|}, \tag{2.3}$$

where $I(x, y)$ represents the intensity field on the grey level of the pixel and its gradient $\vec{\nabla} I = \left(\frac{\partial I}{\partial x}, \frac{\partial I}{\partial y} \right)$ is evaluated over a box of about $L_0 \times L_0$ centered in $\vec{r}$.

[5] In the original procedure suggested by Harrison, all the data were Fourier filtered before further processing, in order to eliminate low-frequency artifacts and high frequency noise from the image.

At this point, a sine and cosine fields could be defined and smoothed by Gaussian averaging each point with its neighbors.[12] In this way, the director is well defined at each point and, from the arctangent of the ratio of these fields, a smooth matrix for the double angle is extrapolated as follows:

$$2\theta = arctan\left(\frac{|\vec{\nabla} I|^2 sin(2\theta)}{|\vec{\nabla} I|^2 cos(2\theta)}\right). \tag{2.4}$$

From the order parameter of eq.2.2, the azimuthally averaged pair correlation function is defined as:

$$g(r) = \langle \psi(\vec{0})\psi^*(\vec{r})\rangle_c. \tag{2.5}$$

In the absence of external directional field, the correlation function for randomly oriented grains could be fitted by a simple exponential decay which finally gives ξ.
Though basically reproducing this idea, the novelty in our procedure consists in the computational routine elaborated for the determination of the local orientation field, as briefly reported thereafter.
High quality[6] SEM images (pixel/nm ratio of about 0.36 and average dimension of 5.6 μm x 4.2 μm) are processed by means of a Matlab routine, which implements an experimental software released by Feng *et al*.[15]
The gradient intensity function of the grey-scale SEM images is calculated, then the images are processed by a subdivision in small blocks of 21x21 pixels. Within each block of pixels, the gradient vectors and the local orientation are on average orthogonal. The components of the gradient vectors are rearranged in a 441x2 matrix. This matrix is then processed through a Singular Value Decomposition (SVD) algorithm [16] which returns the dominant direction of the gradient field as well as the local orientation, which results in a 90° rotation of the former.
The local orientation is then estimated with a resolution of 1 pixel. For each pixel, indeed, the software associates the local orientation of the blocks of pixels centered in it. The main output of this operation is a good estimation of the local orientation field, even in most defective regions without the need of further filtering operations. Indeed the single pixel resolution obtained by means of SVD makes unnecessary the application of filters on the power spectrum of the SEM image.
The software first releases a preliminary fast uploaded image in which the orientational field is visualized by means of a red arrow each square of 10x10 pixels (the set up of this resolution is chosen by user's will), as illustrated in figure 2.14.

Then the complete directional field can be uploaded on the pixel scale and easily visualized by means of a directional map of the entire image in which a color scale assigns an angular information in the range from 0 to 180°. In figure 2.15a SEM image of a lamellar pattern with a well-defined level of lateral order is reported. The dashed lines highlight the profiles of the main ordered domains (grains) which are easily established even by eye. The following picture (figure 2.16) illustrates the corresponding color map which demonstrates the correct running of our MATLAB routine.
As the two pictures are reproduced in the same dimensional scale, it can be easily appreciated the perfect correspondence between the boundaries of the different ordered

[6]The chosen resolution, as already pointed out by Harrison, is the result of a compromise between the need of imaging many grains while at the same time maintaining a good number of pixels describing each microdomain. An additional constrain could be represented by the computational processing time of extreme high definition images.

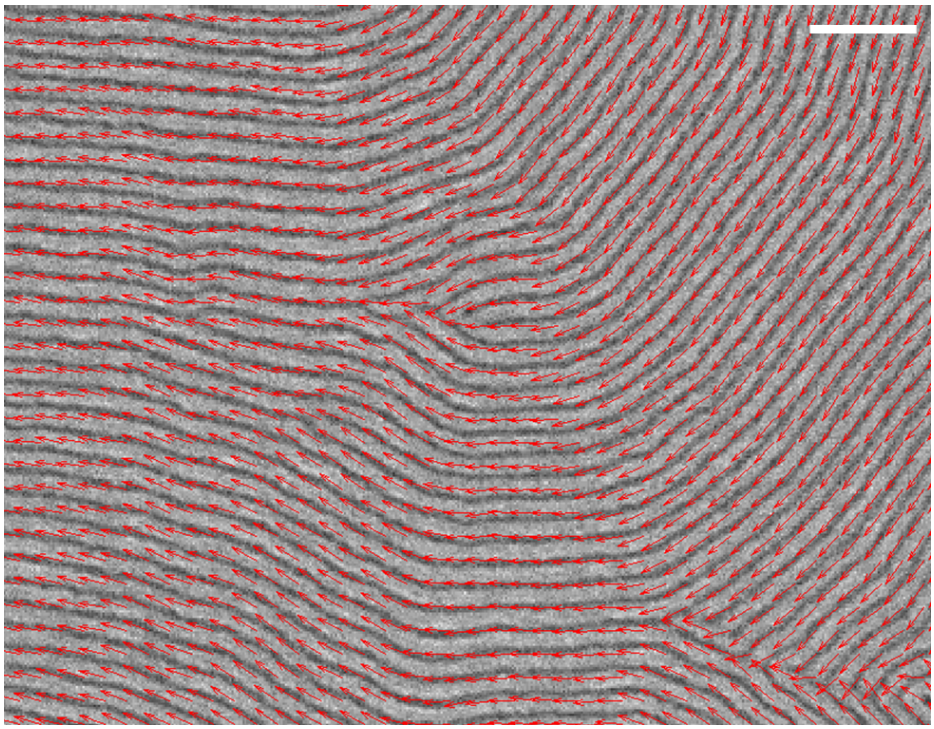

Figure 2.14: Enlarged detailed of a top-view image of a lamellar sample, processed through the software. A red arrow indicates the direction of the lamellar orientational field each square of 10x10 pixels. The white bar corresponds to 140 nm.

grains of the sample.
The extrapolation of the ξ value then follows with the exponential fit ($e^{-r/\xi}$) of the az-

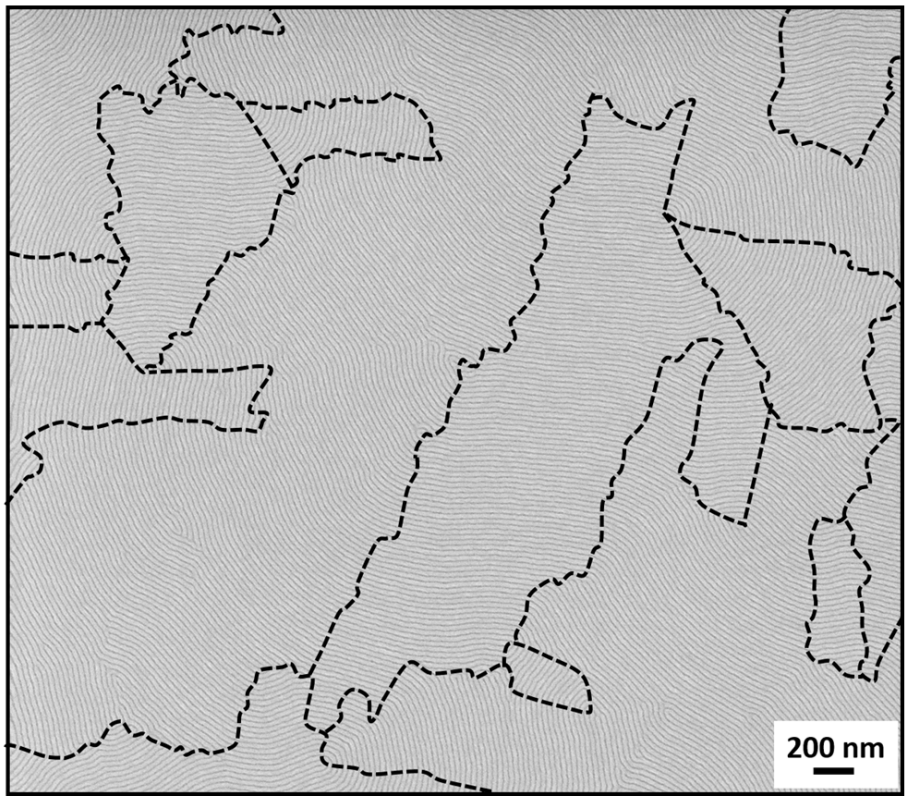

Figure 2.15: Original top-view SEM image of one of the lamellar samples fabricated in this work (submitted to RTP ordering process of 330°C for 10 s). The dashed lines are drawn to delimit the main different lamellar ordered domains.

imuthally averaged autocorrelation function.
The data reported in this thesis finally results from the average ξ value taken over 3 independent images of each sample, with the error reproducing their standard deviation.

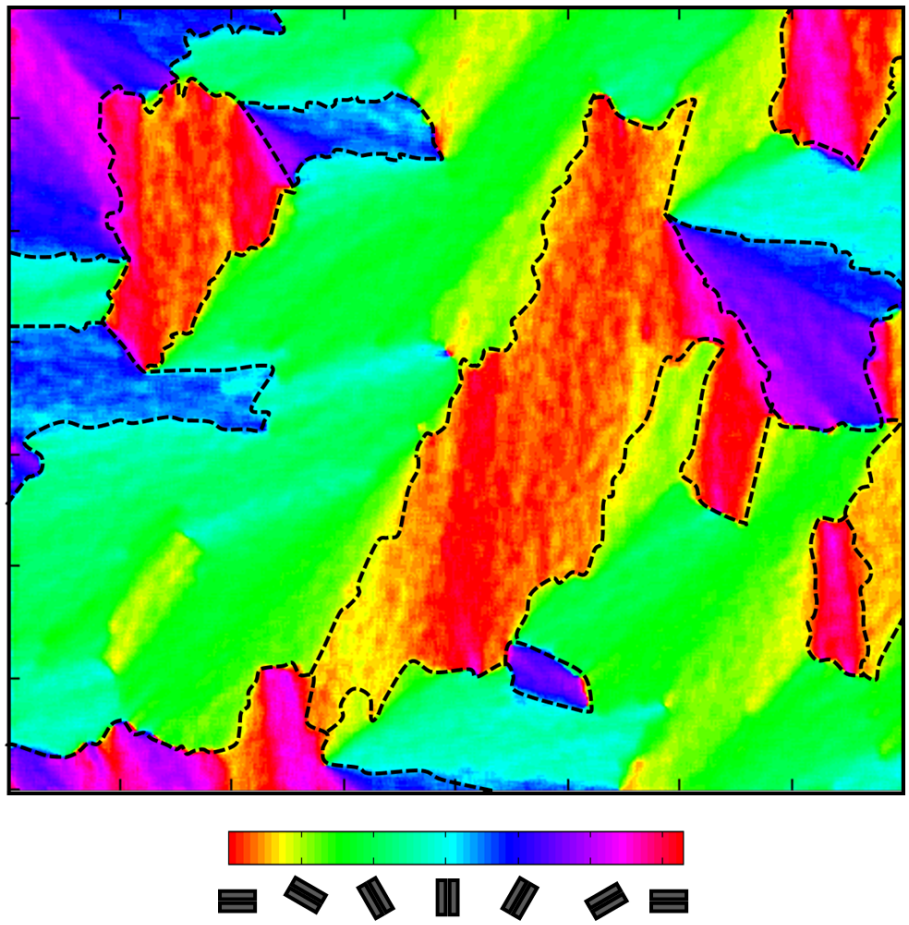

Figure 2.16: Color map corresponding to the original SEM images reported in figure 2.15, computed by software analysis. The dashed lines highlight the boundaries of the main grains in the polymeric film. The color scale corresponding to different lamellar orientations is provided as well.

2.4 Facilities and Collaborations

The entire fabrication process flow of the samples was carried out in the clean room facilities of the MDM laboratory at Agrate Brianza (MB, Italy). The implementation of the MatLab routine for image processing was carried out in a collaboration with Flavio Volpe at MDM lab.
The synthesis of BrR58, the chemical characterization of the polymer samples and in particular the TGA-GC-MS and the DEP analysis were performed by the research group of prof. Michele Laus at Dipartimento di Scienze e Innovazione Tecnologica, Università del Piemonte Orientale ¨A. Avogadro´ (Alessandria, Italy).
At the end of chapter 3 a brief Atomic Force Microscopy (AFM) analysis appears. AFM data were collected by Giampaolo Zuccheri at Dipartimento di Farmacia e Biotecnologie, CNR-Istituto Nanoscienze (Bologna, Italy). AFM characterization of the surface topography of the films was performed on a Multimode NanoScope V with a Jtype piezo scanner (Bruker). Imaging was performed at ambient temperature and humidity in Tapping-mode with NSC15/AIBS MikroMasch noncontact probes. The topography and the phase signals were acquired simultaneously.

Bibliography

[1]F. Roozeboom, "Rapid thermal processing systems: A review with emphasis on temperature control", Journal of Vacuum Science & Tech. B: Microelectronics and Nanometer Structures **8**, 1249 (1990).

[2]R. Ruiz, R. L. Sandstrom, and C. T. Black, "Induced Orientational Order in Symmetric Diblock Copolymer Thin Films", Advanced Materials **19**, 587–591 (2007).

[3]K. Vedam, "Spectroscopic ellipsometry: a historical overview", Thin Solid Films **313-314**, 1–9 (1998).

[4]J. N. Hilfiker, C. L. Bungay, R. A. Synowicki, T. E. Tiwald, C. M. Herzinger, B. Johs, G. K. Pribil, and J. A. Wollam, "Progress in spectroscopic ellipsometry: Applications from vacuum ultraviolet to infrared", J. Vac. Sci. Technol. A, 1103 (2003).

[5]V. Gianotti, D. Antonioli, K. Sparnacci, M. Laus, T. J. Giammaria, M. Ceresoli, F. Ferrarese Lupi, G. Seguini, and M. Perego, "Characterization of ultra-thin polymeric films by Gas chromatography-Mass spectrometry hyphenated to thermogravimetry.", Journal of chromatography. A **1368**, 204–10 (2014).

[6]K. Raemakers, and J. Bart, "Applications of simultaneous thermogravimetry-mass spectrometry in polymer analysis", Thermochimica Acta **295**, 1–58 (1997).

[7]A. I. Roland, and G. Schmidt-Naake, "Thermal degradation of polystyrene produced by nitroxide-controlled radical polymerization", Journal of Analytical and Applied Pyrolysis **58-59**, 143–154 (2001).

[8]D. M. Bate, and R. S. Lehrle, "Thermal degradation of polymer blends: PS/PMMA blend behaviour related to the copolymerization Φ-factor for this system", Polymer Degradation and Stability **55**, 295–299 (1997).

[9]C. Chuai, K. Almdal, and J. Lyngaae-Jorgensen, "Thermal behavior and properties of polystyrene/poly(methyl methacrylate) blends", Journal of Applied Polymer Science **91**, 609–620 (2004).

[10]V. Gianotti, D. Antonioli, K. Sparnacci, M. Laus, T. J. Giammaria, F. Ferrarese Lupi, G. Seguini, and M. Perego, "On the Thermal Stability of PS- b -PMMA Block and P(S- r -MMA) Random Copolymers for Nanopatterning Applications", Macromolecules **46**, 8224–8234 (2013).

[11]M. Perego, F. Ferrarese Lupi, M. Ceresoli, T. J. Giammaria, G. Seguini, E. Enrico, L. Boarino, D. Antonioli, V. Gianotti, K. Sparnacci, and M. Laus, "Ordering dynamics in symmetric PS-b-PMMA diblock copolymer thin films during rapid thermal processing", Journal of Materials Chemistry C **2**, 6655 (2014).

[12]C. Harrison, P. M. Chaikin, D. A. Huse, R. A. Register, D. H. Adamson, A. Daniel, E. Huang, P. Mansky, T. P. Russell, C. J. Hawker, D. A. Egolf, I. V. Melnikov, and E. Bodenschatz, "Reducing Substrate Pinning of Block Copolymer Microdomains with a Buffer Layer of Polymer Brushes", Macromolecules **33**, 857–865 (2000).

[13]Y. Yokojima, and Y. Shiwa, "Hydrodynamic interactions in ordering process of two-dimensional quenched block copolymers", Physical Review E **65**, 056308 (2002).

[14]C. Harrison, Z. Cheng, S. Sethuraman, D. A. Huse, P. M. Chaikin, D. A. Vega, J. M. Sebastian, R. A. Register, and D. H. Adamson, "Dynamics of pattern coarsening in a two-dimensional smectic system", Physical Review E **66**, 011706 (2002).

[15]*Https://users.soe.ucsc.edu/~milanfar/software/local-orientation.html*.

[16]R. A. Sadek, "SVD Based Image Processing Applications: State of The Art, Contributions and Research Challenges", Int. J. Adv. Comput. Sci. Appl., 26 (2012).

CHAPTER 3

Perpendicular Orientation of Nanostructures: Functionalization of the Substrate

In this chapter we investigate in details the grafting process of a PS-*r*-PMMA copolymer for the perpendicular orientation of PS-*b*-PMMA lamellar structure on the top of it.

In the first section of this chapter, the Rapid Thermal Processing (RTP) is validated as a proper technique to bring the ``grafting to'' approach on a time scale fully compatible with Microelectronics industry requirements. All the samples here considered are fabricated with a commercial random copolymer chosen with a PS fraction of 58% that is suitable for the succesive organization of symmetric PS-*b*-PMMA.[1]

The second section studies the whole system made by the symmetric BCP spun on the grafted RCP, when subjected to a RTP treatment for the organization of lamellar thin film. Samples are investigated through SEM images as well as through the analysis of their thermal stability.[2]

The two last sections of this chapter report two different technological approaches for the optimization of the thermal stability of the RCP layer when grafted in a RTP process.[3]).

3.1 From Furnace to RTP: Flash Grafting

The ``grafting to''approach represents a high precision technique to obtain and control the neutralization of the substrate for the subsequent deposition and organization of BCP thin films. The RCP chemical composition indeed can be precisely controlled during the RCP synthesis, this way providing the fine-tuning of the surface characteristics. A straightforward integration of this approach into a lithographic process flow is possible, however its industrial exploitation requires extremely fast grafting procedures.
The time process limitations are dictated by the symbiotic integration of the self-assembling materials into standard lithographic processes. Due to the ITRS requirements, to be competitive with the actual large-scale production lithographic techniques the industrial exploitaion of BCPs looks for a ``grafting to'' approach to be completed within tens of seconds. While the complete processing of BCPs would lay around 4 minutes (see ITRS 2007 [4]).
Though well-established and studied, the grafting process performed in furnace or oven [5] develops on a proper time scale which is definitively far apart from the one just outlined. Moreover reactions comprising polymers are generally slow because they are, at

least partially, diffusion controlled. In this framework, the most obvious solution should be to raise the temperature of the grafting process, but the relatively low thermal stability of the employed functional (co)polymers could prevent the grafting reaction to be performed at high temperatures. In a recent paper Gianotti *et al*. [6] investigated the thermal stability of the commercial available random copolymer TR58 when deposited in layers with different thickness and when submitted to a grafting treatment in a conventional furnace. The results of that work are reported in figure 3.1, through the TGA-GC-MS chromatograms for styrene (S) that is one of the main products of polymer degradation. From the top panel in fig. 3.1, the thermal stability of the as-deposited films appears to increase as the thickness decreases: the main peak of degradation clearly shifts to higher temperature in going from the bulk copolymers to the 30 nm thin film. A reverse shift instead is registered for the grafted 5 nm thin films treated in a furnace at 170°C for 48 h. The thermal stability in this case gets worse than the original bulk chromatogram, with the maximum of the peak that moves back to a temperature well below 400°C. This observation was ascribed to two different effects during the furnace annealing procedure: the occurence of radicals recombinations leading to the formation of weaker bonds such as head-to-head linkages, or alternatively some oxidation leading to thermally labile structures notwithstanding the high vacuum conditions of the process. Analogous results were collected through the methylmethacrylate (MMA) chromatograms, but the instrumental sensibility to this component is worse with respect to the styrene one, for this reason all the following TGA-GC-MS analysis are referred to the styrene profiles only.

The reported results highlights the fact that the thermal stability of the grafted RCP layer is not intrinsically limited by the polymeric film itself, but it is strongly affected by the process employed for the grafting treatment.
In spite of these advices, in a recent paper [7] a fast grafting reaction of a hydroxyl terminated PS-*r*-PMMA copolymer was reported by heating the samples on a hot-plate at 250°C for a few minutes. The authors argued that the combination of high temperature and short time allowed the grafting reaction to occur with limited, if any, degradation of the random copolymer.
On the basis of this considerations we investigated the process-dependent thermal stability of the same RCP used by Gianotti *et al*. [6] by performing a fast grafting reactions operating at very high temperature in a RTP machine.
Whit respect to the treatments performed on a hotplate or in a conventional furnace, in which the heating transfer is governed by conduction or convection mechanism, the radiative sources (normally halogen lamps) of RTP provide several advantages. First, in RTP the temperature on the sample can be tuned with extremely high heating rates (up to 50°C/s) compared to those of conventional furnaces (3-5°C/min). *In situ* monitoring of the temperature induced on the sample is possible and the behavior of the temperature can be controlled during all the three phases of the annealing process: the heating ramp, the isothermal stage, and the cooling ramp. For these reasons annealing in RTP can be performed at temperature very close to the order-disorder transition temperature (T_{ODT}) for very short time periods, thus minimizing the effect of degradation on the thin polymeric film, whether it deals with the RCP or the BCP, and reducing the viscosity of the polymeric film.
A TGA-GC-MS analysis was performed in order to study the thermal stability of TR58 as a function of the specific RTP grafting treatment employed. The S chromathogram

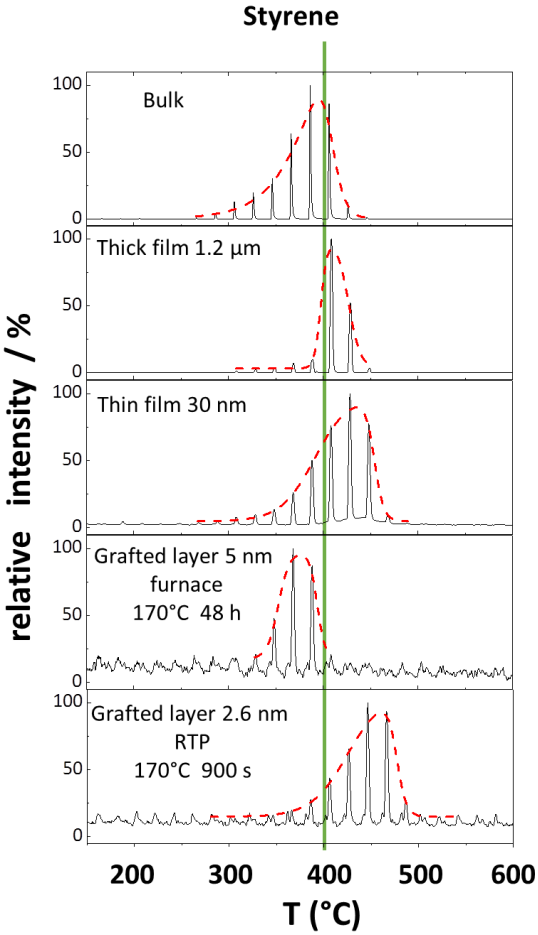

Figure 3.1: TGA-GC-MS analysis of styrene for copolymer TR58 in bulk, as thermally untreated films of different thickness (about 1.2 μm and 30 nm), as grafted thin film of about 5.0 nm thickness submitted to a furnace treatment of 48 h at 170°C as reported in the paper of Gianotti *et al*. [6]. The bottom panel represents the styrene chromatograms for a thin film of 2.6 nm grafted in RTP for 900 s at 170°C. The peaks reported in the chromatograms collect the styrene signals as the main product of degradation produced by heating up the samples over a huge range of temperature. The green line at 400°C is drawn to guide the eye.

of a thin films of 2.6 nm grafted within a RTP treatment of 900 s at the temperature of 170°C is reported in the bottom panel of figure 3.1. The main peak degradation reveals a more stable structure with respect to the sample treated at the same temperature in a furnace (above panel in the figure). Figure 3.2depicts the S chromatograms relative to TR58 thin films grafted in RTP for 900 s at different temperatures in the range between 170 and 250°C. These data interestingly outlined the possibility to increase the grafting temperature without any loss in terms of thermal stability when dealing with a RTP process. [1]

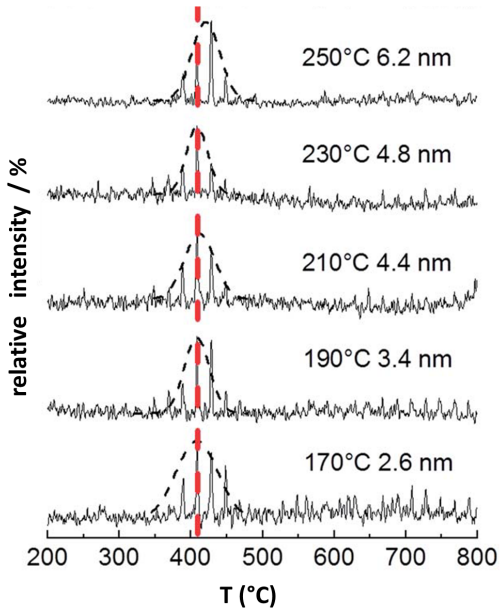

Figure 3.2: TGA-GC-MS analysis o styrene for TR58 after annealing the thin film in RTP for 900 s at temperatures comprised between 170°C and 250°C. The grafted film thickness is reported for each temperature. The dashed red line was added to guide the eye.

A systematic study of the grafted thickness as a function of the time and temperature of annealing has been performed. Figure 3.3 reports the ellipsometric measures of TR58 grafted thickness for samples treated in RTP at 250°C for different time of annealing. The thickness of the film increases very fast at the beginning and then levels off reaching the plateau value of about 5.2 nm, which is very close to the 5 nm thickness obtained with the furnace treatment at 170°C for 48 h. The film growth profile suggests the occurrence of two distinct regimes.[8] [9] [10] [11] Initially, the process is diffusion or reaction limited, where the driving force is the diffusion of the polymers on the surface and the conformational rearrangements of the random coil to appropriately present the functional group to the silica surface. This diffusion/reaction process represents the rate-limiting step and corresponds to a surface grafting process characterized by a negligible interaction among individual polymer chains. Increasing the reaction time, the slope change indicates a transition from the diffusion or reaction limited adsorption regime to the penetration-limited regime. The penetration-limited regime results from

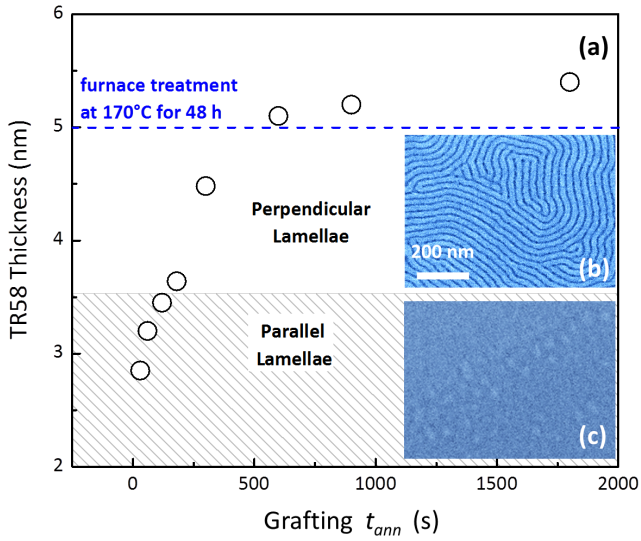

Figure 3.3: Thickness of the RTP grafted films of TR58 at 250°C as a function of time. The two thickness windows corresponding to perpendicular and parallel orientations of the above-deposited lamellae are also indicated. SEM images corresponding to perpendicular (b) and parallel (c) orientation of the lamellar microdomains are reported. The dashed lines indicate the limiting thickness for grafting in a furnace at 170°C for 48 h.

the increased density of the grafted chains on the surface that creates an energy barrier for further grafting. This behavior is accompanied by the transition from random mushroom to brush arrangement of the grafted macromolecules and the grafting stops when the chains form stretched brushes.
The further deposition and organization of a thin layer of the lamellar forming B50 on the samples reported in figure 3.3, allows for the charachterization of the propensity of the random copolymer layer to drive the orientation of BCP microdomains. This propensity depends essentially on the thickness of the grafted layer. The analysis of SEM top views of symmetric BCP layers displays a direct transition from parallel to perpendicular lamellar morphology. The critical thickness, above which a well ordered perpendicular lamellar structure of B50 is observed, is about 3.5 nm, which is established in less then 600 s of annealing.
The evolution of the thickness of the grafted copolymer layer as a function of the temperature of annealing (T_{target}) is reported in figure 3.4 for the costant annealing time of 900 s in RTP. Above 190°C the critical thickness identified in fig. 3.3 for the perpendicular orientation of lamellae, is reached. Above 230°C the thickness levels to the saturation limit, which once again closely resembles the one obtained for the furnace treatment at 170°C.

The above listed results demonstrate that high temperature thermal treatments in a RTP machine can be successfully applied in the procedure of surface energies neutralization, to give rise to perpendicularly oriented lamellae, provided that the time and temperature of annealing allow for the grafting of a proper thickness of the RCP layer. The same trend

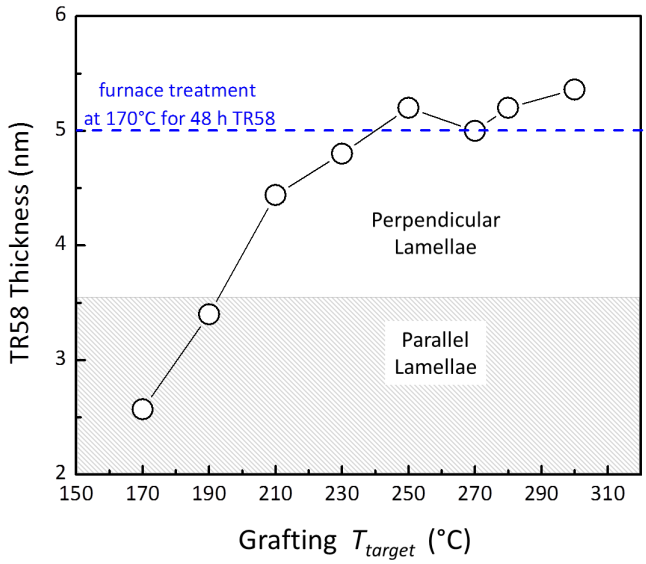

Figure 3.4: Thickness trend for TR58 as a function of the annealing temperature T_{target} after 900 s of annealing time in RTP. The dashed lines indicate the limiting thickness for grafting in a furnace at 170°C annealing for 48 h.

of a rapid increase on short time of annealing and a following saturation, irrespective of the temperature chosen, was obtained for a RCPs produced for the perpendicular organization of cylindrical BCP patterns (XS of RCP of 0.62%). [1] It can be inferred that the higher the annealing temperature, the shorter the time in which the neutralization of substrate surfaces is achieved: in particular operating at 310°C the effective surface neutralization can be achieved in less than 60 s. On the basis of these results, it is possible to finely tune the processing parameters of the RTP process in order to identify the conditions that give rise to a surface neutralization in the shortest possible t_{ann}.

3.2 Thermal Stability of the System RCP + BCP within RTP

The thermal stability of the grafted layer has to be tested during the SA process of the BCP overlayer too. A limited stability of the RCP layer indeed would inhibit from processing BCP at high temperatures this way hampering the improvement into BCP lateral ordering. This problem is specifically addressed in this paragraph: thin film of lamellar BCP were deposited on the grafted RCP layer and the behavior of the system as function of the T_{ann} was investigated in details. The samples considered in this section are then submitted to two subcessive RTP treatments: the first one, for TR58 grafting, involves only the random copolymer layer; the second treatment, for the ordering process of BCP, involves both the TR58 and the B50 layers. For this kind of investigation we first consider a constant RTP grafting process of 600 s at 250°C which is taken in the saturation regime of TR58 grafted thickness (see figure 3.1), and a second RTP treatment of 60 s on a wide range of temperature of annealing from 190°C up to 340°C.

A first analysis focuses on the SEM images taken at the end of the second RTP treatment for different samples. Figure 3.5 displays the progressive growth of ordered lamellar domains during RTP treatments, at different temperatures between 190°C and 290°C. After 60 s at 190°C, phase separation has already taken place and the lamellar morphology emerges progressively better resolved over the entire surface of the samples as the annealing temperature is increased to 290°C. No evidence of degradation in the polymeric film was observed.

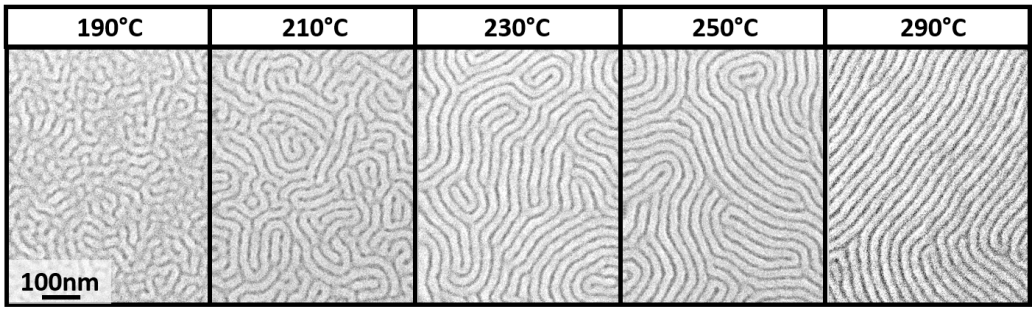

Figure 3.5: SEM images showing morphological evolution as a function of the annealing temperature for B50 thin film treated for 60 s with RTP. All the samples were submitted to a preliminary grafting treatment of TR58 for 600 s at 250°C.

The situation is significantly different when operating at temperatures higher than 290°C. Figure 3.6 reports, at different magnifications, the lateral ordering evolution in BCP thin films for samples subjected to thermal treatments at temperatures between 300°C and 340°C for 60 s. A well-developed lamellar morphology can be observed even in the temperature range between 300°C and 340 °C (figure 3.6, first row) without significant differences in terms of lateral order. However, the observation of larger sample areas reveals the occurrence of some dark spots randomly distributed over the entire film (figure 3.6, second row), indicating the occurrence of some film degradation. At 300°C, the spots are relatively small but increase in size as the RTP temperature increases up to 330°C and then start to coalesce at 340°C. It is interesting to observe the ordering characteristics of the BCPs at the edge of the dark spots (figure 3.6, third row). At 300°C, no evidence of reduced ordering is observed in the lamellar polymeric film and the dark spots correspond to a slightly different contrast in the SEM-enlarged image. On the other hand, in the case of annealing temperatures above 300°C, the dark spots identify damaged areas with no evidence of polymer organization. The abrupt edge between the ordered block and the damaged area behaves as a confining boundary, thus resulting in an enhanced lateral order extending for about 1 μm. In this context the 290°C, seems to represent a limiting temperature for B50 ordering process.

To better understand the origin of the observed film degradation, the thermal behavior of the TR58 and B50 was investigated by mass spectroscopy using the direct exposure probe (DEP) tool, which enables rapid heating of thin polymeric films deposited on a filament.[12] [13] The DEP thermal conditions were set to reproduce the temperature profiles employed in the RTP process. In details, the TR58 was first heated in the mass

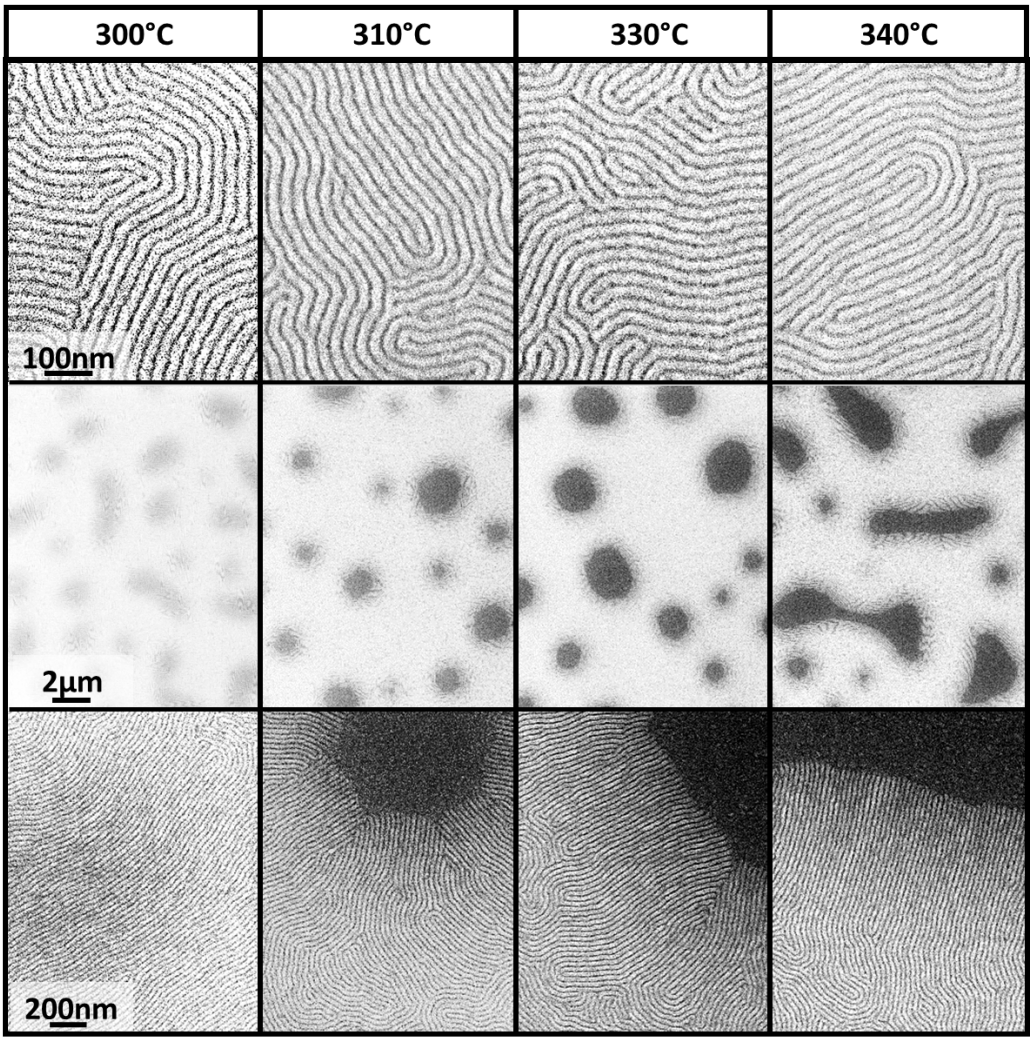

Figure 3.6: SEM images, at different magnifications, of symmetric PS-*b*-PMMA thin films treated with RTP for 60 s at temperatures varying from 300°C to 340°C.

spectrometer to 250°C with a heating rate of 20°C/s[1], maintained at this temperature for 600 s, and then cooled to room temperature. Then the same TR58 sample was heated to the chosen T_{target} with a heating rate of 20°C/s, maintained at this temperature for 60 s, and then cooled to room temperature. Finally, the B50 was heated in the mass spectrometer to the final annealing temperature T_{target} with a heating rate of 20°C/s, maintained at this temperature for 60 s, and then cooled to room temperature.
The first heating treatment of TR58 should have induced the same thermal stress to which the random copolymer was subjected during the surface grafting process, whereas the second would have mimicked the treatment to which the random copolymer was subjected during the thermal treatment after the deposition of the block copolymer film. The above analysis was repeated with T_{target} ranging from 175 to 400°C, following the time evolution of the monomers and oligomers during the annealing process. For both copolymers, the major degradation products were the two monomers, indicating the occurrence of depolymerization via an unzipping process. [6]
Figure 3.7 reports the DEP mass profiles of styrene and methylmethacrylate for the TR58 and B50 samples during the thermal treatment that reproduced the annealing performed to promote the block copolymer self-assembly at two different temperature of annealing. At 250°C, only slight evidence of degradation is detected for the random copolymer TR58. The signal found for B50 is even less marked. A different scenario is observed at 325°C, where the random copolymer DEP mass profile exhibits a strong signature of degradation with intense styrene and methylmethacrylate signals. Conversely, the B50 block copolymer exhibits no significant increment of degradation in respect to the sample treated at 250°C. The same effect, though with less intensity, can be inferred from the DEP mass profiles of the various oligomers (not shown here).

To further compare the behavior of TR58 and B50, the signals corresponding to the integrated peak area of styrene monomer of figure 3.7 are reported in figure 3.8 as a function of the annealing temperature T_{target}. For B50 after the 60 s of annealing time, the onset of degradation occurs at about 350°C, as indicated by the upturn of the peak areas versus temperature curves, whereas for TR58 the degradation starts at lower temperatures. In particular it is quite pronounced even at 300°C where we could fix a treshold for the occurance of inhomogeneity in BCP thin films due to SEM images results shown above. These data indicate that the film degradation starts from the random copolymer layer and produces a detachment of the block copolymer film, because of the formation of bubbles due to the evolution of monomers (as depicted in the following paragraphs). These results clearly indicate that the range of accessible temperatures in the processing of these self-assembling materials is mainly limited by the thermal instability of the grafted random copolymer layer.

From a technological point of view, the 290°C T_{target} has been identified as the limiting processing temperature for the specific system made by TR58+B50, due to significant degradation of the random copolymer film when operating at $T_{target} \geq 300$°C. In principle, according to the degradation data previously discussed, the block copolymer could eventually sustain even higher processing temperatures, provided random copolymer brush layers with greatly increased thermal stability are employed.

[1] A deeper investigation of the role of the heating rate within RTP is reported in the next chapter. In this analysis the value of 20°C/s is taken as the one that better reproduces the 18°C used by the RTP, due to DEP possible settings.

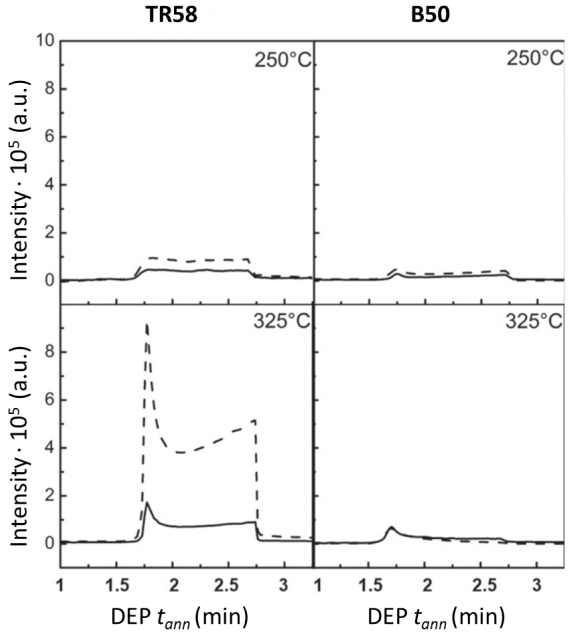

Figure 3.7: Typical mass profiles of DEP analysis for TR58 (left) and B50 (right). The mass profiles report the degradation results during thermal treatment for the block copolymer self-assembling process at 250°C (upper row) and 325°C (lower row). The curves were extracted in selected ion monitoring (SIM) mode by acquiring the signal corresponding to the typical m/z values of styrene (dashed line) at 104 and of methylmethacrylate (continuous line) at 100.

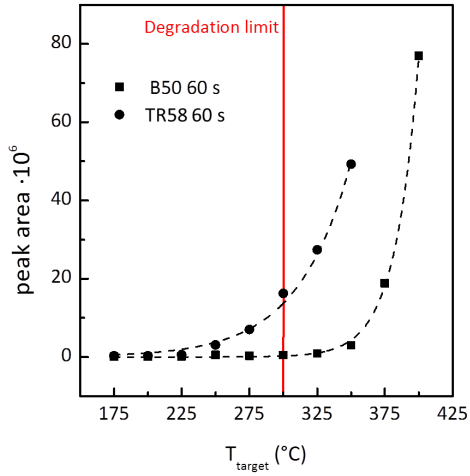

Figure 3.8: Peak areas of the styrene evolved from B50 samples in 60 s of annealing time and from thermally pretreated (250°C for 600 s) TR58 samples in 60 s of annealing time at different annealing temperatures T_{target}. Analogous results could be extracted for methylmethacrylate peak areas.

3.3 Thermal Stabilization of TR58

In this section we investigate the possibility to increase the thermal stability of the copolymer brush layer obtained by the TR58 polymer by properly adjusting the processing conditions during the ``grafting to´´process.
In figure 3.1 we already highlighted the peculiar properties of RTP in getting higher thermal stability of the grafted brush layer in respect to a conventional thermal treatment. Here we try to take advantage of this concept by processing the RCP layer at very high temperatures in a RTP machine in order to further stabilize the grafted layer. For this reason the thermal stability of TR58 was studied for thin films submitted to different grafting processes (600 s in the range of temperature between 170°C and 330°C), and then definitely probed by spin-coating symmetric BCP layers onto the brush layers and subsequently annealing them at high-temperatures.
The thermal stability of the grafted polymeric chains was investigated by TGA-GC-MS analysis. As typical examples, figure 3.9 reports the styrene evolution profiles for TR58 after RTP treatment at 230 and 330°C. The methyl methacrylate evolution (not reported) parallels that of styrene. The same figure reports the degradation contour profile (dashed line) of TR58 in bulk, for comparison purposes. The overall thermal degradation profile, monitored through the evolution of the monomers, appears translated toward higher values along the temperature scale in thin films [6] compared to bulk, irrespective of the temperature of the grafting process. According to literature [14], this effect is explained considering that, because of the small thickness of the film, the residence time in the film of the radicals obtained from chain end scission is too short to allow efficient radical transfer, thus reducing the incidence of the radical transfer processes. As a result, the main degradation peak moves toward higher temperatures[2]. In figure 3.9, comparing the degradation peaks of TR58 when increasing the grafting temperature from 230 to 330°C, we observe a further remarkable shift toward high temperature values.

Figure 3.10 collectively reports the maximum of the degradation peak temperatures for the TR58 samples, taken from the relevant styrene evolution profiles, as a function of the grafting temperature in the range between 170 and 330°C. A sigmoidal trend is observed with a steep increase, when the grafting process is performed at temperatures higher than 230°C. This abrupt variation is followed by a smoother increase and an asymptotic stabilization at temperatures higher than 290°C.
It is important to notice that the thickness of the samples subjected to the above thermal treatments for temperatures higher than 230°C undergoes a negligible reduction. In addition, the water contact angle of all these samples is not influenced by the grafting temperature and results in $\sim 82 \pm 1.0°$ in all cases, supporting the idea that they can be used to provide a proper neutralized surface for subsequent BCP deposition.

According to these data, in the range of temperature here considered, the RCP brush layer acquires more stability when the grafting treatment is performed at higher temperature, till a saturation regime occurs. To test the effective stability of the grafted layer, we consider the whole system RCP + BCP and we proceed with the deposition of a thin film of B50 on top of TR58. The RTP treatment for promoting the lamellar organization is

[2]It is interesting to note that in the range of temperature between 170 and 230°C, when the layer thickness is between 3 and 8 nm, almost identical degradation curves were registered. Consequently, a direct comparison between the degradation profiles of the samples obtained through the various grafting temperatures can be reliably made irrespective of the minor thickness differences.

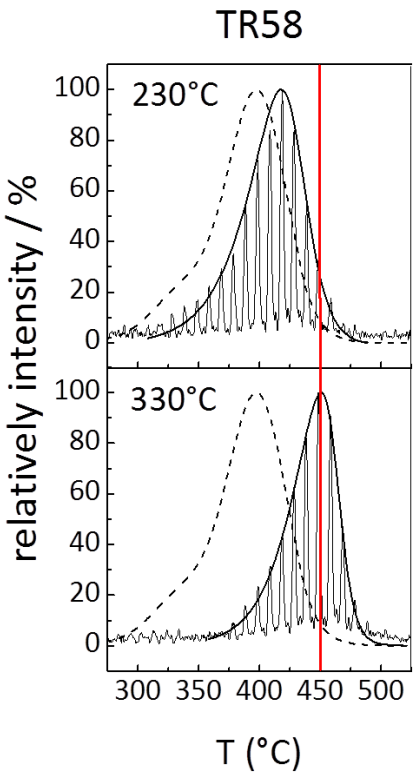

Figure 3.9: TGA-GC-MS analysis of styrene on TR58 films after the grafting process performed at 230 or 330°C. The dashed curves represent the corresponding styrene profiles for the bulk sample. The red lines at 450°C were added as a visual guide.

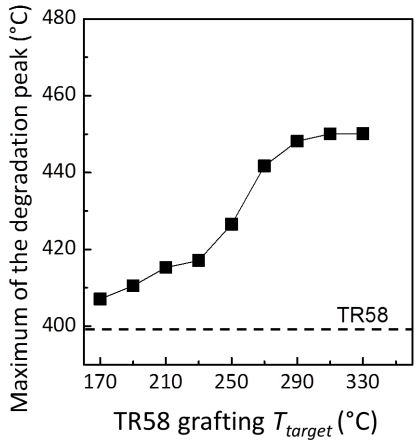

Figure 3.10: Maximum temperature of the degradation peak for TR58 in the TGA-GC-MS analysis of the styrene evolution as a function of the grafting temperature. The horizontal line indicates the corresponding degradation temperature for the bulk sample.

set at 310°C for 60 s. Annealing in RTP at the same conditions, was previously shown to produce damaged samples (see fig.3.6), for this reason it is the optimal choice in testing the effective stabilization ability of our technicque.
In figure 3.11, the SEM plan view images of the self-assembled BCP thin film, obtained at two different magnifications, are reported as a function of the TR58 grafting temperature. When looking at a small scale area, a well-developed lamellar morphology can be observed in all the samples irrespective of the RCP grafting temperature. However, the observation of larger sample areas reveals the occurrence of inhomogeneities in the film. In particular, in the case of the RCP annealed at 250°C, dark spots are randomly distributed over the entire film indicating the occurrence of some film degradation as previously described. Interestingly, in the case of the RCP grafted at 290°C, no discontinuity in the film is observed. On a large area, local variations in the contrast of the image are evident, representing a warning sign of the degradation process, but no film disruption occurred. The magnified SEM images indicate that the lamellar morphology is preserved even on the dark spots of the film. When the sample is annealed at 330°C, the homogeneity of the film further increases, and only very limited modification of the contrast is visible in the large-area SEM image. The depicted system evolution perfectly correlates with the progressive stabilization of the TR58 RCP when annealed at high temperature as shown in figure 3.10.
The collected data indicate that, when grafting the RCPs at 330 °C, the BCP thin films, deposited on top and thermally treated at 310°C for 60 s, are stable and homogeneous with a high level of lateral order. Untill now we discussed the thermal stability results simply considering the main styrene degradation peak. This peak indeed presents the most appreciable stabilization effect, but a more complete explanation of this phenomenon could be highlighted from a supplementary investigation of the secondary styrene degradation peak at lower temperature. A series of analysis was performed by MS using the DEP probe, on samples deposited to the filament and subjected to a RCP

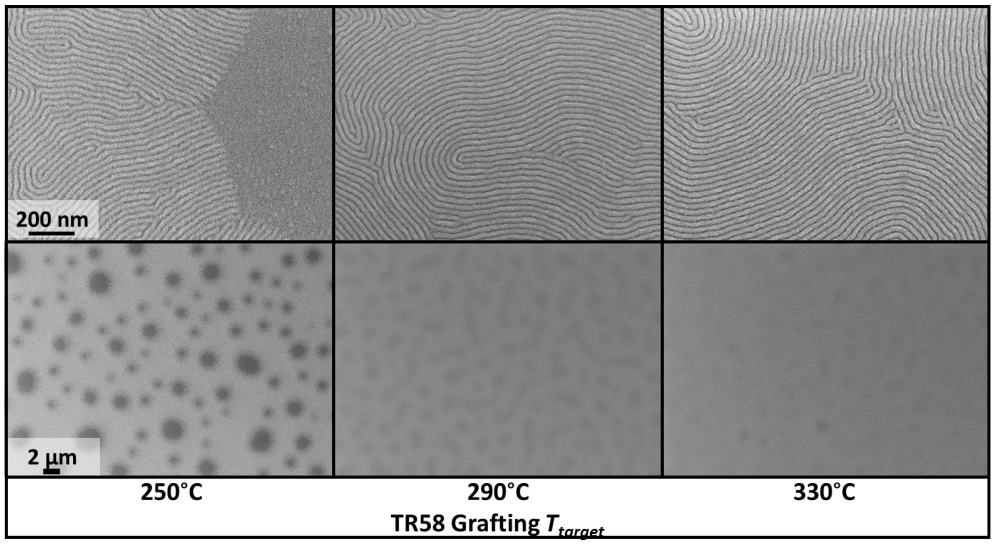

Figure 3.11: SEM plan view images of the self-assembled BCP thin film as a function of the TR58 RCP grafting temperature obtained at two different magnifications. Self-assembly of BCP were promoted with the same RTP treatment of 60 s at 310°C.

grafting simulation treatment at different temperature and time. TR58 samples were first heated in the DEP probe to 250 or 325°C with a heating rate of 20°C/s, maintained at this temperature for different time periods between 10 and 600 s, and then cooled to room temperature. This treatment should simulate the thermal stress to which the RCPs are subjected during the surface grafting process. Next, the samples underwent a simple temperature scan treatment (from 25 to 800°C with a heating rate of 1°C/s) to explore the effect of the thermal annealing at 250 or 325°C.
Figure 3.12 reports the DEP-MS styrene evolution of TR58 subjected to the above listed thermal treatments. After the treatment at 250°C for 600 s, the lower temperature loss peaks are still present. In contrast, when the treatment is performed at 325°C, the intensities of the styrene loss peaks progressively decrease and are no longer visible after a grafting time of ∼300 s. This result indicates that the thermal degradation process, which causes a monomer loss in the low temperature region that precedes the main polymer degradation, can be efficiently offset by subjecting TR58 samples to a high-temperature thermal treatment for relatively short time periods. In addition, combining this result with the trend of the main degradation after the grafting treatments at different temperatures, illustrated in figures 3.9 and 3.10, it may be concluded that during the thermal treatment at high temperatures, the formation of more stable bonds occurs, thus in turn improving the overall thermal stability of the RCP chains.[3]

In summary, the overall framework suggests that by treating the RCP at 330°C, it could be possible to further increase the annealing temperature of the BCP layer overcoming the previously set limit of 290°C. To gain the access to higher and higher temperature of

[3]In particular, radicals resulting from the homolytic cleavage of the end groups, with high local concentration, undergo bimolecular recombination or disproportionation reactions leading to the formation of more stable carbon- carbon bonds.

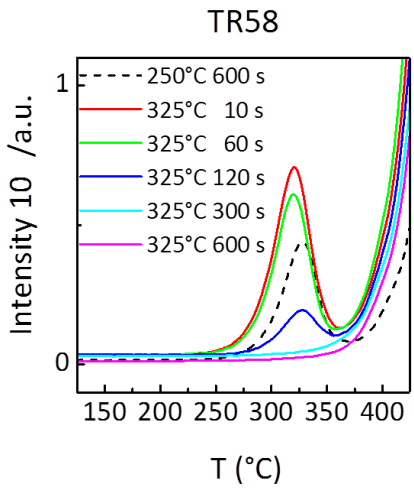

Figure 3.12: Styrene evolution profile of the secondary peak of degradation for TR58 subjected to the following thermal treatments. The samples were first heated, with a heating rate of 20°C/s, in the mass spectrometer to 250°C and maintained at this temperature for 600 s (dashed line) or to 325°C and maintained at this temperature for different time periods and then cooled to room temperature. Finally the samples were analyzed with a heating rate of 1°C/s.

annealing would represent a foundamental key in the technologycal process of lamellar fabrication. Indeed the higher the temperature is, the faster the self-assembly process is, while achieving at the same time a higher level of lateral order for the lamellar pattern[4]. Figure 3.13 compares the results obtained in the case of BCP thin films deposited on a TR58 RCP brush layer grafted at 330°C for 600 s. The BCPs were annealed for 60 s at temperatures ranging from 310 to 350°C. It is important to notice that ordering of the BCP occurs even at this high temperature, because of the weak temperature dependence of the Flory-Huggins parameter for PS-*b*-PMMA copolymers.[15] The SEM plan view images highlight a progressive disruption of the polymeric film when increasing the annealing temperature of the BCP. As it can be easily inferred, the degradation process of the polymeric stack here reported, is similar to the one observed in the case of a TR58 RCP brush layer grafted at 250°C with the formation of dark spots, which gradually evolve when increasing the annealing temperature (fig.3.6).

A detailed investigation of the degraded areas was performed by AFM analysis. The AFM images, reported in figure 3.14, provide information about the morphology of the BCP film after the high-temperature treatments. Upon annealing the BCP film at 310°C, few local inhomogeneities are evident as raised point-like areas (figure 3.14A). The copolymer layer starts corrugating as highlighted by the height profiles (figure 3.14C) along the sections marked in panel A. The film does not break, and the local arrangement of lamellae does not appear significantly different in the flat areas. Annealing at 330°C produces a large number of relatively small ruptured areas in the film with aligned lamellae arranged perpendicularly to the edges of the rupture (resembling the

[4]A quantitative analysis of this point will be widely presented in the next chapter.

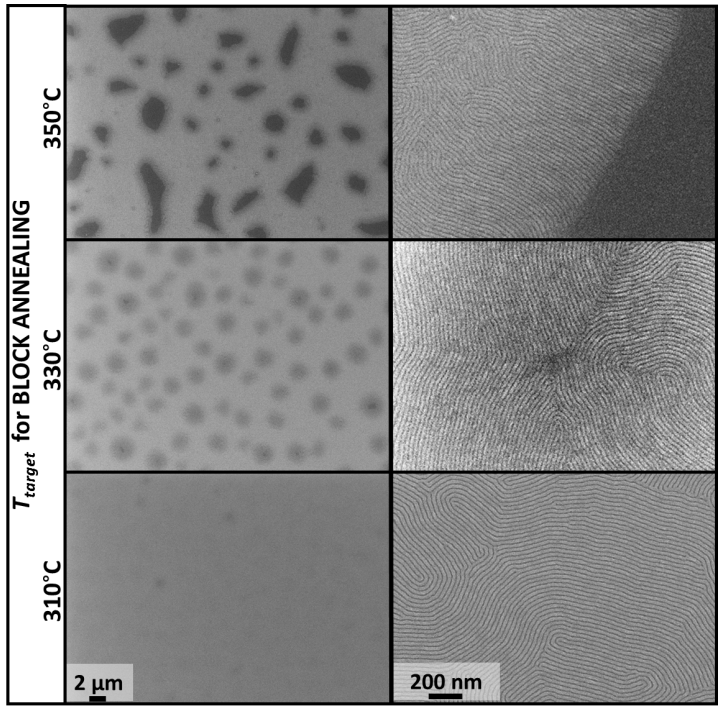

Figure 3.13: SEM plan view images of TR58 samples treated for 600 s at 330°C and then processed at different temperatures for 60 s, once B50 was spun. The right column reports enlargements of a small area of the corresponding images on the left.

same arrangment obtained with a low temperature grafting process). When the film is annealed at 350°C, ruptured areas appear larger than those in the sample annealed at 330°C (figure 3.14B). These areas are ∼25 nm higher than the nanostructured flat copolymer film and present a very flat top portion (figure 3.14D). Additionally, several raised pointlike inhomogeneities arise in the flat areas of the copolymer film. Moreover, the regions of the film rising to the degraded areas display an increased level of structural order than the portions of the film at a distance from these regions, often displaying lamellae arranged perpendicularly to the edge of the cracks (figure 3.14E).

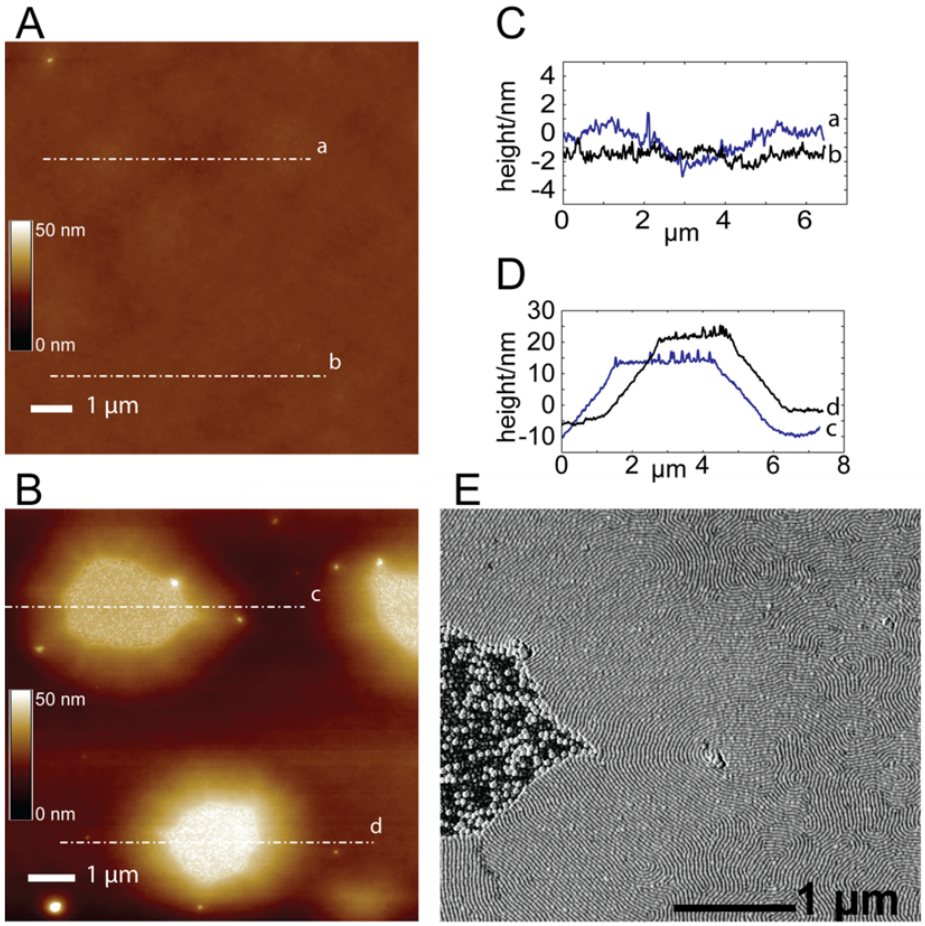

Figure 3.14: AFM analysis of B50 film annealed at different temperatures for 60 s. The BCP film was prepared on TR58 treated at 330°C for 600 s. (A) Tapping-mode topographic image showing the film after annealing at 310°C for 60 s. (B) Tapping-mode topographic image of BCP film annealed at 350°C for 60 s. (C, D) Traces of the height profiles along the sections marked in panels A and B, respectively. (E) Detail of the AFM tapping-mode phase signal showing the organization of lamellae in the proximity of the ruptured area on the BCP film annealed at 350°C.

The collection of the data shown in figure 3.13 and 3.14 states that the grafting treatment performed in RTP can be properly adjusted in order to improve the thermal stability of the TR58 brush layer.

By performing the grafting treatment at high temperature (330°C), the processing T_{target} for the following treatment for lamellar organization could be moved up to 310°C, gaining at least 20°C in respect to the preliminary shown results. Nevertheless, to find a way to get stable polymeric films even at higher T_{target} would mean to speed up lamellar ordering process and to improve the level of lateral order (as depicted in details in the next chapter).

3.4 End-group Changes to Improve RCP Thermal Stability: BrR58

This section focuses on the results obtained with a random copolymer with the same styrene composition and similar molar mass of TR58, but with a bromine end-group instead of the TEMPO moiety termination. This random copolymer was encoded as BrR58. This copolymer was chosen because the difference in the synthesis process itself guarantees a higher thermal stability with respect to TR58[5]. More details about RCPs preparation are reported in chapter 2.

In dealing with this new RCP, we characterized it as a proper neutralization brush layer running again trough the same routine described above for TR58.
Figure 3.15 reports the evolution of the thickness of the BrR58 brush layers after grafting treatments in RTP for 600 s at different temperatures. The overall trend once again displays a first steep increase (diffusion regime) which ends in a leveling around 8.5 nm (penetration-limited regime). This saturation level is about 3 nm higher than the one shown for TR58 due to the slightly higher molar mass of BrR58. The tendency to promote a perpendicular orientation of a lamellar layer was tested by depositing a B50 thin film above the grafted RCP layers and by annealing it in RTP to promote self assembly of the nanodomains. As highlighted in figure 3.15 the perpendicular orientation is achieved for almost every temperature in the analyzed range with the exception of the lower one, 170°C, for which the perpendicular orientation is not complete. In turn at 190°C the lamellar pattern has already reached a perfect perpendicular orientation (see the upper insert in fig. 3.15). For this reason in terms of BrR58 thickness, we approximately fixed the threshold for the perpendicular orientation of the BCP around 4 - 4.5 nm.

Figure 3.16 depicts the thickness dependence of BrR58 brush layers on t_{ann}. The grafting processes were run at 310°C, which is in the saturation region of figure 3.15.Thickness goes to the saturation level after the initial rapid increase. What is truly interesting is that even after the short annealing time of 30 s, the thickness is definitely above the previous defined threshold for the perpendicular orientation of symmetric BCP. This result demonstrates the possibility to properly neutralize the substrate by grafting a RCP film in a time scale that is fully compatible with the requirements of a lithographic application.

The thermal stability of the grafted polymeric chains was investigated by TGA-GC-MS analysis following the previous reported procedure (section 3.3). Figure 3.17 reports the

[5]The incidence of abnormal linkages, such as head-to-head and vinylidene ends, is substantially reduced in controlled radical polymerizations compared to conventional free radical polymerizations, thus increasing the thermal stability of the samples prepared by ATRP.[16] [17] [18]

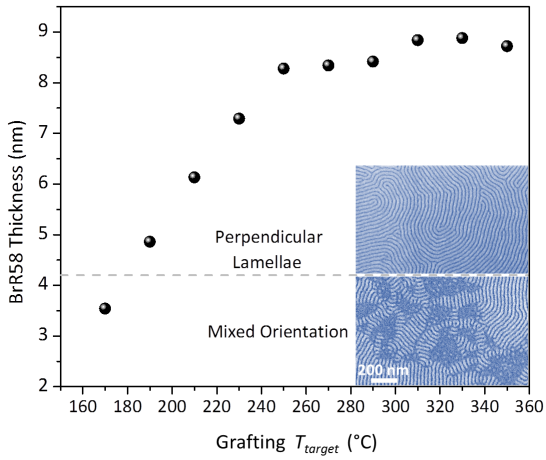

Figure 3.15: Thickness trend for BrR58 as a function of the grafting annealing temperature after 600 s of t_{ann} in RTP. The dash line approximatively indicates the limit of thickness above which the perpendicular orientation of the lamellar pattern is assured.

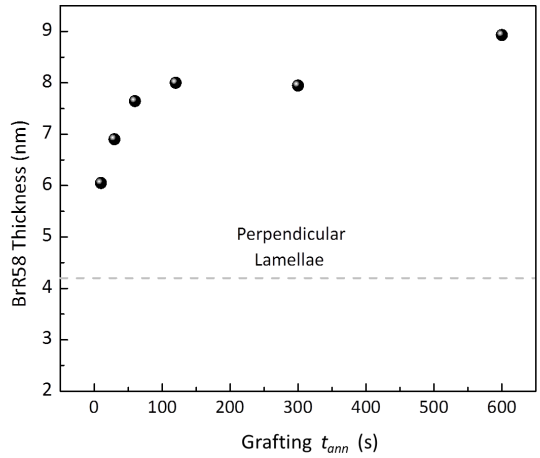

Figure 3.16: Thickness of the RTP grafted films of BrR58 at 310°C as a function of t_{ann}. All the samples report thicknesses in the perpendicular windows of orientation for BCP organization.

styrene evolution profiles for BrR58 thin film grafted on the substrate by RTP treatment at 230 and 330°C. The methyl methacrylate evolution (not reported) parallels that of styrene. The same figure reports the degradation contour profile (dashed line) of BrR58 in bulk, for comparison purposes. As already discussed, the RCP thin films grafted within RTP are definitely more stable than their bulk configuration irrespective of the temperature of annealing. Moreover, the degradation profile of the BrR58 thin sample is not significantly modified when increasing the grafting temperature from 230 to 330°C. This peculiar behavior is even more evident when looking at the entire range of temperature between 170 and 340°C, following the position of the maximum temperature of the degradation peaks, as reported in figure 3.18. The maximum of the degradation peak indeed displays only a smooth shift toward high temperatures as the grafting temperature increases.

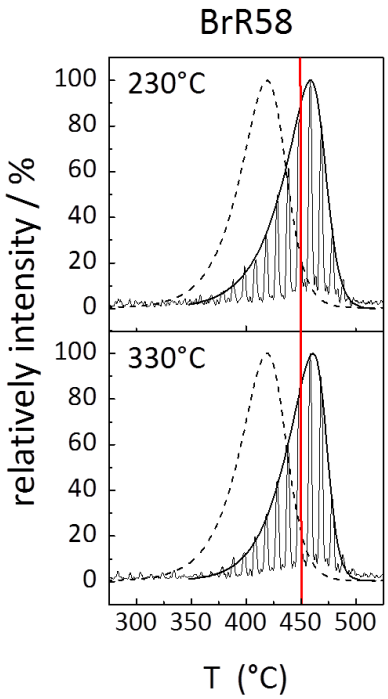

Figure 3.17: TGA-GC-MS analysis of styrene on BrR58 films after the grafting process performed at 230 or 330°C. The dashed curves represent the corresponding styrene profiles for the bulk samples. The red lines at 450°C were added as a visual guide.

The effective stability of the RCP layer, was tested by depositing a symmetric BCP thin film on top of the brush layer obtained by grafting the BrR58 thin films at temperatures ranging from 250 to 330°C for 600 s. The stack was finally annealed at 310°C for 60 s to probe its capability to withstand a severe thermal stress. Figure 3.19 reports the SEM plan view images of the self-assembled BCP thin film, obtained at two diffe-

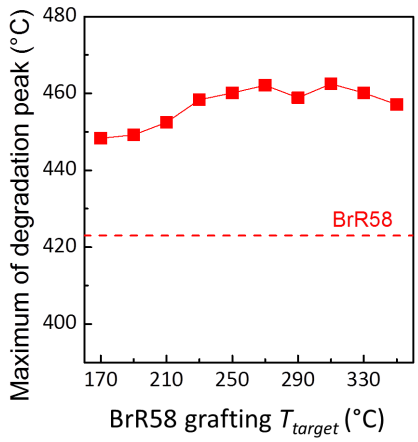

Figure 3.18: Maximum temperature of the degradation peak for BrR58 in the TGA-GC-MS analysis of the styrene evolution as a function of the grafting temperature. The horizontal line indicates the corresponding degradation temperature for the bulk sample.

rent magnifications as a function of the BrR58 RCP grafting temperature. The large-area SEM images provide no evidence of degradation phenomena occurring in the film. The enlarged SEM images demonstrate the occurrence of phase separation in the BCP layer and testify to the perpendicular orientation of the lamellar nanodomains with respect to the substrate. The comparison between the data illustrated in figures 3.11 and 3.19 clearly indicates that the thermal stability of BrR58 is definitely higher than that of TR58, in perfect agreement with the degradation results discussed above. Thus the more stable grafted BrR58 thin films allow for an increase in the temperature of process of BCP.

For a more detailed investigation of the thermal stability of BrR58, a DEP-MS analysis on the lower temperature loss peak of styrene has been carried out. Samples of BrR58 were deposited on the filament of the DEP tool, and then subjected to a grafting simulation treatment at different time and temperature. A successive temperature scan allows for tracing the evolution profile of the styrene monomer loss on a wide range of temperature as a function of the grafting temperature and time. Figure 3.20 displays the DEP-MS styrene evolution of BrR58 focusing on the secondary peak of styrene degradation that is observed at a lower temperatures compared to the main loss peak. This low temperature loss peak is present after the simulated grafting treatment of 600 s at 250°C, but it progressively disappears at 325°C as the annealing time increases. This data demonstrated that by performing a high-temperature grafting process a significant offset in the polymer degradation process is stimulated also in BrR58 polymer chains. A first hint of this effect was also predictable by observing the slight shift in the maximum of the degradation peak of figure 3.18. For this reason we investigated the limit of the thermal stability of the RCP (BrR58) + BCP (B50) system, in raising up the temperature of RTP process for block organization, while maintaining a constant high temperature (330°C) grafting process for the RCP layer.

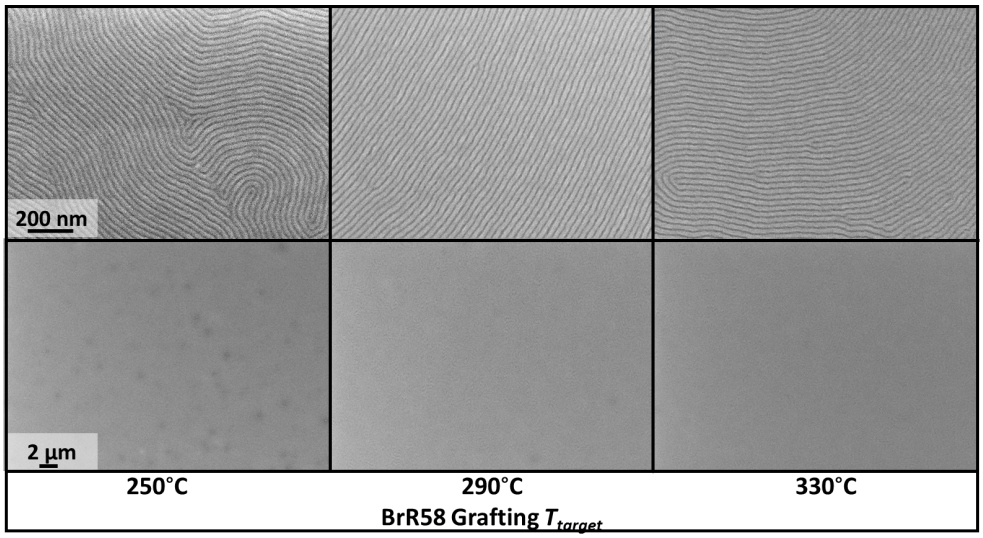

Figure 3.19: SEM plan view images of the self-assembled BCP thin film as a function of the BrR58 RCP grafting temperature obtained at two different magnifications.

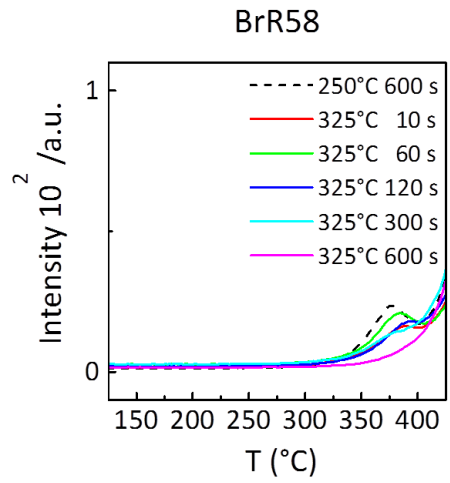

Figure 3.20: Styrene evolution profile for BrR58 subjected to the following thermal treatments: samples were first heated, with a heating rate of 20°C/s, in the mass spectrometer to 250°C and maintained at this temperature for 600 s (dashed line) or to 325°C and maintained at this temperature for different time periods and then cooled to room temperature. Finally the samples were analyzed with a heating rate of 1°C/s.

Figure 3.21 shows SEM images of BCP thin films deposited on a BrR58 RCP brush layer grafted at 330°C for 600 s. The BCPs were annealed for 60 s at temperatures ranging from 310 to 350°C. In the left column in figure 3.21, the SEM plan view images of large areas of the BCP thin films annealed at 310, 330, and 350°C are reported. In the right column enlargements of corresponding small area are presented. When the annealing temperature of the BCP layer was raised from 310 to 330°C, no significant variations in the homogeneity of the BCP film are observed. Conversely, the SEM image of the sample annealed at 350°C shows large areas of well-ordered lamellar pattern, with several bright micrometer-size spots appearing. These spots represent an inhomogeneity of the lamellar pattern which seems to be different from the films degradation discussed previously in section 3.3.

In order to deeper understand this new degradation phenomenon an AFM analysis

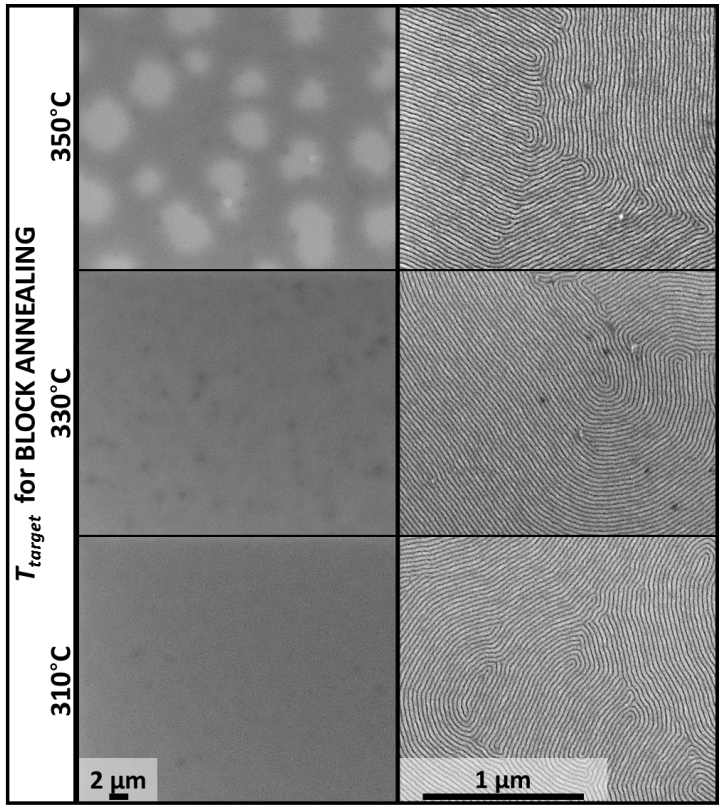

Figure 3.21: (left) The SEM plan view images of BCP films deposited on the BrR58 brush layer (grafted at 330°C for 600 s) and subsequently processed at 310, 330, and 350°C for 60 s. (right) The enlargements of a small area of the corresponding SEM images reported in the left column

was performed on the same samples. The BCP film annealed at 310°C shows an unperturbed flat surface with only very moderate long-range corrugations (figure 3.22, last row). When annealing the films at 330°C for 60 s, the film is still relatively flat and unperturbed. Occasionally, raised pointlike inhomogeneities are found at isolated locations on the surface (figure 3.22 central row), confirming the enhanced stability of the B50 film when spun on the BrR58 brush layer. Annealing at 350°C for 60 s generates a number

of micrometer-sized film inhomogeneities (figure 3.22 first row), as already evidenced by SEM analysis (figure 3.21). AFM images indicate that the nature of these inhomogeneities is significantly different from the film ruptures observed in the case of the B50 BCP film spun on TR58 brush layer. Upon annealing at 350°C, the B50 film deposited on the BrR58 brush layer exhibits large concavities without any evidence of film rupture. The lamellar nanoscale structure is preserved, and no significant discontinuities in the lamellar organization are observed along the concavities. This inhomogeneity could be tentatively ascribed to a thermal instability of the RCP layer, which would ask for further stabilization solution, or of the B50 layer. At the present moment a complete understanding of the effect needs for further investigation, but whatever the triggering cause of the inhomogeneity is, it clearly represents a new technological limit to the RTP processing of the system RCP+BCP.

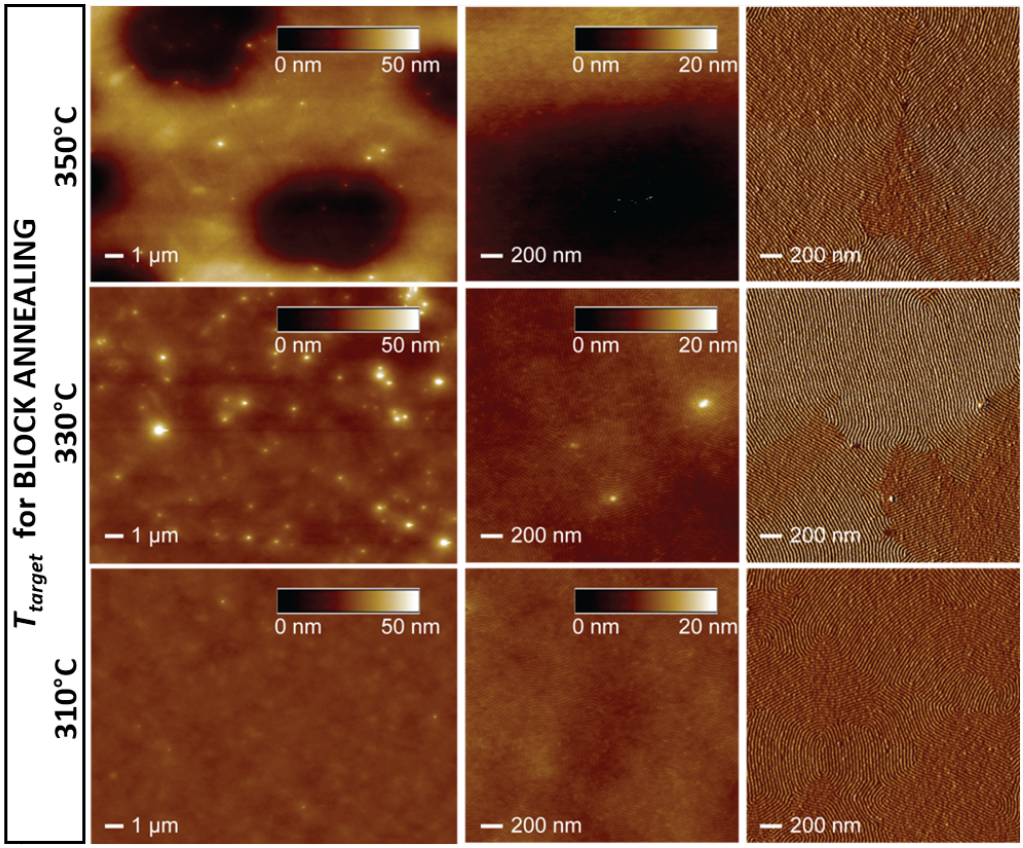

Figure 3.22: AFM analysis of B50 films annealed at different temperatures for 60 s after being spun on BrR58 treated at 330°C for 600 s. On the left and in the central column, the heights of the topographic features and their sizes are coded according to the color tables and scale bars. The tapping-mode phase signal images corresponding to the areas in the central column are outlined in the right column.

3.5 Recalling the Main Results of This Chapter

The thermal stability of RCP thin films can be highly enhanced by performing the grafting process at high temperature in a RTP machine.
Two different RCP were studied. The grafted TR58 RCP exhibited a relatively low thermal stability that limited the processing temperature of the RCP+BCP system at 310°C. The grafted BrR58 RCP presented a definitely more stable structure allowing for the processing temperature of the RCP+BCP system to be shifted up to 350°C. These widespread range of process temperature provides the possibility to deeply investigate the lateral order evolution of lamellar BCP, as depicted in the next chapter.

Bibliography

[1]F. F. Lupi, T. J. Giammaria, G. Seguini, M. Ceresoli, M. Perego, D. Antonioli, V. Gianotti, K. Sparnacci, and M. Laus, "Flash grafting of functional random copolymers for surface neutralization", Journal of Materials Chemistry C **2**, 4909 (2014).

[2]M. Ceresoli, F. Ferrarese Lupi, G. Seguini, K. Sparnacci, V. Gianotti, D. Antonioli, M. Laus, L. Boarino, and M. Perego, "Evolution of lateral ordering in symmetric block copolymer thin films upon rapid thermal processing.", Nanotechnology **25**, 275601 (2014).

[3]K. Sparnacci, D. Antonioli, V. Gianotti, M. Laus, G. Zuccheri, F. Ferrarese Lupi, T. J. Giammaria, G. Seguini, M. Ceresoli, and M. Perego, "Thermal stability of functional P(S-r-MMA) random copolymers for nanolithographic applications.", ACS applied materials & interfaces **7**, 3920–30 (2015).

[4]*ITRS Reports - www.itrs2.net/itrs-reports.html*.

[5]E. Han, K. O. Stuen, Y.-H. La, P. F. Nealey, and P. Gopalan, "Effect of Composition of Substrate-Modifying Random Copolymers on the Orientation of Symmetric and Asymmetric Diblock Copolymer Domains", Macromolecules **41**, 9090–9097 (2008).

[6]V. Gianotti, D. Antonioli, K. Sparnacci, M. Laus, T. J. Giammaria, F. Ferrarese Lupi, G. Seguini, and M. Perego, "On the Thermal Stability of PS- b -PMMA Block and P(S- r -MMA) Random Copolymers for Nanopatterning Applications", Macromolecules **46**, 8224–8234 (2013).

[7]C.-C. Liu, C. J. Thode, P. A. Rincon Delgadillo, G. S. W. Craig, P. F. Nealey, and R. Gronheid, "Towards an all-track 300 mm process for directed self-assembly", Journal of Vacuum Science & Technology B: Microelectronics and Nanometer Structures **29**, 06F203 (2011).

[8]A. V. Berezkin, D. V. Guseva, and Y. V. Kudryavtsev, "Formation of Linear and Graft Block Copolymers at a Polymer/Polymer Interface: How Copolymer Brush and Microdomain Morphology Control Heterogeneous Reactions", Macromolecules **45**, 8910–8920 (2012).

[9]L. S. Penn, H. Huang, M. D. Sindkhedkar, S. E. Rankin, K. Chittenden, R. P. Quirk, R. T. Mathers, and Y. Lee, "Formation of Tethered Nanolayers: Three Regimes of Kinetics", Macromolecules **35**, 7054–7066 (2002).

[10]G. Liu, L. Yan, X. Chen, and G. Zhang, "Study of the kinetics of mushroom-to-brush transition of charged polymer chains", Polymer **47**, 3157–3163 (2006).

[11]R. Hasegawa, and M. Doi, "Dynamical Mean Field Calculation of Grafting Reaction of End-Functionalized Polymer", Macromolecules **30**, 5490–5493 (1997).

[12]R. Lehrle, and A. Shortland, "Reproducibility of filament pyrolysers: Influence of sample deposition and other factors", European Polymer Journal **29**, 1277–1282 (1993).

[13]R. Lehrle, D. Atkinson, D. Bate, P. Gardner, M. Grimbley, S. Groves, E. Place, and R. Williams, "Diagnosing mechanisms of oligomer formation in the thermal degradation of polymers", Polymer Degradation and Stability **52**, 183–196 (1996).

[14]L. E. Manring, "Thermal degradation of poly(methyl methacrylate). 2. Vinyl-terminated polymer", Macromolecules **22**, 2673–2677 (1989).

[15]T. P. Russell, R. P. Hjelm, and P. A. Seeger, "Temperature Dependence of the Interaction Parameter of Polystyrene and Poly(methy1 methacrylate)", Macromolecules **23**, 890 (1990).

[16]C. Granel, P. Dubois, R. Jérôme, and P. Teyssié, "Controlled Radical Polymerization of Methacrylic Monomers in the Presence of a Bis(ortho-chelated) Arylnickel(II) Complex and Different Activated Alkyl Halides", Macromolecules **29**, 8576–8582 (1996).

[17]G. Moineau, M. Minet, P. Dubois, P. Teyssié, T. Senninger, and R. Jérôme, "Controlled Radical Polymerization of (Meth)acrylates by ATRP with NiBr 2 (PPh 3) 2 as Catalyst †", Macromolecules **32**, 27–35 (1999).

[18]D. Colombani, M. Steenbock, M. Klapper, and K. Müllen, "1,3,5,5-tetraphenyl-Δ3-1,2,4-triazolin-2-yl radical–properties in the controlled radical polymerization of poly(methyl methacrylate) and polystyrene", Macromolecular Rapid Communications **18**, 243–251 (1997).

CHAPTER 4

Lateral Order of Symmetric BCPs on Featureless Substrate

This chapter reports the most important results obtained on the study of the lateral order of symmetric BCPs thin films, when deposited on featureless substrate and processed by means of a RTP machine.

The first section highlights the immediate improvements assured in terms of reduction of the annealing time and increase of the correlation length values obtained by processing the BCP thin films at high temperature in a RTP machine.[1] [2].

The second section presents a deep investigation of the mechanism that drives lamellar ordering during the RTP treatment. The peculiar role played by the residual solvent naturally trapped in the polymeric film during the spin coating procedure is addressed and a picture of the morphology evolution of the system explaining the overcoming of the topological limits to lateral order is provided. [3]

In the last part of the chapter the relationship between the thermal stability of thin polymeric films and the effective processing parameters is investigated in details providing quantitative information about the lateral order evolution in the BCP thin film. This gives the possibility to deal with lamellar ordering from a systematic point of view, introducing a study of the activation energy involved in the process.[4]

4.1 From Furnace to RTP: Flash Ordering

The level of order of BCP thin film could be evaluated from SEM images of the samples through the determination of the correlation length ξ (chapter 2). A comparison between the measure of the correlation length of symmetric BCPs thin films submitted to the two distinct procedures, a standard annealing process in a furnace and a RTP treatment, is depicted in the top panel of figure 4.1. The black circles represent the ξ values reported in literature for a 100 minutes long furnace annealing at 190°C in vacuum.[5] The light-blue circles represent the ξ values obtained from the SEM images in the bottom panel of the figure, for the same BCP treated in RTP for 10 minutes. The correlation length relative to the annealing temperature of 190°C is equivalent, within the experimental error for the two different thermal approaches employed.
A simple method to increase the correlation length is to raise the annealing temperature.[6] This method has been demonstrated to be effective on pre-patterned substrates for symmetric and asymmetric BCPs, but it results quite fruitless with symmetric BCPs

on featureless substrates. Lamellar lateral order, indeed, presents only a week dependence on the temperature of annealing. Open circles in figure 4.1 report a slightly change between 42 and 64 nm in the ξ values over more than 100°C of temperature variation. These extremely low correlation length values were explained in terms of topological constraints, which prevent fast coarsening in the lamellar phase. [7]
A completely different scenario occurs when symmetric BCP films are submitted to RTP treatments of 10 minutes (full circles in fig.4.1). These data highlight the significant variation in the lateral ordering of lamellar thin films on featureless substrate when changing thermal annealing conditions and demonstrate, at the same time, the possibility of obtaining high ξ values in very short periods of time. According to these data, RTP provides substancially different results compared with conventional furnace treatment, overcoming the topological constraints that are usually considered the origin of the limited correlation length evolution in lamellar BCP thin films.

4.2 RTP: a new ``solvent-assisted´´ thermal treatment

In order to obtain more specific insight into the principles that drive the morphological development of BCP thin films due to RTP treatment, we focus on the dynamics of the grain coarsening as a function of t_{ann} at the three higher temperatures reported for RTP in fig.4.1. It is worth noticing that the evolution of the lateral order has been investigated even for very short time of annealing ($1 < t_{ann} < 600$ s). The use of radiation sources and the constant temperature control validate RTP as the proper technique to investigate the very early stages of self-assembly, from the early phase separation to the final organization of a lamellar thin film. [2] All the samples discussed in this section were fabricated following the general procedure described in section 2. In particular, all the substrates were neutralized by grafting TR58 with a RTP treatment of 600 s at 250 °C. B50 was then submitted to different RTP treatments as highlighted in the following paragraphs.

4.2.1 Pattern Evolution ξ vs. t_{ann}

Fig. 4.2 reports the sequence of SEM images illustrating the time evolution of the lamellar microdomains at T_{target} = 250, 270, and 290 °C. Measurements at temperatures higher than 290 °C were prevented by the degradation of the random copolymer brush layer. For the shortest annealing time (t_{ann} = 1 s), a clear signature of phase separation is observed at all annealing temperatures, although the specific temperature affects both the lateral ordering and the morphology within the microdomains.
In fact, poor lamellae ordering is observed in the sample annealed at 250 °C whereas, in the samples annealed at 270 and 290 °C, the lamellae are much more defined. In addition, in the samples annealed at 250 and 270 °C, a peculiar morphology is observed including both cylinders and lamellae perpendicularly oriented to the substrate. Conversely, in the sample annealed at 290 °C, small sized lamellar microdomains are mainly detected and only few and isolated cylinders are distinguishable.

It is important to recognize that all the samples were heated up at the constant heating rate of 18 °C/s, which corresponds to about 6 s heating time to move the system from a temperature at which the ordering is extremely slow (see for example the 190 °C point in figure 4.1 where RTP still reproduces the same correlation length of standard furnace though in shorter time of annealing) to the final T_{target}. Consequently, the 1 s annealing

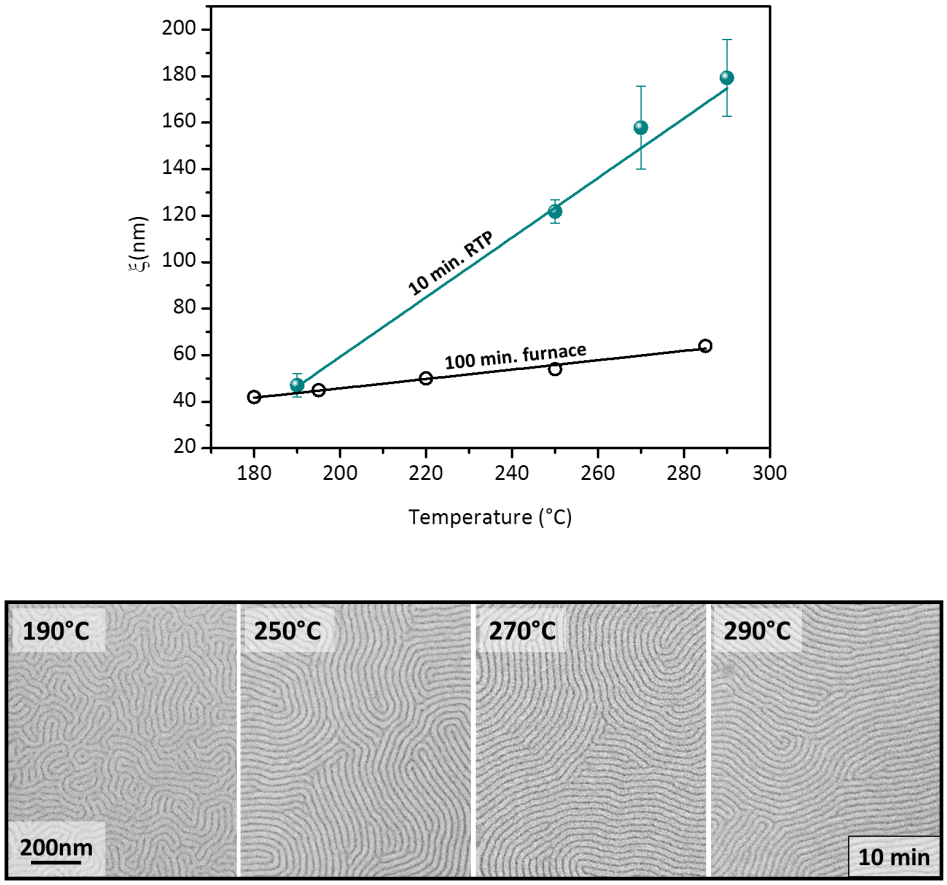

Figure 4.1: Top panel: correlation length values for B50 samples annealed in RTP for 10 minutes at different temperatures (full circles), compared with literature results obtained for the same copolymer treated in a conventional furnace for 100 minutes (open circles).[5] Straight lines are drawn to guide the eyes. Bottom panel: SEM images of B50 samples annealed in RTP for 10 minutes at different temperatures.

time is almost negligible compared to the overall thermal budget and the corresponding morphologies should be considered just as snapshots of the evolution of the system during the heating and cooling stages. In this frame, although a complete picture of the system evolution during the transient stages is still lacking[1], the above data suggest a well-defined path for striped pattern formation involving a transition through a perforated lamellar phase that rapidly evolves to the final lamellar morphology, in agreement with previously reported data on symmetric PS-b-PMMA at 190 °C.[1] For $t_{ann} \geq 5$ s, no more evidence of perforated lamellae is observed and the samples show well-defined

[1] A more complete overview of the transient and isothermal stages of RTP treatment is reported in section 4.4 where a wide range of temperatures is under study.

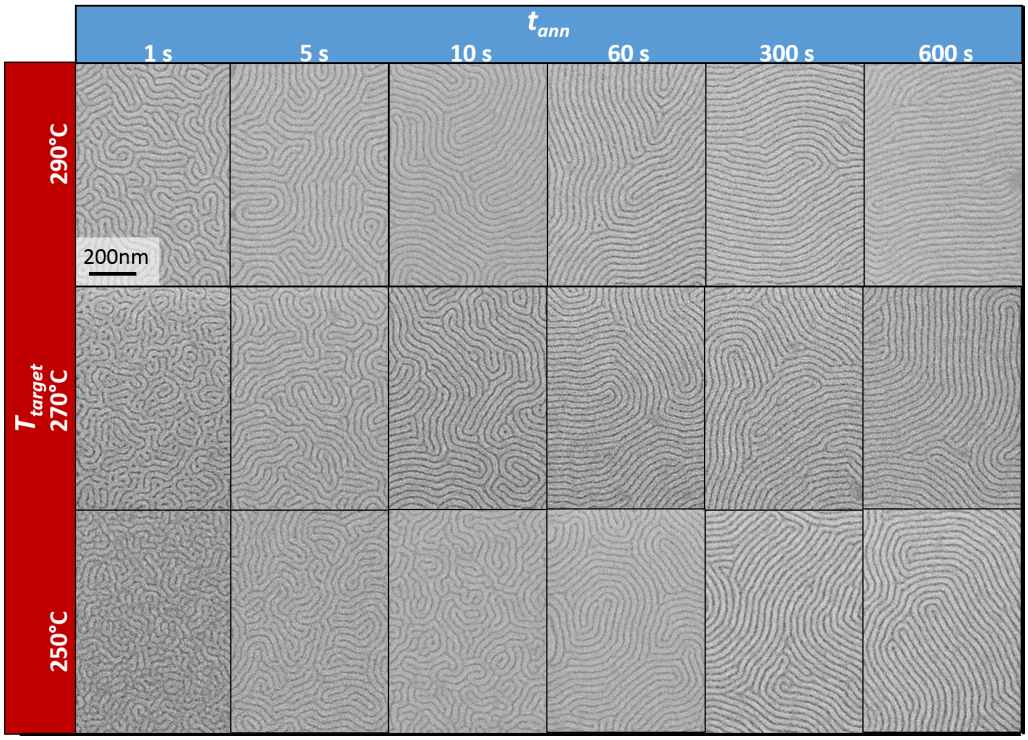

Figure 4.2: Plan view SEM images of B50 films annealed at different temperatures (T_{target}= 250, 270, and 290°C) for different time periods (t_{ann} from 1 to 600 s). The images were acquired after oxygen plasma-etching steps for 60 s in order to remove the PMMA phase and enhance the contrast.

lamellar microdomains, perpendicularly oriented with respect to the substrate.
The lateral organization of the lamellar domains depends on the annealing temperature and time. Within this time frame, the high temperature isothermal stage (T_{target}) predominates over the initial transient period and drives the system evolution towards the final thermodynamic equilibrium condition. In particular, irrespective of the T_{target}, a progressive and significant reduction of defect density is observed as the t_{ann} increases, thus ultimately leading to an increase in the ordering level within the striped patterns.
According to the SEM images reported in fig. 4.2, the self-assembly process in the block copolymer thin film exhibits a strong time and temperature dependence, in contrast with previously reported data.[8] [9] [10]
To monitor the coarsening of the lamellar microdomains at different T_{target} as a function of time, the correlation length ξ values were determined from the above SEM images, following the procedure described in the Experimental Methods and are collectively reported in fig. 4.3 for the different annealing temperatures T_{target}. The correlation length ξ values of the samples annealed at 250 °C for 1 and 5 s and of the sample annealed at 270 °C for 1 s are not included, since their low ordering degree prevented the accurate determination of the correct ξ values. Moreover, in the case of the samples annealed at 290 °C, the point corresponding to t_{ann} = 1 s has not been included in the power law fitting of the data, since it is not representative of the evolution of the system in the isothermal stage but typifies the result of the system evolution during the transient stage.

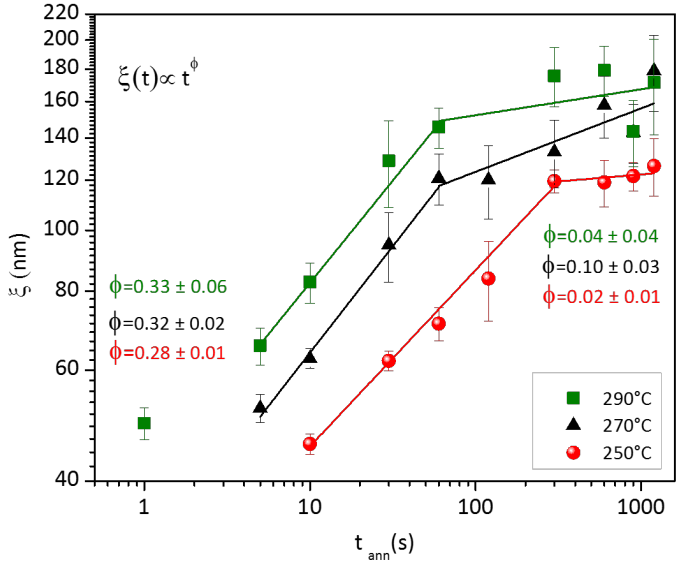

Figure 4.3: Correlation length ξ of the lamellar pattern of B50 thin films as a function of the annealing time at different temperatures

Irrespective of the temperature, the correlation length increases steeply at first and then more gradually as a function of t_{ann}, with a well-defined threshold, which depends on the temperature, thus suggesting the occurrence of two distinct growth regimes. These two regimes are characterized by power laws with markedly different growth

exponents (ϕ). In the fast coarsening regime, an average ϕ value of 0.29 $\pm$ 0.01 is determined whereas, in the slow coarsening regime, ϕ values are more scattered ranging from 0.02 $\pm$ 0.01 to 0.10 $\pm$ 0.03, with an average ϕ value of 0.03 $\pm$ 0.01. The latter growth exponents are perfectly consistent with those reported in the literature pointing to very limited or even no coarsening in perpendicularly oriented symmetric block copolymers.[10] [8] In contrast, the growth exponent corresponding to the initial fast coarsening regime indicates a very effective coarsening process with experimental growth rates equivalent to those observed in sphere or cylinder forming block copolymers.[11] [12]
In the present system, the growth rate values measured during the fast ordering regime correspond to the maximum allowable value for non-entangled polymers having an interconnected matrix, as is the case of asymmetric block copolymer systems. In a somewhat parallel fashion, the growth exponents observed in the slow ordering regime equal those expected in the case of pattern formation in systems without an embedding matrix, as is the case of symmetric block copolymer systems. It is worth to note that the absolute values of the correlation lengths at relatively short annealing times (t_{ann} = 60 s) are much higher than those reported in the literature, for the same block copolymer sample, after very long furnace annealing at the same temperatures. In particular, ξ values from 42 to 64 nm were reported by Ruiz *et al.* for annealing temperatures ranging from 180°C to 285°C and t_{ann} = 6000 s, thus demonstrating a very limited temperature dependence of the final correlation length values (data reported in fig.4.1). In our experiment, ξ values well above 120 nm were obtained at all temperatures in a time scale that is two orders of magnitude lower than the one reported by Ruiz and coworkers.[10]

4.2.2 Morphology Evolution

The morphology throughout the polymeric film was investigated by top-down SEM analysis after oxygen plasma-etching for different time periods. Fig. 4.4 reports the plan view SEM images of the samples annealed at 250, 270, and 290°C for t_{ann} = 1 and 600 s. The morphology of the samples is compared after oxygen plasma-etching times of 60 and 120 s. The SEM images reveal that, irrespective of the annealing temperature, in the samples annealed for 1 s (Fig. 4.4, left side), the perpendicularly oriented lamellae did not propagate through the entire polymeric film and the samples exhibit two closely connected morphologies suggesting the presence of hexagonally packed PMMA cylinders perpendicularly oriented with respect to the substrate underlying the lamellar arrangement. In contrast, the samples annealed for 600 s (Fig. 4.4, right side) exhibit no evidence of cylindrical phase even after prolonged plasma etching. In these samples, the removal of the PMMA phase produces a collapse of the structure due to the reduced mechanical stability of the PS lamellae after the removal of the PMMA phase, thus further supporting the idea that the lamellae spread through the entire film thickness.[13]
To better clarify the observed peculiar morphology, fig. 4.5.a) reports a SEM plan view image of the sample annealed at 250°C for 60 s, after prolonged oxygen plasma exposure. The removal of the PMMA phase clearly confirms the presence of a double morphology. The Fast Fourier Transform (FFT) of a small portion of the image (insert of fig. 4.5.a)) indicates the existence of a phase with hexagonally packed PMMA cylinders that appears to be self-registered with the lamellar structures at the top of the surface. A further

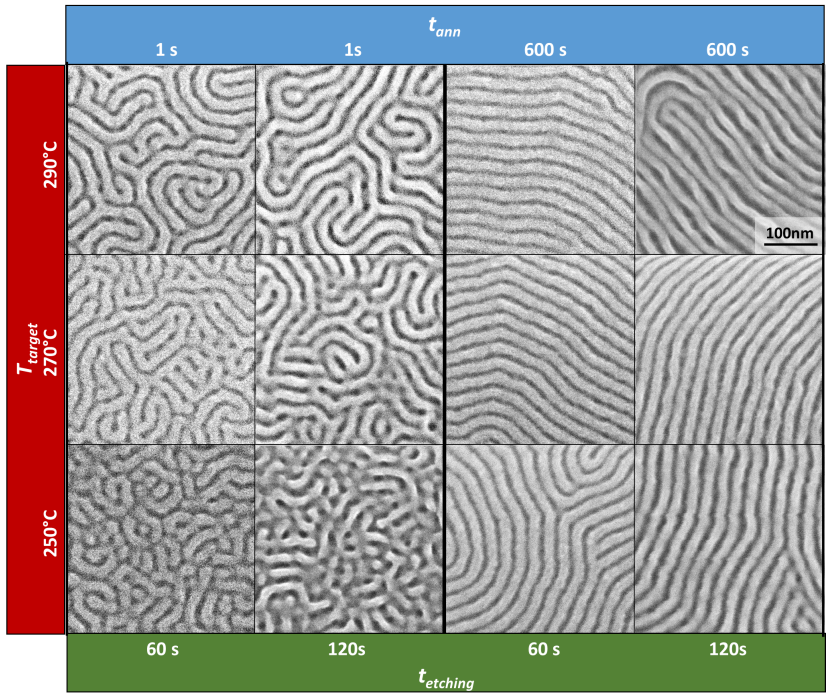

Figure 4.4: SEM Images of the samples annealed at 250, 270 and 290°C for 1 s (left) and 600 s (right) after oxygen plasma-etching steps for 60 s and 120 s respectively. For short annealing times, the lamellae did not propagate through the entire film thickness and the samples exhibit the signature of a double-layer structure with lamellae at the top and cylinders at the bottom.

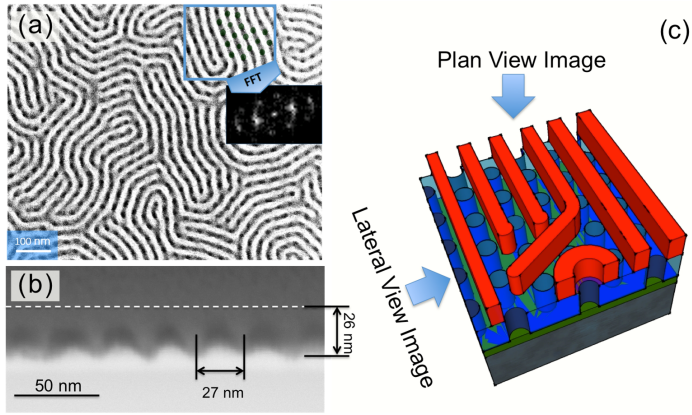

Figure 4.5: SEM plan view (a) and STEM cross-sectional (b) images of the sample annealed at 250°C for 60 s after prolongued oxygen plasma exposure. A cylindrical phase perfectly registered with the lamellar pattern on the surface, is observed, as schematically sketched in the picture on the right (c).

confirmation of this structure is provided by the cross-sectional STEM[2] analysis of the same sample reported in fig. 4.5.b). After the removal of the PMMA phase, the sample was prepared for STEM analysis and the polymeric layer was covered by a protective AuPd thin film. The bright underlying region in the picture corresponds to the substrate. The grey area on top shows the protective AuPd layer deposited that replaced the PMMA phase. The white dashed line indicates the original thickness of the polymeric film. The cross-sectional image confirms the presence of two closely connected lamellar and cylinder structures through the film thickness. The periodicity of the underlying cylindrical structures was determined to be around 27 nm, in good agreement with the characteristic length $L_0 \sim 27$ nm of the lamellar phase for this specific PS-b-PMMA block copolymer.
This experimental evidence further supports the idea of a continuous evolution of the microdomain morphology along the direction perpendicular to the film thickness. The combination of plan and cross-sectional images rules out the possibility of parallel cylinder formation at the surface of the polymeric film and clearly indicates that the morphology of the film is characterized by two closely connected lamellar and cylinder structures, as schematically represented in fig. 4.5.c). Surprisingly, this picture is consistent with the one previously reported by Sakurai et al. [14] in the case of a thermally induced morphology transition from cylindrical to lamellar microdomains in bulk poly(styrene-b-butadiene-b-styrene) block copolymer samples. Despite the fact that di-block and tri-block copolymers have vastly different phase spaces, the similarities between the morphologies of the two systems suggest that a homologous mechanism could be accounted for the transition via coalescence of cylinders without translation of their center-of-mass. Fig. 4.6 describes the morphology evolution as a function of the annealing time of the samples annealed at 290°C, for three etching times ($t_{etching}$ = 60, 120, and 210 s). After the short plasma-etching process (60 s), the presence of the cylindrical phase is evident only in the sample annealed for 1 s whereas, for longer annealing times, the SEM images reveal lamellae perpendicularly oriented to the substrate. After $t_{etching}$ = 120 s, the SEM images reveal a quite different picture indicating the presence of a cylinder phase also in samples annealed for 10 s. A further increase in the plasma-etching time (210 s) reveals a trace of a cylindrical phase even in the sample annealed for 60 s and finally demonstrates the absence of this phase in the polymeric films when the annealing time is longer than 60 s. The above data confirm the idea of two closely connected lamellar and cylinder structures and demonstrate that a transition from the cylindrical phase to the lamellar one occurs during the annealing process and matches the progressive increase in the lateral ordering of the film. Similar results were obtained for the films annealed at 270 and 250°C, with the disappearance of the cylindrical phase occurring at progressively higher t_{ann} values when decreasing the annealing temperature.

4.2.3 Solvent Dynamics

The occurrence of a cylinder morphology, in which the cylinders consist of PMMA, in a film of a symmetric PS-b-PMMA block copolymer suggests that a consistent amount of toluene, which is a preferential solvent for PS, could be entrapped in the film.[15] A related, although reverse, situation was described in the case of a symmetric PS-b-PMMA block copolymer solvent-annealed with the PMMA-selective acetone vapor.[16] In that

[2]The Scanning Transmission Electron Microscopy analysis was carried out by Nano Facility Piemonte, Electromagnetism Division.

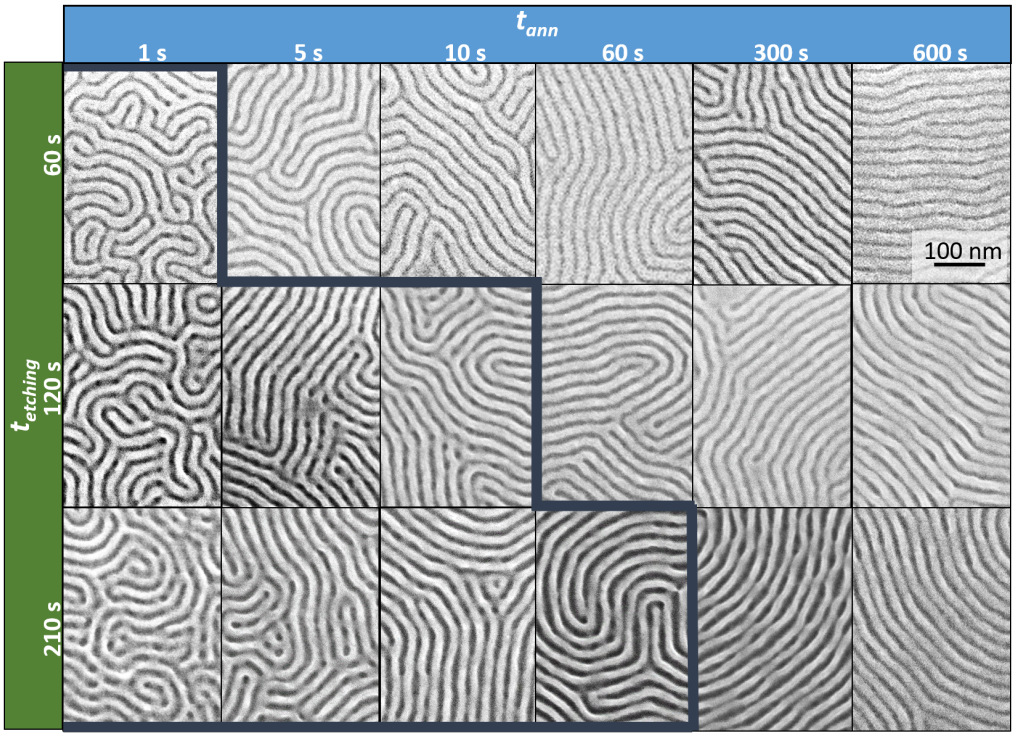

Figure 4.6: Top-down SEM images of 30 nm thick B50 films annealed at 290°C for times ranging from 1 to 600 s after different oxygen plasma-etching times (60, 120 and 210 s). The blue line highlights the samples in which the presence of a cylindrical phase registered with the lamellar-structure is observed.

case, the block copolymer films showed a parallel orientation of the cylindrical PS microdomains over the underlying perpendicular PS cylinders on the substrate. Successive thermal annealing allowed a structural reorganization to take place leading to the equilibrium morphology with the perpendicular orientation of the lamellar microdomains. It is worth noting that, the occurrence of orientation flipping of the nanodomains in cylinder forming PS-b-PMMA thin films confined within topographically defined structures during high temperature thermal treatments in a RTP machine, was recently observed.[17] This peculiar behavior has already been noticed in confined BCP thin films treated via solvent annealing [18], but has never been reported to occur during conventional thermal treatments. The mechanism underlying this evolution of the nanodomain orientation was identified and directly connected to the progressive de-swelling of the film, due to progressive desorption, during the thermal treatment, of the solvent naturally retained in the film. On the basis of these experimental evidence, all the steps involved in the sample preparation were reconsidered from the residual toluene point of view. The absolute amount of toluene in the polymer films was determined by GC-MS analysis after proper extraction in dichloromethane.[3] The extraction conditions were found to be extremely critical and very long extraction times should be employed. The absolute amount of toluene and the geometric characteristics of the films are reported in the following table while, for clarity, all the data in the following discussion are ex-

pressed in terms of the relative volume amount (V_r) of toluene using the toluene bulk density[3].

t_{ann} (S)	250°C				270°C				290°C			
	Toluene (ng)	Sample area (mm^2)	TR58 (nm)	B50 (nm)	Toluene (ng)	Sample area (mm^2)	TR58 (nm)	B50 (nm)	Toluene (ng)	Sample area (mm^2)	TR58 (nm)	B50 (nm)
1	413.8	103.1	5.5	23.7	268.2	95.7	5	22.9	219.6	91.9	5.1	25
5	308.6	88	5.4	23.2	227.6	84.8	5	23.6	184.7	78.4	4.8	25.1
10	337.8	110.6	5.2	22.1	225.7	85.3	5	23.8	215.5	95.8	4.6	25.3
60	283.5	101.2	5.1	22.9	235.9	95.3	5.1	22.7	214.1	100.8	4.8	25.8
300	274.5	102.6	4.9	24	218.1	93.3	5	21.3	187.8	96.0	4.6	25.7
600	238.7	89.9	4.5	24.3	231.2	102.7	4.9	21.1	187.8	97.8	4.8	26
900	233.1	91.6	5.5	23.2	224.3	108.9	4.9	21.2	154.9	82.9	4.4	27.1
1200	220.2	85.7	5.3	24	201.2	98.8	5	21.5	153.7	82.3	4.8	27.1

The relative volume amount of toluene after spinning TR58, but before the thermal treatment to perform the grafting reaction, is V_r = 5.9 $\pm$ 0.4% which reduces to V_r = 4.5 $\pm$ 0.1% after the RTP treatment at 250°C for 600 s. It is interesting to note that although the grafting treatment in RTP is performed at high temperature, the decrease of toluene content is quite limited thus indicating that the toluene is strongly retained in the random copolymer layer. After the washing step to remove the non-grafted TR58 fraction, the toluene amount increases up to V_r = 23.5 $\pm$ 0.3% . The block copolymer B50 was then spin coated on the above random layer and the total amount of toluene averaged over the total thickness of the film, which includes both the random and the block copolymer layers, results V_r = 26.2 $\pm$ 0.3% . These data clearly indicate that the amount of naturally trapped solvent within an ultrathin polymer layer is very high prior to thermal treatments.

Numerous studies were performed to address the solvent retention and distribution in polymeric films. In as-cast thin polystyrene films, the mass fraction of residual toluene was determined by GC, and increased from 2% to 35% with decreasing film thickness (500 to 15 nm). In addition, the amount of toluene reduced to 9% after annealing at 115°C for 16 h, thus indicating that the solvent is retained even in dried films. This finding was also confirmed [19] in absorption/desorption experiments of toluene in several methacrylate polymer films, where some toluene remains trapped even after heating to 50°C for 12 h. Neutron reflectivity, employed to determine the amount of residual solvent in PS, [20] PMMA [21] as well as in PS-b-PMMA samples,[22] [23] confirmed that a

[3] $V_r = [V_t/V_{total}] \times 100$ where V_{total} is the total volume of the polymeric material and toluene estimated from the thickness of the film and the area of the substrate and V_t stands for the toluene volume retained in the film, calculated from the absolute amount of toluene M_t, $V_t = M_t/\rho_t$ where ρ_t is the bulk density of toluene (0.867 g m L^{-1}).

significant amount of toluene as a residual solvent (9% to 15% volume fraction) remains in as-cast films after spin coating. The solvent evaporation during the spin coating process results in an increase in the polymer concentration at the polymer–air surface thus ultimately leading to the formation of a vitrified skin. In turn, the presence of this skin creates a barrier for further solvent evaporation thus inhibiting the transport of solvent out from the film. Consequently, the concentration of the solvent at the polymer–air surface is the lowest one and a gradient in the solvent concentration should develop normal to the surface. In addition, a tendency for the solvent to accumulate near the solid substrate was suggested, due to entropy effects.
To understand the solvent dynamics in the present system, three series of samples, consisting of the block copolymer spin coated on the grafted random copolymer layer, were prepared with exactly the same procedure and were subjected to RTP processing at the same temperatures and for the same time periods of the samples for which the correlation lengths were estimated. Fig. 4.7 reports the relative volume amount V_r of toluene at 250, 270, and 290°C as a function of t_{ann}.

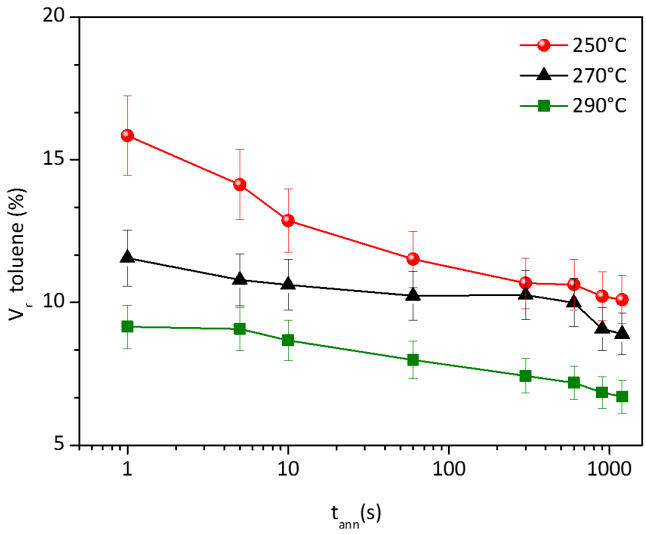

Figure 4.7: Relative volume amount of toluene in B50 thin films deposited on TR58 brush layers as a function of annealing time at different temperatures.

During the thermal treatment, consisting in heating the sample at 18 °C/s from room temperature to T_{target} followed by 1 s at T_{target} and cooling to room temperature, a significant reduction of the solvent content is observed, thus indicating the occurrence of a fast evaporation of the solvent. When T_{target} is 250°C, the solvent amount reduces by 40% of the initial value whereas more than 70% of the solvent evaporates when T_{target} is 290°C. A slight but continuous decrease of the residual toluene is further observed at all temperatures when increasing the annealing time. At the end of the RTP process, a significant amount of residual toluene is still present, ranging from 10 to 7% corresponding to the annealing temperature of 250 and 290 °C, respectively. These data indicate that the solvent evaporation occurs in two distinct stages: a fast stage during heating to the annealing temperature followed by a relatively slow stage once this temperature is reached.

4.2.4 Ordering Mechanism

Comparison of the solvent dynamics with the pattern and morphology evolution clearly indicates that the residual toluene strongly biases the ordering mechanism. Figure 4.8 depicts a schematic diagram that correlates the morphology evolution of the polymeric film with the progressive desorption of the solvent within the layer during the RTP treatment. The experimental data bear out a significant reduction of solvent content during the initial heating period of the thermal treatment. In agreement with a previously proposed ordering mechanism driven by solvent evaporation [24], the burst of solvent is expected to cause an ordering front to propagate throughout the film and to provide a field gradient which assists the perpendicular orientation of the phase separated structures. At the same time, a solvent gradient develops across the layer. The lowest toluene concentration is expected to be located at the free surface of the film while the maximum concentration is located at the polymer/substrate interface. In this context, it is relevant to notice that the toluene amount in the layers of the random and block copolymers could be different, implying a more complex solvent concentration profile along the film. Anyway, such a solvent gradient accounts for the occurrence of the closely connected lamellar and cylinder structures. Indeed in the solvent-poor region of the film close to the free surface, the phase separation results in the formation of lamellar structures as expected for symmetric block copolymers.
Conversely, inside the solvent-rich polymer/substrate interface, as toluene is a preferential solvent for PS, a selective partitioning occurs with preferential swelling for the PS block. This causes an increase in the relative volume fraction of the PS blocks and, when the toluene concentration is sufficiently high, the differential volume change in the swollen state of the PS and PMMA blocks leads to a local order-to-order transition from the expected lamellar morphology to the cylinder one, thus ultimately producing a self-registered structure with lamellae at the upper side of the film and cylinders at the lower side. The progressive solvent evaporation, which occurs during the isothermal annealing period, decreases the differential volume change between the swollen PS and PMMA blocks thus making the cylinder phase metastable so that the PMMA cylinders evolve into lamellae thus progressively moving vertically down the lamellae/cylinder interface until the random layer is reached and the cylinder structure totally disappears.

A clear correlation between the solvent content and the evolution of this double morphology can be obtained looking at the images of the sample annealed for 1 s at different temperatures that are reported in fig.4.4. Apart from the different level of lateral ordering achieved in the superficial lamellar structure, the investigation of the in depth morphology, performed by increasing the duration of the O_2 plasma treatment, revealed a variation of the relative volume occupied by the two phases in the polymeric film: the higher the annealing temperature, the lower the solvent content, the deeper the propagation of the superficial lamellar phase in the polymeric film.
This vanishing cylindrical phase plays a fundamental role in the ordering kinetic of the lamellae. As previously discussed, pattern coarsening in symmetric block copolymer thin films is usually limited by topological constraints resulting in a quite slow kinetics. For perpendicular lamellae, the correlation length values ξ are reported not to change significantly with time and temperature. Just remind that growth exponents $\phi \sim 0.02$ and $\phi \sim 0.14$ are reported for PS-*b*-PMMA block copolymers with molecular weight M_n = 46 kg mol^{-1} and M_n = 32 kg mol^{-1}, respectively.[10]
Conversely, cylinder forming asymmetric block copolymers exhibit a faster ordering ki-

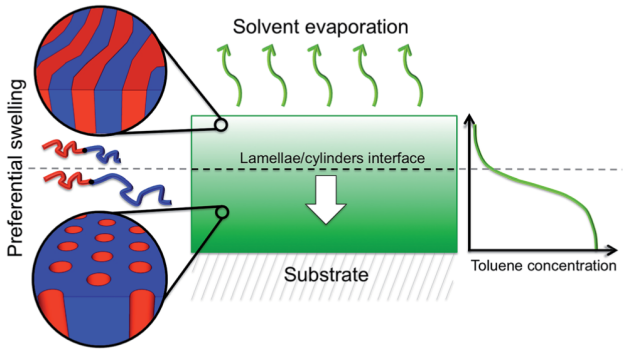

Figure 4.8: Schematic diagram of the solvent evaporation and morphological evolution in the block copolymer thin film during the RTP treatment. A gradient in the concentration of the solvent is established normal to the film surface with the solvent concentration progressively increasing with depth. This increase in solvent concentration induces a preferential swelling of the PS component in the macromolecules close to the film/substrate interface thus leading to a transition from the lamellar to cylindrical phase through the film thickness. As the solvent evaporates, the order-to-order transition front propagates through the film producing highly ordered and perpendicularly oriented lamellar microdomains.

netic since their topological structure provides an alternative path for layer breaking thus significantly decreasing the energy barrier for defect annihilation and consequently boosts the coarsening process in this system.[10] Coarsening in cylinder forming block copolymers has been investigated by several authors both in the bulk phase and in thin films. Bulk cylindrical phase block copolymers have been reported to coarsen with a power law $\xi \propto t^{1.06}$.[25] Harrison *et al.* first reported a growth exponent $\phi \sim 0.25$ for asymmetric block copolymer thin films with parallel orientation of the cylinders with respect to the substrate.[11]. Based on topological considerations, the coarsening kinetic exponent in asymmetric block copolymer thin films has been predicted to be limited to 1/4 in the infinite time limit under isotropic annealing conditions. It is worth noting that the ϕ values we measured in the fast coarsening regime are systematically larger than the one expected according to the theoretical predictions. Nevertheless, several authors reported similar growth exponent $\phi \sim 0.28$ in asymmetric block copolymers with cylinders perpendicularly oriented with respect to the substrate, suggesting the possibility that slightly different defect dynamics could apply when changing sample geometries.[12] [26]

In the present system, two distinct growth regimes are clearly identified. Initially, the correlation length evolves rapidly following a power law $\xi \propto t^{0.29}$. Then, the slope changes in the log ξ vs. log $time$ and coarsening slows down with a growth exponent $\phi \sim 0.03$. This double regime is strictly related to the evolution of the cylinders at the base of the lamellar phase. The initial fast coarsening regime of the lamellar phase is driven by the underlying cylindrical phase with a growth exponent $\phi \sim 0.29$, which is equivalent to those reported in previous experiments for perpendicular-oriented cylindrical phase block copolymers.[12] [26] Then, the cylinder phase disappears and the evolution of the lamellae is limited by the previously described topological constraints and the growth exponent equals those reported in the literature for symmetric block copolymer thin films.[10] [11]

In this context, it is important to recall that fast coarsening in lamellar block copoly-

mer thin films has already been demonstrated by different authors introducing a pre-patterning of the substrate that drives the self-assembly process of the macromolecules deposited on top of it. [27] [28] [29] [6]
Interestingly, a double layer approach has been effectively used in order to achieve a high correlation length lamellar pattern.[8] The parallel oriented cylindrical phase PS-b-PMMA was formed and subsequently immobilized by PS crosslinking via UV irradiation. This layer was successfully used as a template to guide the top layer of the perpendicularly oriented lamellar phase of PS-b-PMMA block copolymers. The final correlation length of the lamellar film coarsens with annealing time and asymptotically approaches that of the respective under layer film with final values much higher than the ones observed in a single layer of the lamellar film. These results indicate that under specific conditions, by properly modulating the surface energy of the substrate, high correlation length values and fast coarsening in symmetric block copolymer thin films are possible. However, the picture just delineated for the polymeric system treated in a RTP machine is substantially different since the coarsening dynamics of the lamellae is essentially driven by the internal evolution of the system that experiences an order-to-order transition determined, at the end, by the progressive desorption of residual solvent originally trapped in the film during the deposition process. In this picture, the cylindrical phase does not simply act as a template that guides the ordering process in the lamellar phase, but actively participates in the evolution of the system, providing alternative paths for macromolecules diffusion and resulting in a significant reduction of the enthalpy barrier for defect annihilation. In this contest we identified RTP as a ``solvent-assisted´´ thermal treatment.

4.3 Thermal Limitation to Lateral order

The experimental results reported so far, outline the pattern coarsening dynamics in symmetric PS-b-PMMA block copolymer thin films, subjected to RTP, from 250 to 290°C. Within this temperature range, the amount of residual solvent boosts the lateral order to higher ξ values than what reported in literature. The metastable cylindrical morphology indeed, acts as a topologycal solution to the limited molecular diffusion expected for a simple lamellar structure.
Once the first limit to lateral order in symmetric BCPs has been pushed forward, a new limit has to be taken into account: the thermal stability one. As already highlighted, the use of RTP to induce and controll the ordering process, opens the possibility to dramatically reduce the processing time by increasing T_{target}. The very fast heating and cooling rates in fact, allowed the sample to be heated to high temperatures and maintained at the target temperature for relatively short time periods, avoiding the substantial degradation of the BCP.
But how far can this ordering process be driven on the considered system?
What is the limit imposed by polymeric thermal degradation, in terms of maximum allowed temperature and maximum achieved lateral order?
The previous chapter suggests an interesting approach to the problem in considering the stability of the whole polymeric system RCP+BCP, this way identifying the first contribution (with TR58 as the random copolymer) as the most affected by thermal degradation. For this reason samples obtained by that random copolymer were studied on the limited range of temperature 250 - 290°C.

The next section reports the results obtained with the same symmetric block copolymer (B50) but with the more stable random copolymer BrR58. In this way the problem of lateral order is addressed on a wider range of temperature, giving rise to a systematic study of samples evolution.
It is worth to note that in further extending the range of processing conditions, up to the very limit imposed by degradation, an accurate study of the influence of every single step of the process on the ordering evolution becomes necessary.

4.4 Scaling of Correlation Length on Wide Process Windows (T_{target}, t_{ann})

This section sistematically deals with the problem of lateral ordering in symmetric BCP thin films thermally treated in RTP at temperatures ranging from 250 to 350°C. The individual contributions of the different steps of the RTP process on the lateral order evolution are investigated and the development of lateral order in symmetric PS-b-PMMA thin films is monitored as a function of annealing temperature and time. In the last paragraph, the systematic analysis aims at obtaining information about the energetic of the lateral ordering process, providing a complete picture of the evolution of the system in this high-temperature range.
All the samples considered in this section were fabricated following the general procedure described in the Experimental Methods. In particular, all the substrates were neutralized by grafting BrR58 with an RTP treatment of 60 s at 310 °C. The Br-terminated random copolymer allows for a wide range of processing temperatures and the grafting treatment was chosen as a good compromise between the thermal stabilization process described in the previous chapter and the Microelectronics requirements for short processing times[4]. B50 was then submitted to different RTP treatments as highlighted in the following paragraphs.

4.4.1 Ordering Dependence on the Heating Ramp

The basic structure of a RTP treatment was described in chapter 2, nevertheless the investigation of ordering over a wide range of temperature above 290°C requires a deeper comprehension of the effect of each single step on the ordering process of BCPs. Following the three steps description consisting of a heating ramp, from room temperature up to the target temperature, an isothermal step, where the sample is maintained at T_{target} for a predetermined t_{ann}, and a cooling ramp from T_{target} back to room temperature, we can determine which are the constant contributions and which are the proper process variables.
The cooling ramp is fixed by the machine recovery time. For this reason, provided that T_{target} is constant, the cooling ramp gives a constant contribution to the ordering process of BCP thin films. To decouple the effect of the isothermal step at T_{target} from the one of the heating ramp, a set of samples was thermally treated at different T_{target} for t_{ann} = 1 s, progressively increasing the heating rate (HR) to reach T_{target}.
Figure 4.9 reports the RTP temperature profiles corresponding to the thermal treatments performed at 290°C with different HRs ranging from 1 to 46°C/s. The zero in the time

[4]The grafted thickness obtained with this treatment is safely above the threshold for perpendicular orientation of B50, though not in the saturation regime yet. Nevertheless it guarantees a perfect perpendicular orientation of lamellae on very short time of annealing.

scale of the entire process time is taken when the sample reaches the T_{target}. The heating time increases as the HR decreases whereas the cooling time is nearly identical. It is worth noticing that the HRs under investigation (from 1 to 46°C/s) are definitely faster than the heating rate achievable in a common furnace (3-5°C/min).

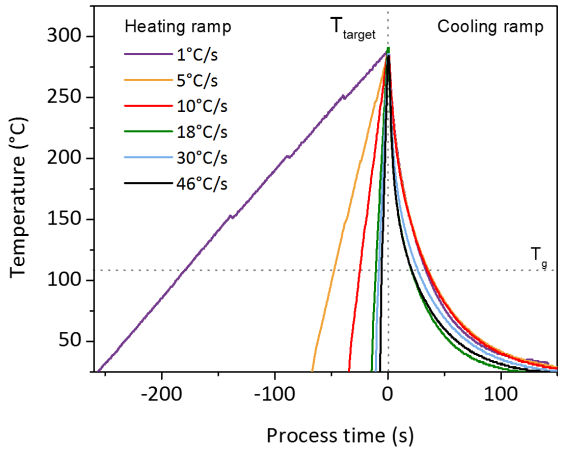

Figure 4.9: Temperature profile vs time during the RTP process involving the heating ramp performed at different HRs, the isothermal step for 1 s annealing time at the T_{target} of 290°C and the cooling ramp in which the cooling rate is fixed by machine recovery time. The zero in the time scale is taken when the sample reaches the T_{target}.

The level of order in the self-assembled BCP films upon annealing was monitored by measuring ξ in the corresponding SEM top view images.
Figure 4.10 (upper row) illustrates the SEM images of the samples processed with T_{target} = 290°C at different HRs. Figure 4.10 (lower row) reports the corresponding orientation color maps obtained by software analysis of high resolution low magnification SEM images. The colored grains correspond to ordered domains of lamellae, aligned to a precise direction. The grain size is nearly constant when the HR is comprised between 46 and 18°C/s. The corresponding ξ values obtained by software analysis of the color maps are approximately 50 nm. On further reducing the HR (1°C/s $<$ HR $<$ 18°C/s), the grain size increases regularly up to ξ values of 260 nm.

Figure 4.11 illustrates the effect of the HR on ξ when heating the samples to different T_{target} from 290 to 350°C. Irrespective of the T_{target}, the ξ is constant until the HR value of 18°C/s is reached and then rapidly increases, as the HR decreases, reaching values higher than 600 nm in the case T_{target} = 350°C. These results suggest the occurrence of a ``slow'' (HR $<$ 18°C/s) and a ``fast'' (HR $\geq$ 18°C/s) regimes. In the ``slow'' regime, we observe a progressive increase of the $\xi$ values as HR decreases. This behavior could be explained considering that, as can be inferred by figure 4.9, lower the HR, longer the time spent above $T_g$. Conversely, in the ``fast'' regime, the ξ values are constant irrespective of the HR, since, the differences in the time spent above the T_g become negligible for HR $\geq$ 18°C/s. The ξ vs. HR curves appear shifted toward higher values along the vertical scale as T_{target} increases.

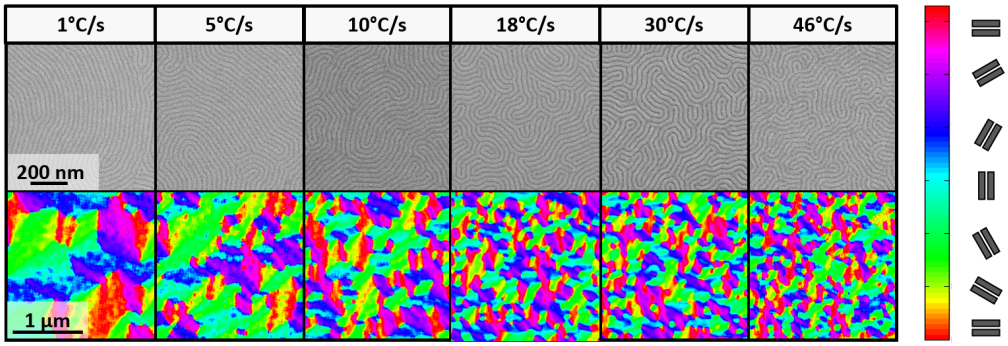

Figure 4.10: SEM top views (upper row) and orientation color map (lower row) of samples treated at T_{target} of 290°C, following the RTP thermal process outlined in Figure 4.9. On the right side, the lamellar orientation is reported in the color scale.

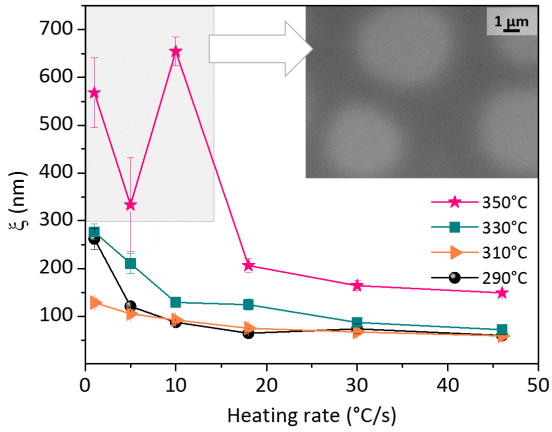

Figure 4.11: Correlation length as a function of the HR of RTP treatments, for different T_{target} from 290 to 350°C . In the inset, a plan view SEM image is included for the sample treated at 350°C with HR = 10 °C/s to illustrate the presence of inhomogeneous regions.

However, corresponding to T_{target} = 350°C, a substantial scattering of the ξ data is observed at low HRs, accompanied by the occurrence of inhomogeneous regions in the polymeric film. In the inset of figure 4.11, a representative low magnification plan view SEM image of these samples (HR = 10°C/s) is reported, highlighting the presence of several bright spots embedded in the dark matrix. Inside these spots, the lamellar structure of the BCP is still present but a lower level of lateral order and a worse contrast between each lamellar period is observed if compared to the surrounding dark areas. Though the occurrence of the bright spots does not involve the polymeric film rupture [30], it still represents an inhomogeneity of the surface, with a local reduction of the level of lateral order, which could eventually prevent a technological exploitation.

Conversely, only homogeneous regions are detected in the BCP thin film when the HR is higher than 18°C/s, even in the case T_{target} = 350°C. In the ``fast'' HR regime, $\xi$ appears to depend only on the selected $T_{target}$, with values increasing from approximately 60 nm at 290 and 310°C, to 80 nm at 330°C, and 150 nm at 350°C. In this ``fast'' HR regime, the transient time of the heating ramp is so short that, for a fixed T_{target}, the effect of this step of the process is minimized. The contribution of the heating step to the final level of lateral order is constant for HR $\geq$ 18°C/s and is mainly determined by the selected T_{target}. This result indicates that in the ``fast'' HR regime, it is possible to decouple the effect of the isothermal step from the one of HR used to achieve the final T_{target} since any further increase of ξ, with respect to the values reported in figure 4.11, will be determined by the duration of the isothermal step.

4.4.2 Ordering Dependence on the Time-Temperature Interplay

To delineate the dynamics of grain coarsening as a function of the annealing conditions (t_{ann} and T_{target}) during the isothermal step, a systematic study of the evolution of lamellar lateral order was performed. The thermal treatments were carried out with a fixed HR of 18°C/s to minimize the contribution of the heating ramp and avoid any dependence of the final ξ values from the HR. Figure 4.12 (upper row) illustrates the SEM images of the samples processed for t_{ann} = 10 s with T_{target} values ranging from 250 to 350°C. Figure 4.12 (lower row) reports the corresponding orientation color maps obtained by software analysis of the SEM images on a large scale. The grain size monotonically increases with T_{target}. The corresponding ξ values reach the maximum ($\xi \approx$ 900 nm) at T_{target} = 350°C. This value is obtained in a sample that comprises inhomogeneous regions. Considering the samples characterized by a homogeneous surface texture, a maximum value of the correlation length (ξ = 500 nm) was observed in the sample annealed at 330°C.

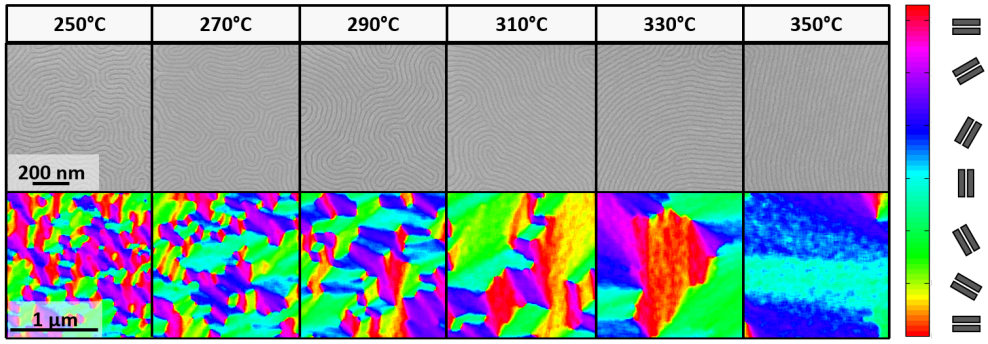

Figure 4.12: SEM top views (upper row) and orientation color map (lower row) of samples treated at T_{target} ranging from 250 to 350°C . On the right side, the lamellar orientation is reported in the color scale.

Figure 4.13 reports ξ as a function of t_{ann} at different T_{target} values, comprised between 250 and 350°C.
For t_{ann} = 1 s, the samples, thermally treated at T_{target} = 250 and 270°C, exhibit a clear

evidence of phase separation between the different polymeric blocks without achieving a significant level of lateral ordering. The ξ values at 250 and 270°C increase regularly with t_{ann}. At 290 and 310°C an initial rapid growth of ξ is followed by a leveling off to a plateau value for long t_{ann}.[5] Above 330°C, the initial, fast growing, regime is observed whereas the plateau value cannot be properly determined because of the appearance of some inhomogeneous regions in the samples. The grey area in the upper right zone of figure 4.13 corresponds to processing conditions leading to inhomogeneous polymeric films. If $T_{target} \leq$ 290°C, uniform polymeric films were observed irrespective of t_{ann}. Differently, if $T_{target} >$ 290°C, inhomogeneities were detected in the samples when increasing t_{ann}; the higher T_{target}, the shorter t_{ann} at which inhomogeneity appeared. For instance, at 350°C traces of local reduction of lateral order are detectable after only 5 s of t_{ann}.
The data indicate a competition between the lateral ordering of the BCP template and the appearance of inhomogeneity in the polymeric film. Raising up T_{target} the inhomogeneity develops increasingly faster and the time interval that allows promoting the lateral ordering without inhomogeneities in the film progressively reduces. In this respect, the lower edge of the grey area in figure 4.13 indicates the combination of processing parameters (e.g. t_{ann} =10/30 s at T_{target} = 330°C or t_{ann} = 60/100 s at T_{target} = 310°C) corresponding to the highest ξ values. An accurate balance of t_{ann} and T_{target} leads to ξ values of approximately 500 nm while maintaining the polymeric film homogeneity.
The occurrence of grains of ordered lamellae with size similar to that obtained in the present investigation, using the same BCP sample, was described in a recent work by Kim *et al.*[31] However, a RCP was added to the BCP sample. The RCP was reported to be preferentially localized near the dislocations of the lamellar structure thus decreasing the BCP diffusion barrier and promoting defect movements across the lamellar domains. Conversely, no polymeric additive was used in this thesis. We take advantage of the residual amount of solvent at the interface between the RCP substrate and the BCP layer. As reported above, residual solvent provides a way to overcome the topological constrains of the lamellar morphology. These correlation length values closely approach the ones obtained in the case of asymmetric block copolymers, with PMMA cylinders parallel to the substrate, when submitted to different thermal treatments such as vacuum annealing [11], zone annealing [32] and photothermal gradients [33].

4.4.3 Activation Energy of the Ordering Process

In viscoelastic materials, there is a correspondence between a temperature and a time shift.[34] For this reason, the uniform relationship between T_{target} and t_{ann} in the RTP process can be investigated by applying the Time-Temperature-Superposition (TTS) [35] principle to the ξ vs. time curves, as reported in figure 4.14. Holding the $\xi(t)$ curve at T_{target} = 250°C as the reference, one at a time all the other curves are rigidly shifted to longer t_{ann} until they match the one at lower temperature (figure 4.14). The amount of time, by which each single curve is shifted, is called horizontal shift factor (a_t). This pro-

[5] This ``leveling off'' corresponds to the slow coarsening regime addressed before, in the case of B50 organized above a TR58 layer. The fact that the same double coarsening is not so evident for samples treated at 250 and 270°C should not surprise the reader. Indeed, the t_{ann} at which the leveling off takes place is influenced by the different random copolymer here involved, which supplied the samples with a slightly thicker grafted layer (7 nm on average of BrR58 with respect to the 5 nm of TR58). The increase in the solvent reservoir could bring the change in the slope of coarsening to longer t_{ann} than the one here considered.

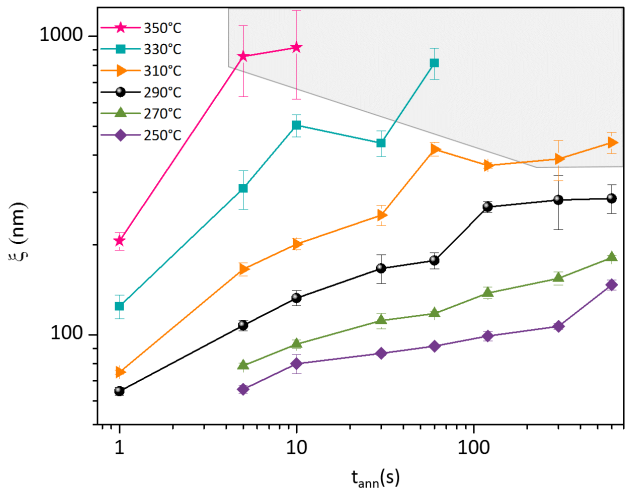

Figure 4.13: Correlation lengths at different T_{target} as a function of the t_{ann}. The grey area corresponds to samples with inhomogeneous regions.

cedure generates a single curve (the master curve) at 250°C describing the evolution of ξ as a function of t_{ann}. The solid line in figure 4.14 represents the master curve obtained by fitting the experimental data with an exponential function.
Two limitations to the range of applicability of TTS should be considered. The first limit consists in the occurrence of inhomogeneous regions in the polymeric film, which hampers the investigation of lateral order evolution at high temperature for long t_{ann}. The second limit occurs when the exponential growth of the ξ turns into the plateau values indicating the system is entering a slow coarsening regime.
Nevertheless, considering the data illustrated in figure 4.14, it is clear that for t_{ann} below 10^4 s ($\log t < 4$), the processing conditions (T_{target}, t_{ann}) leading to a specific ξ value can be easily obtained for ξ values up to 300 nm. In contrast, considering the master curve at 250°C, for $\log t > 4$ no predictions are possible.

The TTS analysis of the time range ($\log t < 4$), where the exponential growth of the correlation length occurs, provides a physical insight on the energetics of the ordering process. As the T_{target} are more than 100°C above the glass transition temperature (T_g),[36] the ordering process should be described by an Arrhenius like dependence [37]: $a_t = exp\frac{E_a}{R}\left[\frac{1}{T} - \frac{1}{T_0}\right]$, where E_a is the activation energy, R is the gas constant, and T_0 is a reference temperature. Figure 4.15 illustrates the logarithm of the horizontal shift factor a_t, as a function of the inverse of T_{target}. Red dashed line corresponds to a linear fit of the experimental data. The first point, relative to the 350°C series, was discarded since it is strongly affected by inhomogeneity of the samples.

From the slope of the fit of figure 4.15, an E_a for grain coarsening of 54 ± 4 kJ/mol can be estimated. A complementary approach for the estimation of the E_a is to directly handle the ξ values as a measure of the ordering kinetics, as suggested by Yager *et al.*[32] The Arrhenius analysis $\xi \propto e^{-E_a/RT}$ performed at a fixed t_{ann}, affords an E_a of 59 ± 16 kJ/mol.

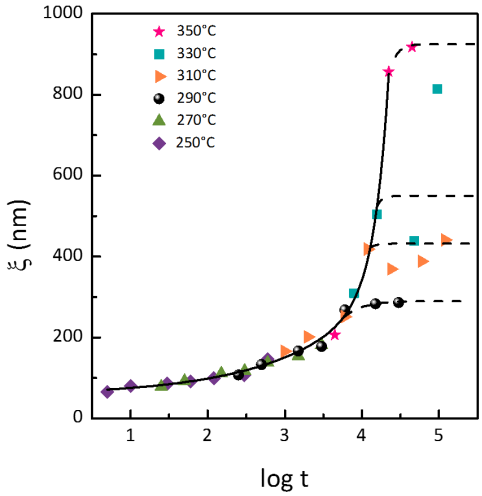

Figure 4.14: Master curve from Time-Temperature-Superposition of the correlation length data of 4.13 keeping 250°C as the reference temperature.

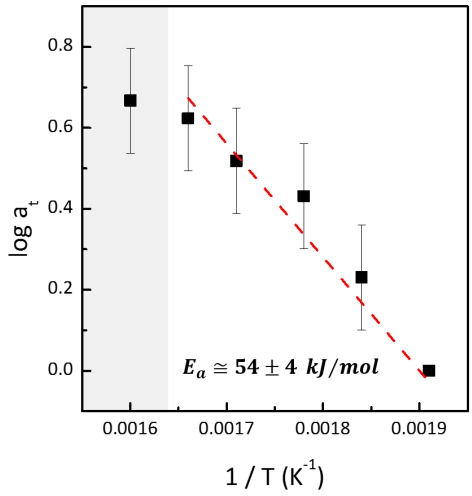

Figure 4.15: Logarithm of the shift factor a_t as a function of 1/T. Grey area collects data most affected by degradation and error bars are representative of the average error in the determination of the horizontal shift factor for each series of data. The point relative to the 250°C series has no error bar as it corresponds to the reference for the master curve in the TTS approach (see fig.4.14).

The E_a values, determined using both approaches are quite similar although the value determined by the TTS approach appears affected by a smaller uncertainty. The present estimation of E_a for the ordering process in a lamellar forming PS-b-PMMA is definitely lower than the value of 8300 kJ/mol reported by Ruiz *et al.*[10] for a PS-*b*-PMMA with M_n = 46 kg/mol, but quite close to that calculated by Yager *et al.* (110 ± 40 kJ/mol) for a cylinder forming PS-b-PMMA with a molar mass similar to that of the BCP employed in

the present investigation (M_n = 47.7 kg/mol). This observation highlights the peculiar ordering process of a lamellar thin film subjected to RTP. In the fast ordering regime, the coarsening of ordered grains resembles the evolution of a cylindrical system as depicted by the estimation of the activation energy. Nevertheless, the appearance of a slow ordering regime reveals a limit in lamellar coarsening. This result can be explained on the basis of the above described observation about the existence of a metastable cylindrical phase at the interface between RCP and BCP which progressively vanishes with the exhaustion of the residual solvent.

4.5 Recalling the Main Results of This Chapter

This chapter summarized the main results accomplished about the problem of lamellar pattern coarsening on featureless substrate, within a RTP treatment. The first series of samples realized with a neutralization random layer of TR58 delt with the dynamics of symmetric PS-b-PMMA ordering in the range of temperature between 250 and 290 °C. Within this temperature range, the correlation length increased steeply at first and then more gradually, with a well defined threshold, which depended on the temperature, thus indicating the occurrence of two distinct growth regimes. These two regimes were characterized by power laws with markedly different growth exponents (ϕ). In the fast coarsening regime, the evolution of the correlation length followed a power law with the growth exponent $\phi \sim 0.32$ typical for sphere or cylinder forming asymmetric block copolymers but never reported for symmetric block copolymers. In contrast, in the slow coarsening regime ϕ values below 0.10 were measured, in perfect agreement with the growth exponent reported in the literature for lamellae forming symmetric block copolymers. These results correlated with the presence, within the polymeric film, of a peculiar morphology involving periodic lamellae laying registered over a hexagonal pattern of PMMA cylinders embedded in the PS matrix and perpendicularly oriented with respect to the substrate. The origin of the two connected phases was related to the presence of a consistent amount of toluene, which was naturally entrapped in the film after the spinning process. Due to the preferential selectivity of toluene for the PS block, a differential swelling occured leading to the formation of cylinders of PMMA embedded into a PS matrix in the toluene rich regions. The evolution of these two structures was governed by desorption of the solvent in the film during the thermal treatment. As the solvent evaporated the cylinder phase became unstable, and an order-to-order transition front propagated through the film thus ultimately producing highly ordered and perpendicularly oriented lamellar microdomains.
The more stable random copolymer BrR58 was then employed to extend the range of processing temperature and to obtain a systematic study of the evolution of the lateral order as a function of the processing parameters T_{target} and t_{ann}. By decoupling the effect of the HR from the one of T_{target} and t_{ann} during the isothermal step of the RTP thermal treatment, the ordering process in the PS-*b*-PMMA film was studied as a function of T_{target} and t_{ann} in order to identify the processing parameters that allows maximizing the lateral order avoiding, at the same time, degradation of the macromolecules. In this way perfectly homogeneous BCP films with high correlation length values ($\xi \approx$ 500 nm) were obtained by properly adjusting the processing parameters (330°C, 10 s). The coarsening kinetic data, recorded at different T_{target}, were masterized by applying the TTS principle. The resulting master curve delimitated the T_{target}/t_{ann} combination

leading to fast and slow coarsening regimes of the lamellar structure. By the TTS procedure, the activation energy ($E_a \sim 55$ kJ/mol) of the ordering process during the fast coarsening regime was estimated. The present data clearly indicate that the fast HR of RTP technology and the excellent temperature control allow the organization of a lamellar system on featureless substrate with exceptionally high ξ obtained in very short time.

Bibliography

[1]F. Ferrarese Lupi, T. J. Giammaria, M. Ceresoli, G. Seguini, K. Sparnacci, D. Antonioli, V. Gianotti, M. Laus, and M. Perego, "Rapid thermal processing of self-assembling block copolymer thin films", Nanotechnology **24**, 315601 (2013).

[2]M. Ceresoli, F. Ferrarese Lupi, G. Seguini, K. Sparnacci, V. Gianotti, D. Antonioli, M. Laus, L. Boarino, and M. Perego, "Evolution of lateral ordering in symmetric block copolymer thin films upon rapid thermal processing.", Nanotechnology **25**, 275601 (2014).

[3]M. Perego, F. Ferrarese Lupi, M. Ceresoli, T. J. Giammaria, G. Seguini, E. Enrico, L. Boarino, D. Antonioli, V. Gianotti, K. Sparnacci, and M. Laus, "Ordering dynamics in symmetric PS-b-PMMA diblock copolymer thin films during rapid thermal processing", Journal of Materials Chemistry C **2**, 6655 (2014).

[4]M. Ceresoli, F. G. Volpe, G. Seguini, D. Antonioli, V. Gianotti, K. Sparnacci, M. Laus, and M. Perego, "Scaling of correlation length in lamellae forming PS-b-PMMA thin films upon high temperature rapid thermal treatments", J. Mater. Chem. C **3**, 8618–8624 (2015).

[5]R. Ruiz, N. Ruiz, Y. Zhang, R. L. Sandstrom, and C. T. Black, "Local Defectivity Control of 2D Self-Assembled Block Copolymer Patterns", Advanced Materials **19**, 2157–2162 (2007).

[6]A. M. Welander, H. Kang, K. O. Stuen, H. H. Solak, M. Müller, J. J. de Pablo, and P. F. Nealey, "Rapid Directed Assembly of Block Copolymer Films at Elevated Temperatures", Macromolecules **41**, 2759–2761 (2008).

[7]R. Ruiz, H. Kang, F. A. Detcheverry, E. Dobisz, D. S. Kercher, T. R. Albrecht, J. J. de Pablo, and P. F. Nealey, "Density multiplication and improved lithography by directed block copolymer assembly.", Science **321**, 936–9 (2008).

[8]R. Ruiz, R. L. Sandstrom, and C. T. Black, "Induced Orientational Order in Symmetric Diblock Copolymer Thin Films", Advanced Materials **19**, 587–591 (2007).

[9]S.-M. Park, M. P. Stoykovich, R. Ruiz, Y. Zhang, C. T. Black, and P. F. Nealey, "Directed Assembly of Lamellae- Forming Block Copolymers by Using Chemically and Topographically Patterned Substrates", Advanced Materials **19**, 607–611 (2007).

[10]R. Ruiz, J. K. Bosworth, and C. T. Black, "Effect of structural anisotropy on the coarsening kinetics of diblock copolymer striped patterns", Physical Review B **77**, 054204 (2008).

[11]C. Harrison, D. H. Adamson, Z. Cheng, J. M. Sebastian, S. Sethuraman, D. A. Huse, R. A. Register, and P. M. Chaikin, "Mechanisms of Ordering in Striped Patterns", Science **290**, 1558–1560 (2000).

[12]S. Ji, C.-C. Liu, W. Liao, A. L. Fenske, G. S. W. Craig, and P. F. Nealey, "Domain Orientation and Grain Coarsening in Cylinder-Forming Poly(styrene- b -methyl methacrylate) Films", Macromolecules **44**, 4291–4300 (2011).

[13]Y.-H. Ting, S.-M. Park, C.-C. Liu, X. Liu, F. J. Himpsel, P. F. Nealey, and A. E. Wendt, "Plasma etch removal of poly(methyl methacrylate) in block copolymer lithography", Journal of Vacuum Science & Technology B: Microelectronics and Nanometer Structures **26**, 1684 (2008).

[14]S. Sakurai, T. Momii, K. Taie, M. Shibayama, S. Nomura, and T. Hashimoto, "Morphology transition from cylindrical to lamellar microdomains of block copolymers", Macromolecules **26**, 485–491 (1993).

[15]C. M. Hansen, *Hansen Solubility Parameters: A User's Handbook, Second Edition - CRC Press Book*, 2007.

[16]J. Gong, H. Ahn, E. Kim, H. Lee, S. Park, M. Lee, S. Lee, T. Kim, E.-A. Kwak, and D. Y. Ryu, "Rapid structural reorganization in thin films of block copolymer self-assembly", Soft Matter **8**, 3570 (2012).

[17]F. Ferrarese Lupi, T. J. Giammaria, G. Seguini, M. Laus, E. Enrico, N. De Leo, L. Boarino, C. K. Ober, and M. Perego, "Thermally induced orientational flipping of cylindrical phase diblock copolymers", Journal of Materials Chemistry C **2**, 2175 (2014).

[18]P. Mokarian-Tabari, T. W. Collins, J. D. Holmes, and M. A. Morris, "Cyclical Flipping of Morphology in Block Copolymer Thin Films", ACS Nano **5**, 4617–4623 (2011).

[19]A. C. Saby-Dubreuil, B. Guerrier, C. Allain, and D. Johannsmann, "Glass transition induced by solvent desorption for statistical MMA/nBMA copolymers — Influence of copolymer composition", Polymer **42**, 1383–1391 (2001).

[20]J. Perlich, V. Korstgens, E. Metwalli, L. Schulz, R. Georgii, and P. Muller-Buschbaum, "Solvent Content in Thin Spin-Coated Polystyrene Homopolymer Films", Macromolecules **42**, 337 (2009).

[21]X. Zhang, K. G. Yager, S. Kang, N. J. Fredin, B. Akgun, S. Satija, J. F. Douglas, A. Karim, and R. L. Jones, "Solvent Retention in Thin Spin-Coated Polystyrene and Poly(methyl methacrylate) Homopolymer Films Studied By Neutron Reflectometry", Macromolecules **43**, 1117–1123 (2010).

[22]X. Zhang, B. C. Berry, K. G. Yager, S. Kim, R. L. Jones, S. Satija, D. L. Pickel, J. F. Douglas, and A. Karim, "Surface morphology diagram for cylinder-forming block copolymer thin films.", ACS nano **2**, 2331–41 (2008).

[23]X. Zhang, J. F. Douglas, and R. L. Jones, "Influence of film casting method on block copolymer ordering in thin films", Soft Matter **8**, 4980 (2012).

[24]S. H. Kim, M. J. Misner, T. Xu, M. Kimura, and T. P. Russell, "Highly Oriented and Ordered Arrays from Block Copolymers via Solvent Evaporation", Advanced Materials **16**, 226–231 (2004).

[25]H. J. Dai, N. P. Balsara, B. A. Garetz, and M. C. Newstein, "Grain Growth and Defect Annihilation in Block Copolymers", Physical Review Letters **77**, 3677–3680 (1996).

[26]C. T. Black, and K. W. Guarini, "Structural evolution of cylindrical-phase diblock copolymer thin films", Journal of Polymer Science Part A: Polymer Chemistry **42**, 1970–1975 (2004).

[27]S. O. Kim, H. H. Solak, M. P. Stoykovich, N. J. Ferrier, J. J. De Pablo, and P. F. Nealey, "Epitaxial self-assembly of block copolymers on lithographically defined nanopatterned substrates.", Nature **424**, 411–4 (2003).

[28]M. P. Stoykovich, M. Müller, S. O. Kim, H. H. Solak, E. W. Edwards, J. J. de Pablo, and P. F. Nealey, "Directed assembly of block copolymer blends into nonregular device-oriented structures.", Science **308**, 1442–6 (2005).

[29]L. Rockford, Y. Liu, P. Mansky, T. P. Russell, M. Yoon, and S. G. J. Mochrie, "Polymers on Nanoperiodic, Heterogeneous Surfaces", Physical Review Letters **82**, 2602–2605 (1999).

[30]K. Sparnacci, D. Antonioli, V. Gianotti, M. Laus, G. Zuccheri, F. Ferrarese Lupi, T. J. Giammaria, G. Seguini, M. Ceresoli, and M. Perego, "Thermal stability of functional P(S-r-MMA) random copolymers for nanolithographic applications.", ACS applied materials & interfaces **7**, 3920–30 (2015).

[31]B. H. Kim, S. J. Park, H. M. Jin, J. Y. Kim, S.-W. Son, M.-H. Kim, C. M. Koo, J. Shin, J. U. Kim, and S. O. Kim, "Anomalous Rapid Defect Annihilation in Self-Assembled Nanopatterns by Defect Melting", Nano Letters **15**, 1190–1196 (2015).

[32]K. G. Yager, N. J. Fredin, X. Zhang, B. C. Berry, A. Karim, and R. L. Jones, "Evolution of block-copolymer order through a moving thermal zone", Soft Matter **6**, 92–99 (2010).

[33]P. W. Majewski, and K. G. Yager, "Millisecond Ordering of Block Copolymer Films via Photothermal Gradients.", ACS nano **9**, 3896–3906 (2015).

[34]S. Naya, A. Meneses, J. Tarrío-Saavedra, R. Artiaga, J. López-Beceiro, and C. Gracia-Fernández, "New method for estimating shift factors in time–temperature superposition models", Journal of Thermal Analysis and Calorimetry **113**, 453–460 (2013).

[35]K. Fukushima, H. Cai, M. Nakada, and Y. Miyano, "Determination of Time-Temperature Shift Factor for Long-Term Life Prediction of Polymer Composites", in Int. conf. compos. mater. proc., 17th. (2009).

[36]C.-Y. Liu, J. He, R. Keunings, and C. Bailly, "New Linearized Relation for the Universal Viscosity-Temperature Behavior of Polymer Melts", Macromolecules **39**, 8867–8869 (2006).

[37]G. R. Strobl, *The Physics of Polymers - Concepts for Understanding Their Structures and Behavior* (Springer, 1997).

Conclusions

CHAPTER 5

Conclusions and Perspectives

This thesis focuses on the problem of the ordering process in lamellar forming BCP thin film, in view of their application as lithographic nanostructures. In particular this thesis offers a basic study of the properties of a symmetric PS-*b*-PMMA system, when organized on a featureless substrate, by means of high temperature processes performed in a RTP machine. Considering the peculiar approach followed in this work, we can identify some main experimental achievements:

1)The thermal stability of RCP thin films can be highly enhanced by performing the grafting process at high temperature in a RTP machine.
Two different RCP were studied in order to addressed a wide range of grafting temperature. The grafted TEMPO-terminated RCP exhibited a relatively low thermal stability that limited the processing temperature of the RCP+BCP system at 310°C. The grafted Br-terminated RCP presented a definitely more stable structure allowing for the processing temperature of the RCP+BCP system to be shifted up to 350°C.

2)The thermodynamic and kinetics of self-assembly of symmetric lamellar forming BCP was systematically addressed over a wide range of temperature and time of thermal treatment. The ordering mechanism reveals its process-dependent characteristics. First of all, a fast heating rate of the sample allows to take advantage of the presence of a consistent amount of toluene, which was naturally entrapped in the film after the spinning process, and is not completely evaporated when the target temperature is reached. Grain coarsening in symmetric PS-*b*-PMMA thin films deposited on the TEMPO-terminated RCP and processed in the range of temperature between 250 and 290 °C, highlights the presence of two distinct growth regimes characterized by power laws with markedly different growth exponents (ϕ). In the fast coarsening regime, the evolution of the correlation length followed a power law with the growth exponent $\phi \sim 0.32$ typical for sphere or cylinder forming asymmetric block copolymers but never reported for symmetric block copolymers. In contrast, in the slow coarsening regime ϕ values below 0.10 were measured, in perfect agreement with the growth exponent reported in the literature for lamellae forming symmetric block copolymers. These results correlated with the presence, within the polymeric film, of a peculiar morphology involving periodic lamellae laying registered over a hexagonal pattern of PMMA cylinders embedded in the PS matrix and perpendicularly oriented with respect to the substrate. The origin of the two connected phases was related to the presence of a consistent amount of toluene originally trapped in the film during the spinning process. Due to the preferential selectivity of toluene for the PS block, a differential swelling occurred leading to the formation of

cylinders of PMMA embedded into a PS matrix in the toluene rich regions. The evolution of these two structures was governed by desorption of the solvent in the film during the thermal treatment. As the solvent evaporated the cylinder phase became unstable, and an order-to-order transition front propagated through the film thus ultimately producing highly ordered and perpendicularly oriented lamellar microdomains.
The presence of the solvent together with the enhancement of PS-*b*-PMMA kinetics in working at very high temperatures of processing, gives the possibility to lower the energetic barrier to molecules diffusion. In this way high level of lateral order could be fabricated even on symmetric BCPs thin films on featureless substrate. The more stable Br-terminated RCP was then employed to extend the range of processing temperature and to obtain a systematic study of the evolution of the lateral order as a function of the processing parameters T_{target} and t_{ann}. The processing parameters that allows maximizing the lateral order avoiding, at the same time, degradation of the macromolecules were identified. In this way perfectly homogeneous BCP films with high correlation length values ($\xi \approx 500$ nm) were obtained by properly adjusting the processing parameters (330°C, 10 s). The coarsening kinetic data, recorded at different T_{target}, were masterized by applying the TTS principle. The resulting master curve delimitated the T_{target}/t_{ann} combination leading to fast and slow coarsening regimes of the lamellar structure. By the TTS procedure, the activation energy ($E_a \sim 55$ kJ/mol) of the ordering process during the fast coarsening regime was estimated.

Perspectives.
On the basis of the experimental results presented in this thesis work, we can identify some interesting developments for this research activity that are described in more details in the following sections.

Self-registration
For most of the lithographic applications of BCP thin films the ability to generate defect-free microdomains and precisely control their placement and self-registration on the substrate is fundamental. As already mentioned in chapter 1, *Graphoepitaxy* is based on the idea that surface relief structures can direct the self-assembly of microdomains in block copolymer thin films. The specific surface topography employed (alternation of trench and mesa) strongly affects the formation and alignments of BCPs domains. Some of the main parameters that have to be taken into account are the ratio between the thickness of the structures and of polymeric films, as well as the commensurability between the characteristic BCP period and the width of the trenches, and the wetting properties of the trenches. In particular, in the case of lamellar microdomains, when the bottom surface of the trench is neutral to both PS and PMMA blocks, the side wall that is selectively wetted by one of the block induces orientation of the lamellae parallel to the side wall surface. In this contest the study of the high temperature self-assembly kinetics of BCPs on predefined structures represent an interesting possibility for the implementation of *Graphoepitaxy* into existing lithograpic process flow. Interesting results for example,were recently shown for the confinement of asymmetric cylinder-forming PS-*b*-PMMA treated within RTP.[1]

Pattern Transfer Fidelity
The graphoepitaxy would allow achieving high lateral order and self-registration of the BCP pattern. Besides this, in order to be suitable for lithographic applications, a good pattern transfer fidelity has to be assured. In this contest the use of a lamellar morphology would disclose the possibility to obtain high aspect ratio striped patterns provided that the correct neutralization of the surfaces is obtained. Nevertheless the feasible transferability on hard patterns has to be evaluated.
Very recently Wan *et al.*[2] reported that although a nearly perfect DSA by chemical prepatterning can be obtained with lamellar forming PS-*b*-PMMA with L_0 as short as 18.5 nm, a high-fidelity pattern transfer is limited to a large L_0 of about 22 nm. Most of the problems were attributed to the low-$\chi_{PS-PMMA}$ value which brings the $\chi_{PS-PMMA}N$ product next to the WSL when dealing with such a small characteristic period. In this conditions indeed the interface dimension becomes non negligible with respect to the critical dimension of the single line ($L_0/2$).[3] A large interfacial width affects the ability to selectively remove one of the two lamellar component getting for example worse level of Line Edge Roughness (LER[1]) once the pattern is used as mask.
In this framework an interesting route to improve the quality of the polymeric pattern is proposed by Darling *et al.* based on the application of Atomic Layer Deposition (ALD) technology into a *Sequential Infiltration Synthesis* (SIS) of polymeric samples.
ALD is a thin films growth technique based on sequential, self-limiting, binary reactions of the surface with two chemical (gas phase) precursors.[4] The deposition indeed proceeds by exposing the surface to the precursors one at a time in non-overlapping pulses. The four main steps giving rise to an ALD Cycle may be listed as follows: exposure of the

[1] LER is defined as the root mean squared variation in the edge position of a patterned feature.

first precursor, purge or evacuation of the reaction chamber to remove the non-reacted precursors, exposure of the second precursor, purge or evacuation of the reaction chamber. In this cycle a precise amount of material is deposited, depending on the number of active sites in the surface-precursor reaction. For this reason the process is self-limited and ALD growth control is at the Å level. A model system for ALD deposition process is the one used for the growth of Alumina films. Thin films of Al_2O_3 could be grown using trimethylaluminum (TMA) and water as precursors.
The same model revealed extremely suitable for the application of ALD on polymeric substrates. TMA indeed is sufficiently reactive even at low temperature which is a prerequisite to prevent polymer degradation and pursue the growth of inorganic film on polymeric substrate by ALD. Figure 5.1 [5] reports a scheme of an Al_2O_3 ALD cycle on a polymer, in the presence of functional groups working as active sites for the precursor.

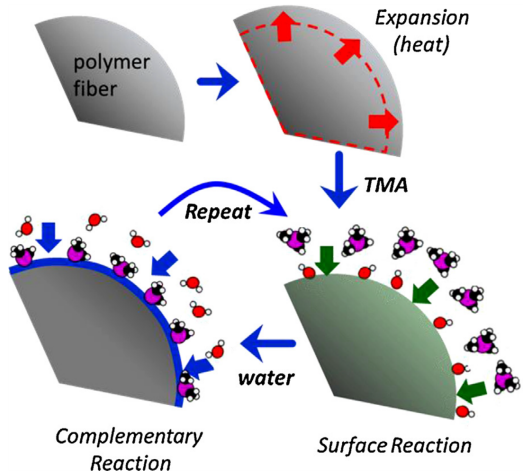

Figure 5.1: Scheme of an ideal TMA/water cycle on a polymer surface, in the presence of a large amount of reactive sites for TMA (taken from[5]).

In the case of PMMA, the interaction of TMA with carbonyls groups was exploited to enhance its etch-resistance when employed as resist in standard lithography and EBL process flow. This technique prevents collapses of striped pattern during the transferring process into deep silicon without the need of further hard mask deposition.[6] In this way the ALD-treated resist could be directly employed as an etch mask for the definition of high aspect ratio nanostructures, through plasma etching processes (300 nm deep structures in silicon starting from 33 nm of PMMA [7]). Morover this treatment does not induce any degradation of the LER of the pattern.
These results can be extended to phase separating polymeric substrates. In this case the polymeric materials can be chosen in order to induce a selective growth into one polymeric component alone. This Sequential Infiltration Synthesis of one block gives rise to inorganic structures with the same order and structure dictated by the phase separation. It is the case of cylinders forming PS-*b*-PMMA thin films processed with Al_2O_3 ALD cycle. The preferential interaction of TMA with PMMA carbonyl groups ruther then with the PS componet is at the origin of the formation of inorganic Alumina cylinders. Once the ALD SIS is performed the polimeric material could be easily removed.[8] A

schematic picture is reported in figure 5.2.

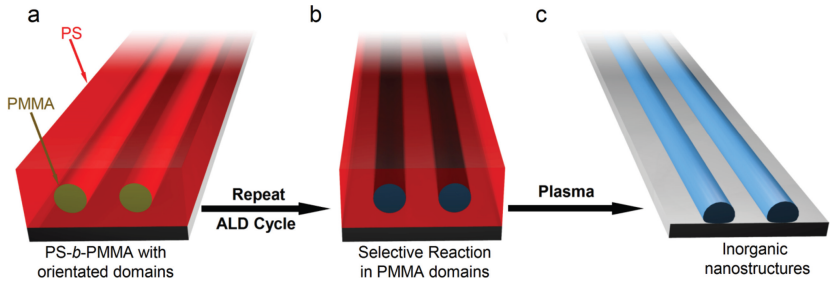

Figure 5.2: Schematic representation of the application of ALD on a PS-*b*-PMMA template of parallel cylinders (a). The raction preferentially occurs in the PMMA domains (b). The polymeric component is etched within O_2 plasma treatment to leave a striped pattern of Alumina (taken from[8]).

The first advantage of this protocols is to convert the polymeric template into an inorganic one with an enhanced etch resistivity with respect to the original one. While the depth of the conventionally etched structured in silicon was reported to be around the order of the thickness of the polymeric film, the SIS-modified BCP could be used as a mask for new lithographic approach in the definition of extremely higher aspect ratio structures.[7]. The second benefit of this approach is that the critical dimension of the striped pattern could be easily controlled by playing with the number of cycles of SIS, starting from relatively large L_0. The easiness of alumina infiltration in PMMA disclosed a wide interest to the optimization of processes for the realization of striped pattern composed by different materials such as SiO_2, ZnO and W and to the investigation of their suitability as lithografic mask.[9] Once again PS-*b*-PMMA revealed to be a suitable model system, but further researches on different materials could in principle bring to a wider range of organometallic patterns.[10]

The SIS approach could be easily implemented for the lamellar pattern fabrication starting from the symmetric PS-*b*-PMMA templates described in this thesis as demonstrated by a few preliminary results. Thin films of B50 were deposited on BrR58 grafted layers (60 s at 310°C in RTP) and then treated at 290°C for 60 s in RTP. Samples were then submitted to different number of TMA/water cycles in a ALD Savannah 200 reactor keeping a temperature of growth of 90°C. The SEM images of the polymeric templates before SIS treatment and the SEM images of the alumina structures obtained after different SIS cycles are reported in figure 5.3. After the SIS procedure samples were treated in a O_2 plasma for 5 minutes at 50 W in order to remove the polymeric components. The characteristic L_0 for each sample maintains around 27 nm, while the CD of the remaining alumina striped structures results to be of 7, 11 and 13 nm for 1, 5 and 10 cycles respectively.
The obtained results are very promising for the controlling of CD within SIS procedure, for the fabrications of striped pattern with sub-20 nm features.

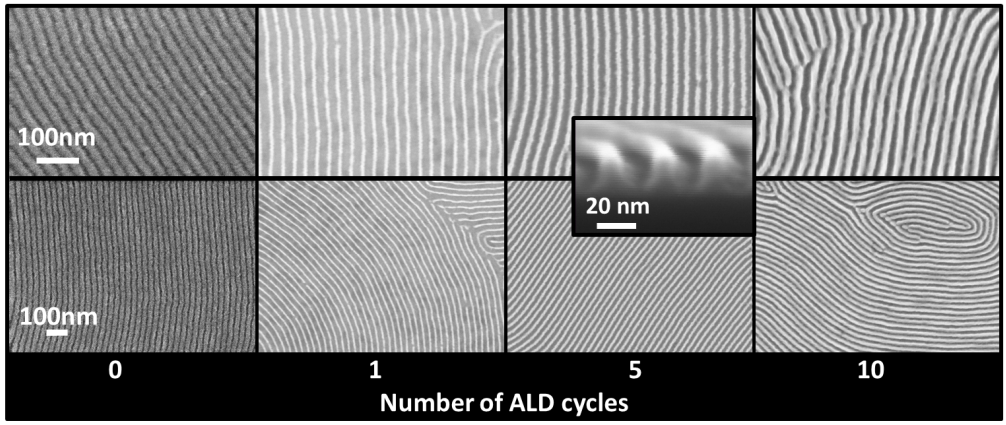

Figure 5.3: SEM top-down images at two different magnitude of B50 lamellar samples organized in RTP and then submitted to different number of cycles of Alumina SIS. On the left the 0-cycle sample corresponds to the test sample treated in RTP and then processed with UV exposure and with a short O_2 plasma treatment in order to remove the PMMA component and to enhanced the contrast in the striped pattern. The other samples were submitted to 1, 5 and 10 cycles of SIS respectively and then processed for 5 minutes in O_2 plasma to completely remove the polymeric components. The leaving alumina lamellae were then imaged with SEM. For this reason the contrast in the resulting pictures is reversed with respect to the original one. A cross section detail for the 5 SIS cycles sample is reported in the inset.

Beyond PS-b-PMMA

The possibility to fabricate and control domains resolution below the 10 nm level is at the basis of the study of high-χ BCPs. These BCPs are particularly promising to extend BCP lithography beyond PS-*b*-PMMA beacuse their high-χ value can enable phase separation, even at a low degree of polymerization (N), with the formation of nanostructures below 10 nm. In this contest silicon containing BCPs are particularly convenient because during the removal of the organic block, the silicon-containing block can be oxidized to form a SiO_x structure, providing proper etch contrast for the subsequent pattern transfer into the substrate. Among them, polystyrene-*b*-polydimethylsiloxane (PS-*b*-PDMS), has attracted more and more interest due to the very high Flory-Huggins interaction parameter of 0.11 (at 150°C, [11]) and small domain resolution. Nevertheless, the high incompatibility between the two blocks in silicon-containing BCPs inhibits the thermal diffusion of the polymeric chains and results in an extremely slow kinetic of the self-assembly and lateral-ordering processes. Because of the progressive slow down into self-assembly kinetic for increasing segregation strength (χN) [12], it would be highly desirable to thermally treat these BCPs at high temperatures to speed the process for a fixed given N value. A deep investigation of the kinetics of self-assembly at high temperatures, such as the one proposed in this thesis for PS-*b*-PMMA system, appears to be hampered by the low thermal stability of the siliconcontaining block with respect to the PS one [13], resulting in a limited processing temperature and, consequently, in a limited mobility of the macromolecules during the thermally induced ordering. Nevertheless in a recent study the self-assembly of cylinder-forming polystyrene-block-poly(dimethylsiloxane-random-vinylmethylsiloxane) (PS-*b*-P(DMS-r-VMS)) BCP

on flat substrates was promoted by means of a simple thermal treatment at high temperatures.[14] This work opens the possibility to study the thermodynamic and kinetic of the high temperature process-dependent self-assembly on a broad range of polymers.

Bibliography

[1]F. Ferrarese Lupi, G. Aprile, T. J. Giammaria, G. Seguini, G. Zuccheri, N. De Leo, L. Boarino, M. Laus, and M. Perego, "Thickness and Microdomain Orientation of Asymmetric PS-b-PMMA Block Copolymer Films Inside Periodic Gratings.", ACS applied materials & interfaces **7**, 23615–22 (2015).

[2]L. Wan, R. Ruiz, H. Gao, K. C. Patel, T. R. Albrecht, J. Yin, J. Kim, Y. Cao, and G. Lin, "The Limits of Lamellae-Forming PS-b-PMMA Block Copolymers for Lithography.", ACS nano **9**, 7506–7514 (2015).

[3]D. F. Sunday, E. Ashley, L. Wan, K. C. Patel, R. Ruiz, and R. J. Kline, "Template-polymer commensurability and directed self-assembly block copolymer lithography", Journal of Polymer Science Part B: Polymer Physics **53**, 595–603 (2015).

[4]S. M. George, "Atomic layer deposition: an overview.", Chemical reviews **110**, 111–31 (2010).

[5]G. N. Parsons, S. E. Atanasov, E. C. Dandley, C. K. Devine, B. Gong, J. S. Jur, K. Lee, C. J. Oldham, Q. Peng, J. C. Spagnola, and P. S. Williams, "Mechanisms and reactions during atomic layer deposition on polymers", Coordination Chemistry Reviews **257**, 3323–3331 (2013).

[6]Y.-C. Tseng, A. U. Mane, J. W. Elam, and S. B. Darling, "Enhanced Lithographic Imaging Layer Meets Semiconductor Manufacturing Specification a Decade Early", Advanced Materials **24**, 2608–2613 (2012).

[7]Y.-C. Tseng, Q. Peng, L. E. Ocola, D. A. Czaplewski, J. W. Elam, and S. B. Darling, "Enhanced polymeric lithography resists via sequential infiltration synthesis", Journal of Materials Chemistry **21**, 11722 (2011).

[8]Q. Peng, Y.-C. Tseng, S. B. Darling, and J. W. Elam, "Nanoscopic patterned materials with tunable dimensions via atomic layer deposition on block copolymers.", Advanced materials **22**, 5129–33 (2010).

[9]Q. Peng, Y.-C. Tseng, S. B. Darling, and J. W. Elam, "A route to nanoscopic materials via sequential infiltration synthesis on block copolymer templates.", ACS nano **5**, 4600–6 (2011).

[10]J. Kamcev, D. S. Germack, D. Nykypanchuk, R. B. Grubbs, C.-Y. Nam, and C. T. Black, "Chemically enhancing block copolymers for block-selective synthesis of self-assembled metal oxide nanostructures.", ACS nano **7**, 339–46 (2013).

[11]C. Sinturel, F. S. Bates, and M. A. Hillmyer, "High χ-Low N Block Polymers: How Far Can We Go?", ACS Macro Letters, 1044–1050 (2015).

[12]J. M. Kim, Y. Kim, W. I. Park, Y. H. Hur, J. W. Jeong, D. M. Sim, K. M. Baek, J. H. Lee, M.-J. Kim, and Y. S. Jung, "Eliminating the Trade-Off between the Throughput and Pattern Quality of Sub-15 nm Directed Self-Assembly via Warm Solvent Annealing", Advanced Functional Materials **25**, 306–315 (2015).

[13]G. Deshpande, and M. E. Rezac, "Kinetic aspects of the thermal degradation of poly(dimethyl siloxane) and poly(dimethyl diphenyl siloxane)", Polymer Degradation and Stability **76**, 17–24 (2002).

[14]T. J. Giammaria, F. F. Lupi, G. Seguini, M. Perego, F. Vita, O. Francescangeli, B. Wenning, C. K. Ober, K. Sparnacci, D. Antonioli, V. Gianotti, and M. Laus, "Micrometer-Scale Ordering of Silicon-Containing Block Copolymer Thin Films via High-Temperature Thermal Treatments", ACS applied materials & interfaces **8**, 9897–9908 (2016).

Appendix

CHAPTER 6

Homopolymer Blends: Alternative Route to Obtain a Neutral Brush Layer.

As widely discussed in chapter 3 the most common approach to generate a neutral surface was introduced by Mansky [1] and consists in the use of end-functional poly(A-r-B) random copolymers to induce the perpendicular orientation of polyA-b-polyB block copolymers. This concept was initially applied to polystyrene-b-poly (methyl methacrylate) (PS-*b*-PMMA) block copolymers through the use of hydroxyl-terminated poly(styrene-r-methyl methacrilate)s (P(S-r-MMA)) that, upon thermal treatment, undergo a "grafting to" process with the HO-Si moieties of the SiO_2 substrate. By properly adjusting the random copolymer composition, a precise control of the interfacial energies obtained and the perpendicular orientation of lamellar or cylinder-forming block copolymer is achieved when non-preferential surfaces are employed. This concept has been further developed as a kind of leitmotif, leading to a great variety of random copolymers bearing not only end-chain but also side-chain thermal- or photo-crosslinkable functional groups [2][3], and neutral layers for PS-*b*-PMMA can be deposited regardless of the chemistry of the underlying substrates.[4]
As the synthesis of tailor-made functional random copolymers for each specific block copolymer could be quite demanding and not always feasible, an alternative and apparently forthright possibility resides in the use of a binary blend of end-functional homopolimers A and B. In general, the preparation of homopolymers featuring reactive functional groups, so that they can form a covalent bond with the substrate and create a polymer brush, is relatively simple, and the control over the molar mass, including the molar mass distribution, can be efficiently exerted by the use of living or controlled polymerization techniques. The use of homopolymer blends to tune the substrate surface could be efficient, provided that no macroscopic phase separation occurs or that the chemically different polymer brushes are mixed over a sufficiently small length scale to create a chemically neutral surface for the self-assembly of vertically oriented block copolymer microdomains in the overlying polymeric film (see the scheme in figure 6.1).

In spite of the apparent simplicity of the process, few studies have been reported so far on surface neutralization using homopolymer mixtures. Most of the studies available in the literature focus on the PS/PMMA system.
The PS/PMMA system is an upper critical solution temperature (UCST) blend [5], and for symmetric molar mass pairs below 7000 g/mol the two homopolymers are miscible above T_g. Mixtures of low molar mass hydroxyl-terminated polystyrene (PS-OH) and polymethylmethacrylate (PMMA-OH) (PS Mn=3800, Mw=4900; PMMA Mn=4000, Mw=4400) were grafted to activated silicon surfaces by annealing them for 48 h at 160°C

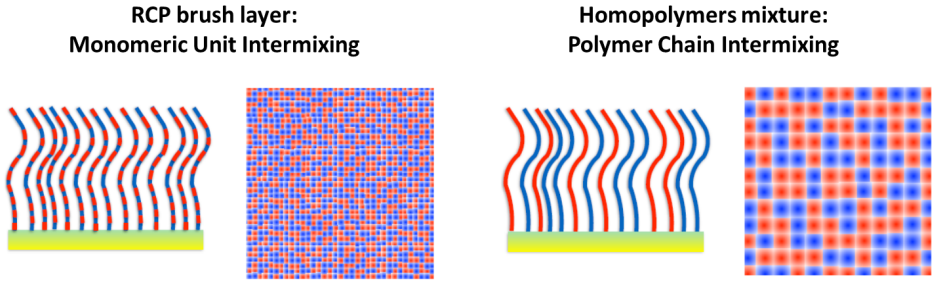

Figure 6.1: A RCP brush layer (see chapter 1 and 3) achieves the neutrality of surface interactions through a monomeric unit intermixing (left scheme). If chemically different polymer brushes are mixed over a sufficiently small length scale, neutralization could result from polymer chain intermixing (right scheme).

in order to form a brush of PS and PMMA molecules randomly attached to the surface [6]. An efficient tuning of the surface energy was reported by controlling the composition of the blend cast onto the surface. The measured contact angles were proportional to the blend composition used for surface treatment, in agreement with the miscible nature of the blend components. Although the PS/PMMA brushes were claimed as an alternative approach to generate neutral surfaces, no data regarding the ordering characteristics of PS-*b*-PMMA on these functionalized substrates were provided.
Somewhat higher molar mass end-functional PS-OH and PMMA-OH homopolymers (PS Mn=6000, Mw=6400; PMMA Mn=6300, Mw=6700) were employed by Nealey [7] and grafted onto the silicon surface for 48 h at 160°C . The preparation of a neutral brush layer was not successfully accomplished using pure homopolymer blends due to the occurrence of demixing accompanied by phase segregation. To inhibit phase separation of the homopolymers, ternary blends, including PS-OH and PMMA-OH as well as a PS-*b*-PMMA block copolymer, were prepared. Perpendicular orientation of both lamellae and cylinder-forming block copolymer domains was observed only in a very narrow composition window of the ternary blend. Although the effect of the neutralizing layer thickness was not explicitly dealt with, the formation of a thin layer of about 4–5 nm was reported, thus possibly explaining the relatively high defect density in the relevant SEM pictures. Obviously, higher molar mass PS-OH and PMMA-OH homopolymers should be employed to obtain thicker grafted layers. However, the increased demixing propensity of the two homopolymers could not be fully compensated by the addition of the block copolymer.
In principle, a neutral surface can be prepared in a single step not only by a grafting process involving a homogeneous blend, but also by performing the grafting reaction from a bi or multilayer system of immiscible functional homopolymers lying parallel to the substrate surface. However, the formation of a PS overlayer during annealing of a PS/PMMA thin film polymer blend at 142°C was reported [8] only once, whereas the results observed in annealed PS/PMMA systems indicated in most cases the occurrence of phase-separated films without any wetting layer at the air interface [9].
On the basis of thermodynamic equilibrium considerations, it was demonstrated that the spreading parameter for PMMA spreading on PS remains negative at all achievable

temperatures. However, the spreading parameter for PS spreading on PMMA can be also estimated from the literature data [9][10] and accounts to -1.8 mJ/m^2 at 140°C but turns to the positive value of 1.7 mJ/m^2 at 290°C. As a silicon surface is preferential for the PMMA, this result suggests that a PS layer can spread on a PMMA layer, laying over the silicon surface, once the thermal treatment is performed at sufficiently high temperatures.
In this contest, results reported in the previous chapters on the possibility to perform a grafting process at high temperature and short time of annealing within a RTP, open new possibilities to promote the grafting of binary homopolymer mixtures to modify the surface. In the next sections the grafting characteristics of homopolymer blends with two functional PS-OH and PMMA-OH with a molar mass of about 16000 g/mol were studied in detail as a function of the original composition of the blend and of the processing parameters. Thin films of PS-*b*-PMMA (symmetric and asymmetric) were subsequently deposited on top of the various brush layers and used to probe the effect of the surface modification and eventual surface neutralization on the ordering and orientation characteristics of PS-*b*-PMMA domains.

6.1 Experimental Details

6.1.1 Materials

Two block copolymers PS-*b*-PMMA with a styrene fraction of XS = 0.70 (asymmetric copolymer, Mn = 67100 g/mol and PDI = 1.09, PMMA syndiotactic rich contents >78%) and XS = 0.50 (symmetric copolymer, Mn = 51000 g/mol and PDI = 1.06, PMMA syndiotactic rich contents >78%) were purchased from Polymer Source Inc. and used as obtained. The block copolymers (BCPs) were marked B50 and B70, where B stands for block, and the number represents the percent styrene unit.
Two homopolymers were synthesized for the styrene and methyl methacrylate component: PS_{16}-OH with Mn=16000 g/mol and PDI= 1.14; $PMMA_{15}$-OH with Mn=15000 g/mol and PDI= 1.22. The complete procedure of synthesis of the homopolymers can be found elsewhere.[11]

6.1.2 Substrate preparation

Substrates of 1 cm^2 area were cut from (100) oriented Si wafers with a native SiO_2 layer. The oxidized substrates were cleaned with Piranha solution (H_2SO_4/H_2O_2 with 3/1 vol. ratio at 80°C for 40 min) to eliminate any residual organic material and to increase the surface concentration of hydroxyl groups. This step of the process was effective in reducing the water contact angle of the substrate from 63.5° to 8°. The activated substrates were rinsed in H_2O and dried in N_2. Finally, the cleaning process was completed by an ultrasonic bath in 2-propanol.

6.1.3 Annealing procedure

A first series of samples was obtained by spin coating $PMMA_{15}$-OH or PS_{16}-OH solutions (18.0 mg in solution with 2.00 mL of toluene) for 30 s at 3000 rpm on the activated SiO_2 surface, leading to a polymeric film of $\sim$30 nm. A second series of samples was prepared by mixing the homopolymer solutions in toluene to obtain a blend at a predeter-

mined composition. These blends were identified by the general acronym PS/PMMA-n, where n represents the weight percent of the PS_{16}-OH in the polymeric blend. All samples were then annealed in RTP in order to promote the grafting process. The removal of the non-grafted polymer was performed by means of a toluene ultrasonic bath. The samples of the second series were spin coated with a solution of PS-*b*-PMMA B50 or B70 (18.0 mg in 2.0 mL of toluene) for 30 s at 3000 rpm, leading to a polymeric film of $\sim$30 nm.
The grafting of $PMMA_{15}$-OH, PS_{16}-OH, and PS/PMMA-n blends was achieved by RTP treatments with T_{target} in the range 170–350°C, whereas the grafting time ranged from 1–600 s. To promote BCPs self-assembly, after deposition of the PS-*b*-PMMA films, the samples were further annealed in RTP at 250°C for 300 s.

6.1.4 Characterization of Thickness and Morphology

The thickness of the polymeric films was measured by means of an M-200U spectroscopic ellipsometer (J. A. Wollam Co. Inc.) using a Xe lamp at a 70° incident angle. Water contact angle measurements were performed using an optical tensiometer Attension Theta.
The morphology of the block copolymer films was characterized by scanning electron microscopy (SEM) images (Zeiss Supra 40 SEM). Opening of the cylindrical or lamellar nano-template was completed by selective removal of the PMMA blocks in order to ensure a good contrast in the SEM images. The degradation of the PMMA component via chain scission was achieved by exposing the samples to UV radiation (5 mW/cm^2, λ= 253.7 nm, 15 min). The degraded PMMA for B70 was then removed by washing the samples in an acetic acid bath for 8 min.[1] An O_2 plasma treatment was performed on B70 and B50 samples to cross-link the PS chains and remove the grafted PS-OH and PMMA-OH at the bottom.
Atomic force microscopy (AFM) characterization was performed in tapping mode in a Nanoscope V system (Bruker, U.S.A.) equipped with a Multimode head and using NSC15 probes (MikroMasch, Estonia). Topography data was recorded in light and hard tapping mode, and the phase information was recorded simultaneously.

6.1.5 TGA-GC-MS Copolymer Characterization

The TGA-GC-MS analyses were performed using a Mettler TGA/SDTA 851^e purged with a steady flow of inert gas at a scanning rate of 20°C/min from room temperature to 1100°C. The polymeric films on the substrate were directly placed on the thermo-balance plate. The evolved gas from thermogravimetric analysis (TGA) was transferred to the GCMS using the interface well described elsewhere.[12] The transfer lines from the TGA to the interface and from the interface to the gas chromatography (GC) were set at the temperature of 200°C, the temperature of the interface was 150°C, and the sampling frequency was 30 s^1. The sampled gas from the loop to the waste was switched after 10 s, and the capacity of the injection loop was 2.5 mL. The GC-MS analysis was performed using a Finnigan TRACE GC-Ultra and TRACE DSQ. The GC separation was carried out using a Phenomenex DB5-5 ms capillary column (30 m, 0.25 mm, i.d., 0.25 μm thickness). The injector temperature was set at 250°C in splitless mode, and helium was used as a

[1] This step is not performed when dealing with B50 lamellar structures because it could induce a collapse of PS walls.

carrier gas at a constant flow of 1.0 mL/min. The mass spectrometry (MS) transfer line and the oven temperatures were set at 280 and 150°C, respectively.
The MS signal was acquired in EI+ mode with ionization energy of 70.0 eV and at the ion source temperature of 250°C. The acquisition was performed both in full-scan mode, in the 20–350 m/z range, and in single ion monitoring mode by acquiring the signals corresponding to styrene at m/z = 104 and methyl methacrylate at m/z = 100.

6.1.6 Determination of the Grafted Layer Composition

If a proper calibration procedure is provided, it is possible to determine the chemical composition of the grafted layers. The calibration was performed, reporting the styrene content of the blend versus the ratio of the interpolated chromatographic areas relative to the evolution of the Styrene (S) and Methylmethacrylate (M) monomers, in the TGA-GC-MS. Silica wafers spin coated with different blend compositions (from 95:5 PS:PMMA to 5:95 PS:PMMA) were employed as calibration samples and subjected to the TGA-GC-MS scanning treatment from room temperature to 1100°C, at the scanning rate of 20°C/min. The obtained calibration was employed to calculate the relative composition of the samples subjected to the different thermal treatments.
The expected composition of the grafted layer was computed, starting from a simple ideal model of the as-spun blend consisting in a perfect segregated and layered structure with the PMMA layer in contact to the substrate surface and the PS layer at the top. As the thickness of the as-spun blend is 30 nm, from the composition of the blend and the (bulk) densities of the two homopolymers, the thickness of the PMMA layer can be estimated. If the thickness of the PMMA layer is higher than or equal to the thickness of the grafted layer (about 6–7 nm), then the amount of PS in the grafted layer is zero. Otherwise, if the thickness of the PMMA layer in the as-spun blend is lower than the thickness of the grafted layer, the amount of PS is computed from the difference between the thickness of the grafted layer and the estimated thickness of the PMMA layer in the as-spun blend.

6.2 Homopolymer Grafting

Figure 6.2 reports the thickness of the grafted layer of PS_{16}-OH and $PMMA_{15}$-OH as a function of grafting time, after the removal of the non-grafted polymeric chains, when the grafting reaction is performed at 290°C. The layer thickness increases very fast at the beginning and then levels off, in agreement with the strongly self-limiting nature of the ``grafting to´´reaction.[13] [14] [15]
The limiting saturation value amounts to about 8.3 $\pm$ 0.3 nm for both homopolymer samples as they present very similar molar masses. This thickness is large enough to guarantee the physical decoupling between the BCP thin film and the underlying SiO_2 substrate. In this condition, the orientation of the BCP nanodomains is exclusively determined by the composition of the brush layer [16] [1] [4].
For short grafting times, although within the experimental errors, the thickness of PS_{16}-OH appears slightly higher than $PMMA_{15}$-OH. This difference becomes evident when the thickness of the film is reported as a function of the grafting temperature at the fixed grafting time of 600 s (figure 6.3).
When the temperature is higher than 230°C, the curves reporting the growth of the

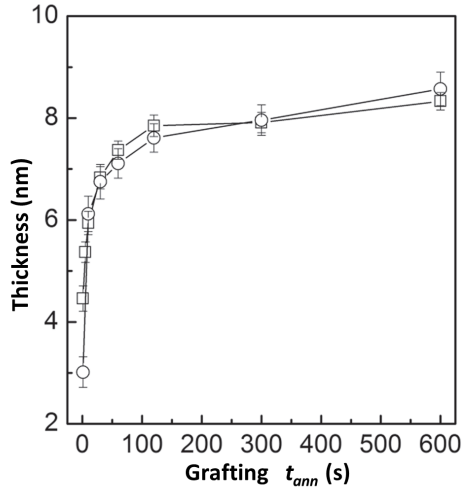

Figure 6.2: Thickness of the grafted films of PS_{16}-OH (square) and $PMMA_{15}$-OH (circle) at 290°C for 600 s as a function of grafting time.

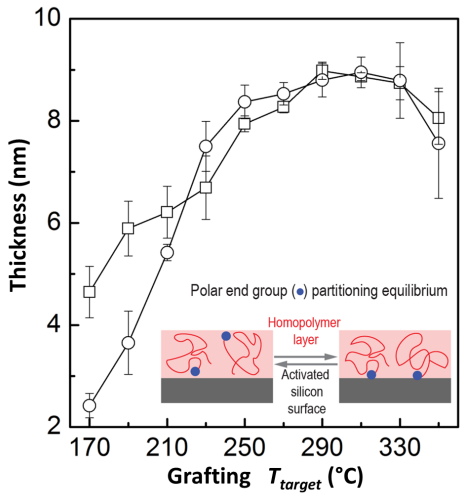

Figure 6.3: Thickness of the grafted films of PS_{16}-OH (square) and $PMMA_{15}$-OH (circle) for 600 s as a function of the grafting temperature. In the inset, the partitioning equilibrium of the hydroxyl group between the polymer layer and the SiO_2 surface is illustrated.

thickness of the two homopolymer layers are identical, within the experimental error, indicating that saturation values can be achieved at this temperature range in a grafting time equal or even lower than 600 s. In contrast, for grafting temperatures lower than 230°C, the thicknesses of the homopolymer layers are significantly lower than the saturation value. Due to the low mobility of the homopolymer chains in this temperature range, the grafting process cannot be accomplished reaching the final equilibrium configuration. In this condition, it is worth noting that the PS_{16}-OH grafted layer is systematically higher than that of the $PMMA_{15}$-OH. Since the molar mass of the two homopolymers is quite similar, chain mobility and diffusivity of the macromolecules cannot explain this experimental finding.
This result can be understood, considering that the hydroxyl-bearing end group is very polar and could undergo a partitioning equilibrium between the polymer layer and the SiO_2 surface, as schematically illustrated in the inset of figure 6.3. In case of PS_{16}-OH, the hydrophobic nature of the PS layer should drive the equilibrium partitioning toward the right side, since the polar chain ends should be located preferentially onto the SiO_2 surface, whereas in case of $PMMA_{15}$-OH, some polar end groups could be also accommodated within the polymer layer because of the higher polarity of the PMMA. Consequently, the effective concentration of the functional end groups at the SiO_2 surface should be higher for PS_{16}-OH than $PMMA_{15}$-OH, thus finally leading to a faster thickness growth for the former polymer. Finally, when the grafting temperature is higher than 310°C, a decrease in the layer thickness is obtained, possibly due to the onset of polymer degradation.[17] [18]

6.3 Homopolymer Blend Grafting

Several blends were prepared by mixing PS_{16}-OH and $PMMA_{15}$-OH solutions in toluene at predetermined compositions. The characteristics of the various samples, together with the processing conditions are reported in the table.

Initially blends with two different compositions, namely, PS/PMMA-50 and PS/PMMA-90, were grafted on SiO_2 substrates at different temperatures, keeping the grafting time constant (600 s). Water contact angle measurements were performed on samples before and after the grafting treatment and were repeated after removal of the non-grafted polymeric chains. The water contact angle for all the samples from PS/PMMA-90 and PS/PMMA-50 blends, before and after the grafting reaction but before the removal of the unreacted materials, is about 90°. The water contact angles reported in the table conversely were taken after the removal of the non-grafted chains for all the samples.
The composition of the grafted layer was determined, after removal of the non-grafted material, by TGA-GC-MS, using the signals corresponding to the evolved styrene (m/z 104) and methylmethacrylate (m/z 100) to build up a calibration curve. As a typical example, figure 6.4 reports the TGA-GC-MS chromatograms, with specific reference to the mass peaks at m/z 100 and at m/z 104, after grafting PS/PMMA-90 and PS/PMMA-50 to the SiO_2 substrate at 290°C for 600 s.
From the ratio of the interpolated chromatographic areas relative to the evolution of the styrene and methyl methacrylate, taking into account the calibration curve, the composition of the grafted layer was determined and amounted to PS% = 15.0 and 61.9 for PS/PMMA-50 and PS/PMMA-90, respectively.

Sample	As-spun thickness (nm)	RTP T_{target} (°C) for 600 s	Grafted thickness (nm)	Water Contact Angle (°)	PS in the grafted layer (%)
PS/PMMA-90	28	230	4.1	79.6	35.2
	29.3	250	6.8	81.9	45.9
	28.5	270	7	82.2	48.8
	27.8	290	7.8	82.5	61.9
	28.5	310	8.2	82.9	57.5
	28.6	330	7.8	84.4	58.3
PS/PMMA-50	28.5	230	6.3	69.8	13.3
	29.2	250	9	69.6	15.2
	28.7	270	9.5	69.6	14.5
	27.8	290	9.9	70.1	15
	28.3	310	8.4	70.4	15.7
	27	330	9.2	70.5	14.4
PS/PMMA-95	27.6	290	8.9	88.8	77.3
PS/PMMA-90	27.8	290	7.8	82.5	61.9
PS/PMMA-85	27.8	290	7.7	79.8	50.1
PS/PMMA-80	26.6	290	7.1	76.1	37
PS/PMMA-75	27.3	290	7.3	73.6	33.2
PS/PMMA-70	26.4	290	7.5	72.1	23.8
PS/PMMA-65	26.4	290	7.6	70.6	21.4
PS/PMMA-50	27.8	290	9.9	70.1	15

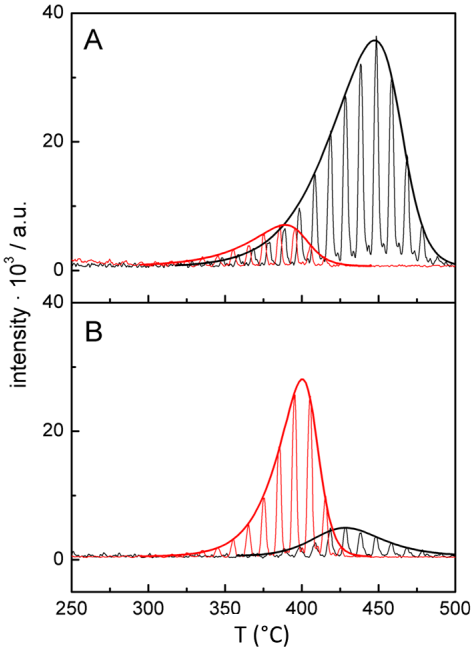

Figure 6.4: TGA-GC-MS chromatograms for PS/PMMA-90 (A) and PS/PMMA-50 (B), after grafting at 290°C for 600 s and removal of the unreacted material, with specific reference to the mass peaks at m/z 100 and at m/z 104, corresponding to methylmethacrylate (red line) and styrene (black line), respectively.

The composition data of the grafted layers after reacting PS/PMMA-90 and PS/PMMA-50 blends at different grafting temperatures (from 230–330°C) for 600 s, as well as the water contact angles for the grafted samples after removal of the non-grafted material, are reported in the table. In both sample series, the grafted layers are PMMA-rich, and the percentage of polystyrene is much lower than in the original blend. In the case of PS/PMMA-50, the percentage of grafted polystyrene amounts to about 13% – 16% and does not change with grafting temperature. For PS/PMMA-90 blends, the percentage of grafted polystyrene increases from 35%, when the grafting reaction is performed at 230°C, up to about 60%, corresponding to the grafting temperature of 330°C. The water contact angle for the sample prepared by grafting the two homopolymers are 69° for $PMMA_{15}$-OH and 92° for PS_{16}-OH. The water contact angles of series PS/PMMA-50 are comprised between 69.8°– 70.5°, whereas for series PS/PMMA-90 the contact angles increase regularly from 79.6°– 84.4°as the grafting temperature increases.
The overall picture of the above data indicates that once the blend is spun, due to the strong attractive interactions between the carbonyl groups of PMMA and the silanol groups on the SiO_2, the $PMMA_{15}$-OH is preferentially adsorbed at the hydrophilic SiO_2 surface. Consequently, a layer of $PMMA_{15}$-OH rich phase is located at the SiO_2 surface, whereas a PS_{16}-OH rich phase can be found at the air/polymer interface, as indicated by the water contact angle measurement performed before and after grafting reactions. This phase separation ultimately leads to the preferential grafting of $PMMA_{15}$-OH chains on the substrate, leading to PMMA-rich grafted layers.
In addition, as the limiting layer thickness of the two homopolymers is about 8.3 nm (figure 6.2), and considering that the thickness of the as-spun blends is in all cases about 30 nm, we can correlate the composition of this PMMA-rich grafted layer to the composition of the blend. For PS/PMMA-50 and PS/PMMA-90 the thickness of the $PMMA_{15}$-OH rich phase before grafting would be about 15 and 3 nm, respectively. Accordingly, for PS/PMMA-50 a negligible amount of PS_{16}-OH is expected to graft to the surface due to the screening effect induced by the saturated PMMA brush layer. Conversely, for PS/PMMA-90 we observed a progressive increase of the grafted layer thickness (as reported in the table) as a function of the grafting temperature and a correspondent increase of the amount of grafted PS_{16}-OH. This experimental evidence suggests that, since the 3 nm-thick $PMMA_{15}$-OH rich phase in the as-spun film is lower than the limiting layer thickness (about 8.3 nm), the PS_{16}-OH molecules in the film can diffuse through the PMMA-rich layer and react with the substrate, leading to a progressive increase of the film thickness and enrichment in the PS content as a function of the grafting temperature.
The same grafting procedure was performed at 290°C for 600 s for several PS/PMMA-n blends with n ranging from 50 to 95. The thickness of the grafted layer was found to be about 7–8 nm for all the samples, confirming the limiting saturation thickness. Figure 6.5 illustrates the compositions of the different PS/PMMA-n blends obtained by TGA-GC-MS analysis and the corresponding water contact angle data.

For all the samples, the amount of PS_{16}-OH grafted to the SiO_2 surface is considerably lower than in the original blend (dashed red line), in agreement with data in the literature. [7]
However, if we consider the composition of a layered structure consisting of a PS_{16}-OH rich phase at the polymer/SiO_2 interface (featuring a variable thickness as a function of the blend composition) covered by a PS_{16}-OH rich phase, then the experimental data are

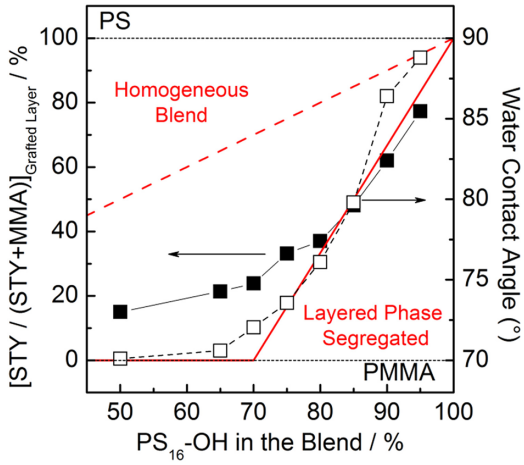

Figure 6.5: Polystyrene percentage (full square) in the grafted layer as well as water contact angle (open square) after reacting PS/PMMA-n at 290°C for 600 s. The red dashed line represent the expected composition in the case of grafting from a homogeneous blend, whereas the continuous red lines represent the expected composition in the case of grafting from a layered phase-segregated structure with the $PMMA_{15}$-OH rich phase located at the silicon substrate and the PS_{16}-OH rich phase at the polymer/air interface, as described in the experimental details.

in agreement with the expected compositions (continuous red line).

6.4 Block Copolymer Self-Assembly

The effective surface neutralization was investigated by spinning B50 and B70 over samples grafted at 290°C for 600 s with blends having a PS % ranging from 75–100. Figure 6.6 reports a collection of SEM images which illustrate the orientation of nanodomains in the B50 and B70 films deposited on the different grafted layers.

For both block copolymers, using PS/PMMA-n blends with n $<$ 85%, a heterogeneous texture is observed, comprising circular domains in which perpendicular cylinders or lamellae are observed, whereas a mixed or parallel morphology can be observed outside. The size and density of the circular domains increase with increasing PS_{16}-OH percentage in the grafting blend. Corresponding to PS/PMMA-85, no more circular domains are observed. In particular, homogeneous textures of perpendicularly oriented lamellae are obtained for the symmetric block copolymer, indicating that proper neutralization of the substrate has been achieved for symmetric BCPs. Conversely, a mixed morphology consisting of parallel and perpendicularly oriented cylinders is observed for the asymmetric block copolymer, thus indicating that the surface is neutral for the former but not for the latter block copolymer. However, corresponding to PS/PMMA-90, homogeneous textures of perpendicularly oriented cylinders are obtained, thus indicating the achievement of a perfect surface neutralization for the asymmetric block copolymer. In this case, a parallel arrangement of the lamellar structure of the symmetric block copolymer is obtained.
The effective percentage of PS homopolymer in the grafted layers of the PS/PMMA-85

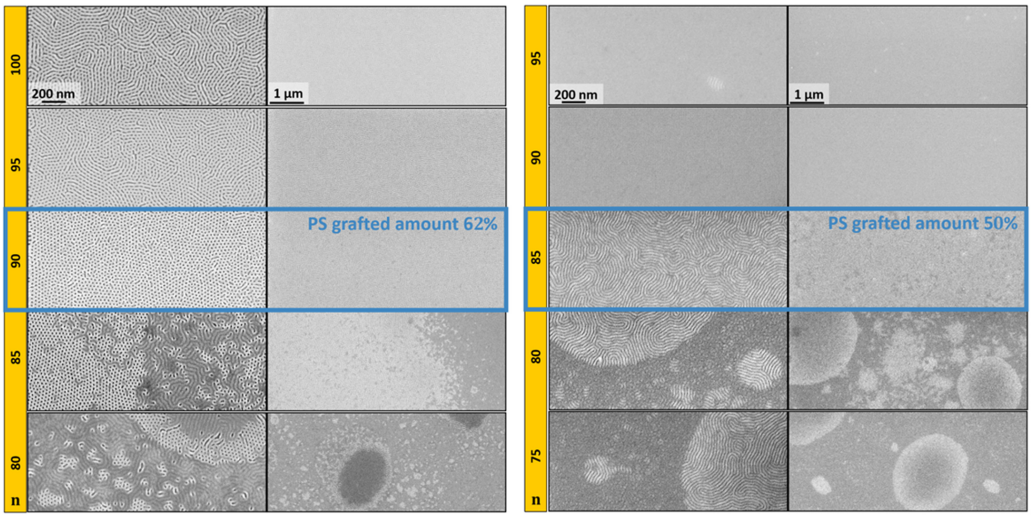

Figure 6.6: Morphologies of B70 (left panel) and B50 (right panel) on the silicon wafer after the grafting reaction at 290°C for 600 s of PS/PMMA-n blends with different n values. Images at two different magnitudes are reported.

and PS/PMMA-90 is 50±2 and 62±2% (figure 6.5). These values are quite close the optimum styrene content, which is reported to provide an effective surface neutralization for symmetric and asymmetric block copolymers in the case of hydroxyl-terminated PS-*r*-PMMA random copolymer brush layers.[1] [19] [20] Further increasing the PS amount in the grafting blend, homogeneous textures are obtained, but the orientation of both lamellae and cylinders turns to parallel, in agreement with an exceedingly high amount of PS in the grafted layer, which does not result in a neutral layer for the block copolymers.

6.5 Grafted Layer Morphology

The effective morphology of the grafted layer was directly studied by AFM, and additional information was obtained from the morphological arrangement of the phase-separated B70 and the B50 block copolymers overlying the different grafted layers.
Figure 6.7 illustrates, in parallel, representative AFM topographic images of grafted PS/PMMA-n samples upon grafting at 290°C for 600 s (top row) and SEM images of B50 thin films deposited on the grafted substrates and subsequently annealed at 250°C for 300 s (bottom rows).

In the blends with PS$\geqslant$85%, a homogeneous texture is observed in the AFM images of the grafted layers, and the corresponding SEM images show a homogeneous morphology in the B50 film spun on top of the grafted layer and thermally treated (right column). This observation indicates that, for high PS% in the blends, a smooth and compositionally homogeneous layer is obtained because of the grafting process.
On the other hand, the topographic images of the samples grafted with blends having PS$<$85% are characterized by the presence of topographic structures. The AFM images highlight the presence of large structures with a circular shape and diameter comprised

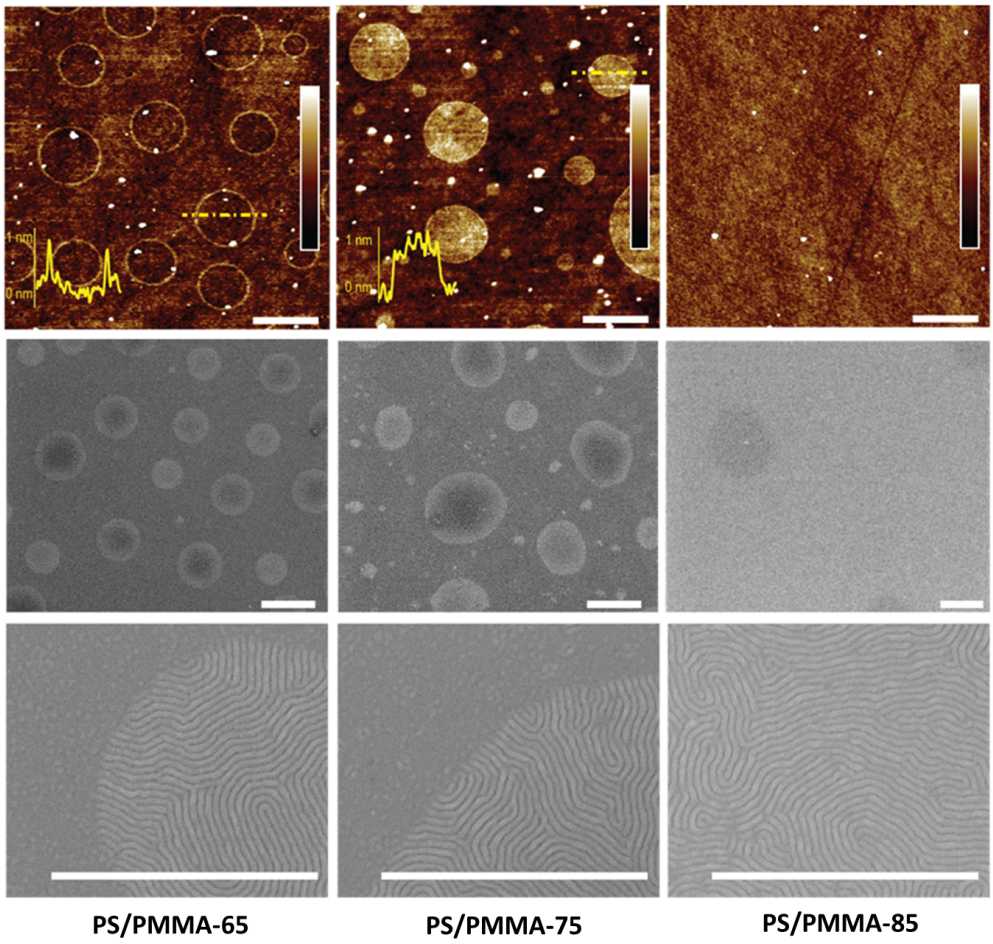

Figure 6.7: AFM topographic images of grafted PS/PMMA-n samples at 290°C for 600 s (top row) and SEM images after deposition of B50 on the same samples, followed by annealing at 250°C for 300 s (bottom rows). The horizontal size bars are 2 μm in the images of the first two rows from the top and 1 μm in the third row. The color range in the AFM images is equivalent to a 2 nm height range, as coded in the included color bars. The overlay plots in the AFM images show the height profiles along the dashed traces in the images on the round surface structures.

between 1–3 μm. In addition, a second set of small circular structures with a size of about 0.2–0.5 μm can be noticed (central and left columns).
As shown in figure 6.8, circular ``drops´´of homopolymer are evident in these specimens after RTP thermal treatment of spun blends but prior to washing the non-grafted polymer chains.
The size distribution of these dewetted drops is indistinguishable from that of the circular structures shown in figure 6.8 for specimens with PS<85%.

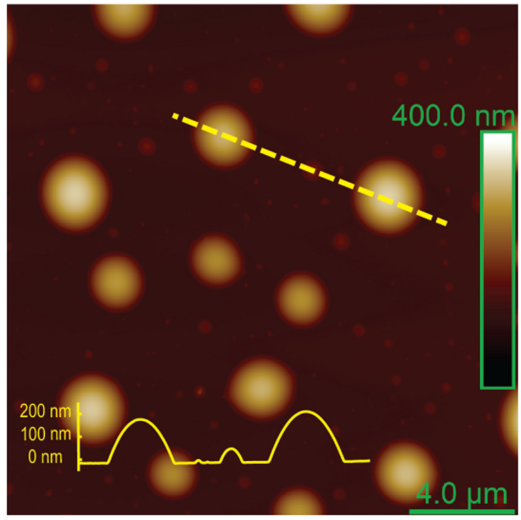

Figure 6.8: AFM topographic images of a PS/PMMA layer after spin coating of PS/PMMA-70 and RTP treatment at 290°C for 30 s. The image was recorded before solvent wash of the ungrafted polymer; thus it shows the drops of polymer (presumably mainly PS) that have dewetted from the substrate upon thermal treatment. Feature sizes and heights are as coded in the included size bar and colour bar.

When B50 is deposited on these samples and thermally treated, circular islands with perpendicular orientation of the lamellae emerge from an ill-defined background (figure 6.7). The close similarity between the circular elements observed in the AFM analysis and the ordered block copolymer circular region observed in the SEM image clearly indicated that the grafting reaction leads to the formation, in the grafted layer, of a heterogeneous structure in which the composition inside the circular elements is different from that of the background. Such a compositional difference inside the circular elements is clearly evident from the AFM micrographs obtained for the blend with PS = 75%, where the circular elements are disks with an apparent height of about 1 nm with respect to the surface outside the circular features (see the height profile overlaid on the corresponding AFM image). Based on the orientation of the PS-b-PMMA on top of the grafted layer, we suppose that such additional height might report on a thicker grafted layer where PS chains protrude from a PMMA ``carpet´´. In AFM micrographs of the blend with PS = 65%, the circular structures appear as rings with a 1 nm-thick border but not showing any significantly different surface height in their inner portions, if compared with the substrate outside of the circular structures. Yet the orientation of the nanodomains in the PS-b-PMMA film deposited on top of the grafted layer support the idea of a different

composition of the grafted layer inside and outside these circular structures. It could be supposed that at such lower PS fraction, the grafting of PS in the internal area is slightly lower, not leading to sufficient AFM contrast with respect to the outside. On the edges of the dewetted PS drops, capillary forces could provide an additional stress on the underlying PMMA layer so as to enable more extensive PS grafting in the border regions. Alternatively or concurrently, at the PS/air interface, the polymer concentration could be higher than in the bulk of the drops, or chains at the interface could be more extended [21], leading to a localized faster grafting reaction. Such effects might disappear at saturation, such as at PS = 75% in the blends.

Phase Segregation vs. Grafting Process.

From the data so far described, it appears that a critical interplay exists between the phase segregation of the homopolymer blends in the deposited film and their grafting process on the SiO_2 surface. Although a complete description of this mechanism is under investigation, a general scheme is offered in figure 6.9. PS and PMMA present a UCST that depends on blend composition, and the blend separates into two coexisting phases with different compositions at a T<UCST for any given blend composition. During the spin coating of these very thin films using toluene as the solvent, the polar SiO_2 surface is preferential for the PMMA-rich phase that thus forms a homogeneous layer on the substrate. Conversely, the PS-rich phase is located at the polymer/air interface. Depending on the blend composition and processing temperature, partial wetting or complete wetting of the PS-rich phase on the PMMA-rich phase is expected to occur.[9] [22] [23] However, during the RTP heating treatment, phase segregation and grafting proceed simultaneously.
In turn, as the grafting reaction proceeds, the composition of the grafted layer changes. In the case of partial wetting, an enrichment in the PS component underneath the PS-rich phase making up the circular domains is observed.
In the case of complete wetting, leading to the formation of a PS/PMMA bilayer, the progressive diffusion of PS chains, from the top of the layer to the polymer substrate interface, followed by grafting, produces a continuous and homogeneous change in the substrate surface characteristics over the entire sample surface. In addition, as the grafting reaction is self-limited, the amount of graftable PS depends also on the density of the grafted chains deriving from the PMMA-rich phase.

6.6 Conclusions

In summing up the main results collected in this appendix it is important to highlight that this study indicates the possibility to obtain the surface neutralization for the ordering of PS-*b*-PMMA block copolymers by using a mixture of functional PS and PMMA homopolymers.
In particular, an efficient surface neutralization is obtained when homopolymer blends with 85% and 90% of PS are grafted to the surface at 290°C for 600 s. This enables the formation of homogeneous textures of lamellae or cylinders oriented perpendicularly to the substrate upon self-assembly of symmetric or asymmetric BCPs.

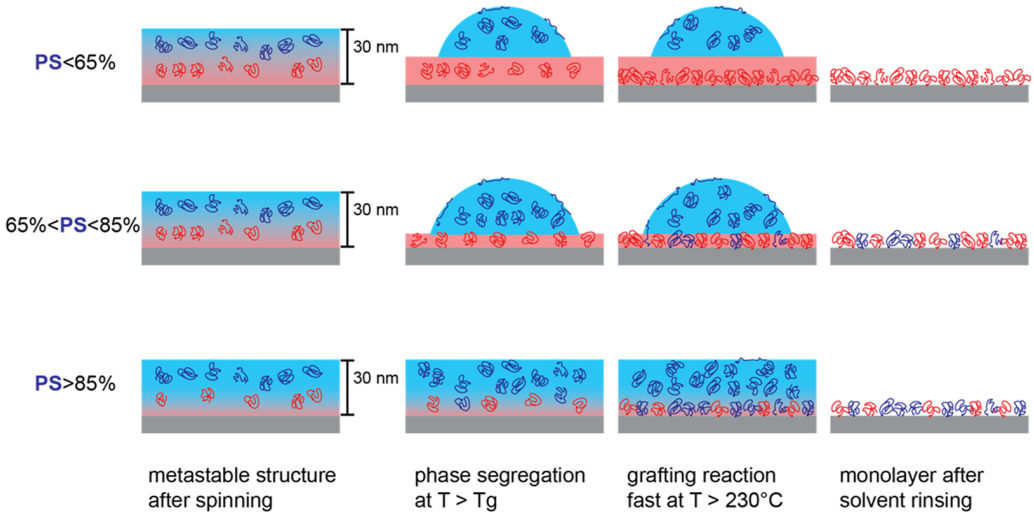

Figure 6.9: Schematic representation of the phase segregation and grafting processes during the RTP treatment.

A delicate balance between blend morphology and grafting characteristics leads to the formation of a homogeneous surface whose average composition is effectively tuned by controlling the blend composition. Interestingly, corresponding to the blend compositions of PS = 85% and 90%, grafted layers featuring styrene unit contents of 50% and 62% are obtained, respectively. The styrene content in these two grafted layers is close to the optimum composition for the surface neutralization of lamellar and cylinder forming block copolymers promoted by random copolymers with the corresponding styrene mole fraction.

Bibliography

[1]P. Mansky, Y. Liu, E. Huang, T. P. Russell, and C. Hawker, "Controlling Polymer-Surface Interactions with Random Copolymer Brushes", Science **275**, 1458–1460 (1997).

[2]S. Ji, C.-C. Liu, J. G. Son, K. Gotrik, G. S. W. Craig, P. Gopalan, F. J. Himpsel, K. Char, and P. F. Nealey, "Generalization of the Use of Random Copolymers To Control the Wetting Behavior of Block Copolymer Films", Macromolecules **41**, 9098–9103 (2008).

[3]E. Han, K. O. Stuen, M. Leolukman, C.-C. Liu, P. F. Nealey, and P. Gopalan, "Perpendicular Orientation of Domains in Cylinder-Forming Block Copolymer Thick Films by Controlled Interfacial Interactions", Macromolecules **42**, 4896–4901 (2009).

[4]E. Han, and P. Gopalan, "Cross-Linked Random Copolymer Mats As Ultrathin Nonpreferential Layers for Block Copolymer Self-Assembly", Langmuir **26**, 1311–1315 (2010).

[5]T. P. Russell, R. P. Hjelm, and P. A. Seeger, "Temperature Dependence of the Interaction Parameter of Polystyrene and Poly(methy1 methacrylate)", Macromolecules **23**, 890 (1990).

[6]D. A. Winesett, S. Story, J. Luning, and H. Ade, "Tuning Substrate Surface Energies for Blends of Polystyrene and Poly(methyl methacrylate)", Langmuir **19**, 8526–8535 (2003).

[7]S. Ji, G. Liu, F. Zheng, G. S. W. Craig, F. J. Himpsel, and P. F. Nealey, "Preparation of Neutral Wetting Brushes for Block Copolymer Films from Homopolymer Blends", Advanced Materials **20**, 3054–3060 (2008).

[8]C. Ton-That, A. G. Shard, R. Daley, and R. H. Bradley, "Effects of Annealing on the Surface Composition and Morphology of PS/PMMA Blend", Macromolecules **33**, 8453–8459 (2000).

[9]M. Harris, G. Appel, and H. Ade, "Surface Morphology of Annealed Polystyrene and Poly(methyl methacrylate) Thin Film Blends and Bilayers", Macromolecules **36**, 3307–3314 (2003).

[10]S. Wu, "Surface and interfacial tensions of polymer melts. II. Poly(methyl methacrylate), poly(n-butyl methacrylate), and polystyrene", The Journal of Physical Chemistry **74**, 632–638 (1970).

[11]M. Ceresoli, M. Palermo, F. Ferrarese Lupi, G. Seguini, M. Perego, G. Zuccheri, S. D. Phadatare, D. Antonioli, V. Gianotti, K. Sparnacci, and M. Laus, "Neutral wetting brush layers for block copolymer thin films using homopolymer blends processed at high temperatures.", Nanotechnology **26**, 415603 (2015).

[12]V. Gianotti, D. Antonioli, K. Sparnacci, M. Laus, T. J. Giammaria, M. Ceresoli, F. Ferrarese Lupi, G. Seguini, and M. Perego, "Characterization of ultra-thin polymeric films by Gas chromatography-Mass spectrometry hyphenated to thermogravimetry.", Journal of chromatography. A **1368**, 204–10 (2014).

[13]S. T. Milner, T. A. Witten, and M. E. Cates, "Theory of the grafted polymer brush", Macromolecules **21**, 2610–2619 (1988).

[14]A. Kopf, J. Baschnagel, J. Wittmer, and K. Binder, "On the Adsorption Process in Polymer Brushes: A Monte Carlo Study", Macromolecules **29**, 1433–1441 (1996).

[15]B. Zhao, and W. Brittain, "Polymer brushes: surface-immobilized macromolecules", Progress in Polymer Science **25**, 677–710 (2000).

[16]K. Sparnacci, D. Antonioli, V. Gianotti, M. Laus, F. F. Lupi, T. J. Giammaria, G. Seguini, and M. Perego, "Ultrathin random copolymer-grafted layers for block copolymer self-assembly.", ACS applied materials & interfaces **7**, 10944–51 (2015).

[17]I. McNeill, M. Zulfiqar, and T. Kousar, "A detailed investigation of the products of the thermal degradation of polystyrene", Polymer Degradation and Stability **28**, 131–151 (1990).

[18]Y.-H. Hu, and C.-Y. Chen, "The effect of end groups on the thermal degradation of poly(methyl methacrylate)", Polymer Degradation and Stability **82**, 81–88 (2003).

[19]D. Y. Ryu, S. Ham, E. Kim, U. Jeong, C. J. Hawker, and T. P. Russell, "Cylindrical Microdomain Orientation of PS- b -PMMA on the Balanced Interfacial Interactions: Composition Effect of Block Copolymers", Macromolecules **42**, 4902–4906 (2009).

[20]S. Ham, C. Shin, E. Kim, D. Y. Ryu, U. Jeong, T. P. Russell, and C. J. Hawker, "Microdomain Orientation of PS- b -PMMA by Controlled Interfacial Interactions", Macromolecules **41**, 6431–6437 (2008).

[21]H. R. Brown, and T. P. Russell, "Entanglements at Polymer Surfaces and Interfaces", Macromolecules **29**, 798–800 (1996).

[22]J. Raczkowska, R. Montenegro, A. Budkowski, K. Landfester, A. Bernasik, J. Rysz, and P. Czuba, "Structure evolution in layers of polymer blend nanoparticles.", Langmuir **23**, 7235–40 (2007).

[23]S. Coveney, and N. Clarke, "Pattern Formation in Polymer Blend Thin Films: Surface Roughening Couples to Phase Separation", Physical Review Letters **113**, 218301 (2014).

List of Publications

Refereed publications

Rapid thermal processing of self-assembling block copolymer thin films,
F Ferrarese Lupi, T J Giammaria, M Ceresoli, G Seguini, K Sparnacci, D Antonioli, V Gianotti, M Laus, M Perego, Nanotechnology **24**, 315601 (2013).

Flash grafting of functional random copolymers for surface neutralization,
F Ferrarese Lupi, T J Giammaria, G Seguini, M Ceresoli, M Perego, D Antonioli, V Gianotti, K Sparnacci, M Laus, Journal of Materials Chemistry C **2**, 4909-4917 (2014).

Ordering dynamics in symmetric PS-b-PMMA diblock copolymer thin films during rapid thermal processing,
M Perego, F Ferrarese Lupi, M Ceresoli, T J Giammaria, G Seguini, E Enrico, L Boarino, D Antonioli, V Gianotti, K Sparnacci, M Laus, Journal of Materials Chemistry C **2**, 6655-6664 (2014).

Evolution of lateral ordering in symmetric block copolymer thin films upon rapid thermal processing,
M Ceresoli, F Ferrarese Lupi, G Seguini, K Sparnacci, V Gianotti, D Antonioli, M Laus, L Boarino, M Perego, Nanotechnology **25**, 275601 (2014).

Characterization of ultra-thin polymeric films by Gas chromatography-Mass spectrometry hyphenated to thermogravimetry,
V Gianotti, D Antonioli, K Sparnacci, M Laus, T J Giammaria, M Ceresoli, F Ferrarese Lupi, G Seguini, M Perego, Journal of Chromatography A **1368**, 204-210 (2014).

Thermal Stability of Functional P (S-r-MMA) Random Copolymers for Nanolithographic Applications,
K Sparnacci, D Antonioli, V Gianotti, M Laus, G Zuccheri, F Ferrarese Lupi, T J Giammaria, G Seguini, M Ceresoli, M Perego, ACS applied materials & interfaces **7**, 3920-3930 (2015).

Scaling of correlation length in lamellae forming PS-b-PMMA thin films upon high temperature rapid thermal treatments,
M Ceresoli, F G Volpe, G Seguini, D Antonioli, V Gianotti, K Sparnacci, M Laus, M Perego, Journal of Materials Chemistry C **3**, 8618-8624 (2015).

Neutral wetting brush layers for block copolymer thin films using homopolymer blends processed at high temperatures,
M Ceresoli, M Palermo, F Ferrarese Lupi, G Seguini, M Perego, G Zuccheri, SD Phadatare, D Antonioli, V Gianotti, K Sparnacci, M Laus, Nanotechnology **26**, 415603 (2015).

Enhanced Lateral Ordering in Cylinder Forming PS-b-PMMA Block Copolymers Exploiting the Entrapped Solvent, G Seguini, F Zanenga, T J Giammaria, M Ceresoli, K Sparnacci, D Antonioli, V Gianotti, M Laus, M Perego, ACS Applied Materials and Interfaces **8**, 8280-8288 (2016).

Composition of ultrathin binary polymer brushes by thermogravimetry-gas chromatography-mass spectrometry,
D Antonioli, K Sparnacci, M Laus, F Ferrarese Lupi, T J Giammaria, G Seguini, M Ceresoli, M Perego, V Gianotti, Analytical and Bioanalytical Chemistry **408**, 3155-3163 (2016).

Acknowledgments

First of all I should thank Dr. Michele Perego and prof. Paolo Milani for giving me the opportunity to attein this PhD.
Special ackowledgments go to everyone who collaborates in this experimental activity in particular to the group of Dr. Michele Perego of the laboratory MDM of the Institute of Microelectronics and Microsystems (CNR) at Agrate Brianza; and to the group of Prof. Laus at Università del Piemonte Orientale.

As previously mentioned... Grazie a Michele Perego per questi anni di dottorato e in particolare per avermi insegnato (o almeno per averci provato) a partire sempre dai dati, senza avere la fretta di fargli dire quello che vogliamo; perchè solo così i risultati (e gli articoli) arrivano. Grazie per la pazienza avuta anche di fronte al mio desiderio di realizzare dispositivi! e per avermi mostrato la bellezza di fare ricerca scientifica. Grazie ovviamente a Gabriele Seguini, per la guida dall'alto, e in particolare per il bel lavoro di revisione degli articoli fatto insieme. Grazie a Michele Laus, Diego Antonioli, Katia Sparnacci e Valentina Gianotti: poter collaborare con voi e vedere all'opera dei chimici è stato un vero piacere. Ringrazio i miei due mentori Federico Ferrarese Lupi e Tommaso Jacopo Giammaria, che mi hanno introdotto e guidato fin dai primi passi nella ricerca sui copolimeri a blocchi. Dopo quattro anni sono certa di aver fatto breccia nei vostri cuori. Grazie a Jacopo Frascaroli per aver condiviso questi anni di dottorato, e a tutti i tesisti che ci hanno accompagnato (Filippo, Marcello, Fabio, Massimo, Stefano). Grazie a Davide Rotta per avermi insegnato a stare in una clean room e per aver risposto a tutte le domande con cui l'ho assillato. Ringrazio tutti i membri del laboratorio MDM e in particolare coloro che mi hanno più sopportato, come Mario Alia, con i nostri infiniti test sulle termocoppie, e Mara che veglia su tutto l'ufficio. Grazie a Simone Selmo per la sua amicizia.
Grazie ad Elisa Arduca: condividere l'attività lavorativa è stato un grande privilegio, condividere una maternità è stato eccezionale.
Da ultimo un grande ringraziamento a mio marito Andrea che durante questo dottorato mi ha sposato!...e che mi ha corretto le versioni latex di questa tesi fino all'ultimo warning.